HIGH RESOLUTION RADIO SPECTROSCOPY OF CONTINUUM RADIO BURSTS AT DECAMETER WAVELENGTHS FROM THE SUN

A Thesis

Submitted for the Degree of

Doctor of Philosophy in the Faculty of Science

BANGALORE UNIVERSITY

By

K.R.SUBRAMANIAN

INDIAN INSTITUTE OF ASTROPHYSICS

BANGALORE 560034

INDIA

1992 MARCH

DECLARATION

I hereby declare that the matter embodied in this thesis is the result of the investigations carried out by me in the Indian Institute of Astrophysics and the Dept of Physics, Bangalore University, under the supervision of Prof.Ch.V.Sastry and Dr.M.N.Anandaram and has not been submitted for the award of any degree,diploma,associateship,fellowship etc of any university or institute.

K.R. Subramanian

(K. R. Subramanian)

Ch.V. Sastry

Ch.V.Sastry

M.N. Anandaram

M. N. Anandaram

Supervisors

Bangalore

Date 16/3/1992

DEDICATION

I dedicate this thesis to the memory of my late parents

ACKNOWLEDGEMENTS

I am greatly indebted to Prof.Ch.V.Sastry who introduced me to this research problem and took keen interest in all aspects of the work presented in this thesis. His guidance, encouragement, inspiration and suggestions helped me widen my understanding of the problem. I express my deep gratitude to Dr. M. N. Anandaram for his continued interest during the course of this work and for many useful suggestions and comments. I am grateful to Prof. Vinod Krishan for many valuable discussions and suggestions, regarding theoretical interpretations presented in this work.

I am indebted to Prof. J. C. Bhattacharya for his constant encouragement and continued support during this work.

My thanks are due to the staff of Gauribidanur radio observatory for their help in the construction of the antenna and receiver system and collection of solar burst data. In particular I would like to thank C. Nanje Gowda, G. N. Rajasekar,

H.A.Asthawappa and A.T.Abdul Hameed.

I feel indebted to Prof.V. Radhakrishnan and the entire Raman Research Institute for providing me all facilities at Raman Research Institute.

I am thankful to Dr.G.Thejappa, Dr.N. Udayshankar,Dr.A. Desphande and Dr.R.K. Shevgaonkar for useful discussions.

The excellent library at Indian Institute of Astrophysics has been of great help and I would like to thank the library staff.I am thankful to the Librarian Ms.A. Vagiswari for allowing me to use the xerox and binding facilities of the Institute. My thanks are also due to the staff of the xerox and the binding section in particular Mr. R. Krishnamoorthy.

My thanks are due to Mr. S. Muthukrishnan for preparing the drawings in this thesis.

My acknowledgement beyond words are due to my wonderful family,my wife Geetha, and my daughter Raji who gave me love, affection, apppreciation, criticism and everything and brought this work to a success.

ABSTRACT

Observations of solar radio bursts at decameter wavelengths with high time, frequency and sensitivity are presented. The time and intensity characteristics of type IIIb burst observed at 25 MHz are compared with those of type III burst which follows the type IIIb burst. A theoretical model which accounts for the various aspects of these bursts is proposed. The time profile of isolated and type IIIb associated type III bursts are compared. It is observed that while there exists a correlation between exciter duration and decay constant for isolated type III bursts, it is absent in the case of type IIIb associated type III bursts.

The Gauribidanur radio telescope operating at a frequency of 34.5 MHz and an eight channel filter bank spectrograph are described. Fine structures in the radio emission of the sun observed with the above system are presented. Observations on the pulsation pattern in the time profile of short duration solar radio bursts, are presented. These pulsations are found to be present in the saturation phase of the burst. A tentative physical model to explain the observed characteristics is proposed. From the bandwidth and

drift rate of slowly drifting spike bursts,the strength of the magnetic field at 1.5 solar radii is determined. From the time profiles of diffuse echo bursts, the distance between the plasma layers corresponding to frequencies 17.25 MHz and 34.5 MHz is derived.

To study solar radio bursts over wide bandwidth a broadband array operating in the frequency range of 30 to 70 MHz was designed and constructed. Using this array and a four channel spectral receiver,low frequency radio spectrum of the continuum emission from the undisturbed sun is determined for 24 days over the period 1985 May - Sept. It is found that the spectral index varied from + 1.6 to + 3.6 during this period. It is suggested that the large positive spectral indices are due to the existence of temperature gradients in the outer corona. Temporal and spectral characteristics of microbursts observed in the frequency range of 38 to 65 MHz are compared with those of normal type III radio bursts. It is shown that the microbursts are low frequency extension of the brightness temperature spectrum of type III bursts.

CONTENTS Page

CHAPTER 1

INTRODUCTION

1.1 Introduction

The sun is studied by astrophysicists as a star, the only one that can be seen in detail. Its atmosphere provides a laboratory where unique condition of temperature,density,and fluid motion exist which cannot be reproduced in any laboratory. The sun can be studied in the optical and radio domain from ground based instruments. Radio studies of the sun was started with the serependitious discovery by Hey in the year 1942.The close association between metrewave bursts and solar flares was discovered by Hey. Southworth detected thermal radiation from the sun in the same year. The contributions by several groups in Australia,France and Cambridge led to the detection of three basic components in the radio emission of the sun. They are (i) the Quiet sun component, (ii) the Slowly varying component and (iii) the Radio bursts. The quiet sun component is the radiation from the sun when there are no active regions on the sun and is due to thermal emission from the million degree corona. The slowly

varying component arises in high density regions called "condensations" and is again due to thermal emission. This component varies in time scale of the order of 27 days. The third component radio bursts result from impulsive processes in active centers called flares. Solar flares are explosions in the solar atmosphere and are seen as a sudden brightening in the H_{α} line with the intensity few times the background intensity. In radio flares the brightness temperature rises from 10^9K to 10^{12}K in a few seconds. The observed brightness and the speed with which it varies indicate the existence of nonthermal processes such as gyromagnetic and plasma oscillations in the corona. The large brightness temperature at the expense of small fraction of flare energy suggests that radio bursts are sensitive indicators of flares in the sun. The solar bursts had been recognized over wide range of wavelengths from millimeter to decameter from ground based instruments. The burst emission which is always associated with solar active regions start at the time of a flare. The characteristics of the burst depends on the wavelength of observation. Near the millimeter wavelength the bursts are weak and of short duration.As the wavelength increases the intensity and duration of the bursts increases. The bursts are also complex in

nature. At meter and decameter wavelengths the bursts are rich in variety and substantial changes in the charateristics of emission may occur within time scales of the order of few seconds.

1.2 Solar radio bursts

The first spectral observations of solar burst at meter wavelengths was made by Wild and McCready (1950). They classified the bursts into three spectral classes, Type I, Type II and Type III. Observations by Boischot (1959) and Wild et al (1959) added two more spectral types in the above classification called type IV and type V. Type I bursts occur during noise storms accompanied by a background emission. Radio noise storms are a common kind of long lived activity which may last for several days in solar cycle maximum year. Their spectral properties vary with the wavelength of observation. At meter wavelengths a large number of type I bursts appear superimposed on the continuum emission (Kundu 1965). At decameter wavelengths a large number of type III bursts occur in quick succession with their starting frequency usually below 100 MHz. These type III bursts called storm type III bursts are accompanied by fine structure emission. These fine structures have

narrow bandwidth and short duration. These fine structures were discovered when decameteric noise storms were observed with spectrographs having high time and frequency resolution.

The decametric radiation is mostly emitted in 1-2 solar radii. The study of this region of the corona is important because the solar wind is accelerated here and the magnetic field configuration changes from closed to open lines. High time and frequency resolution studies of fine structures may serve as tracers for spatial structure and magnetic field configuration in the outer corona that are otherwise inaccesible. The fine structure can be used as tracers only if their physical mechanism is established. The fine structure encouraged the study of Langumir turbulence under cosmic conditions.

High sensitivity and high time and frequency resolution studies of so called decametric continuum revealed that the continuum is composed of several kinds of bursts (Ellis 1969). Among these one finds type I bursts,storm type III bursts, type IIIb bursts (de la Noe & Boischot 1972), drift pairs (Roberts 1958) and unclassified fine structure emission.

1.3 Thesis organisation

This work is a study of solar radio bursts at decameter wavelengths with high time and frequency resolution along with high sensitivity. In the first chapter observations of type IIIb - type III burst with time resolution of 20 msec and frequency resolution of 100 KHz are presented.The time profile can be measured accurately with the receiver system used. The time structure and intensity of type IIIb bursts are compared with that of type III bursts. The nonlinear evolution of an electron beam magnetoplasma system is studied inorder to interpret the characteristics of type IIIb bursts. The interpretation differs from that of Smith & de la Noe in the treatment of electric field corresponding to electrostatic instability. Smith & de la Noe considered the electric field interaction with the normal modes of the plasma system. The electromagnetic modes of the plasma immersed in electric and magnetic field is considered in the treatment given here. The electric field enters at a single particle level and is therefore accounted in a more exact manner.

The time profile of isolated type III burst

and type IIIb associated type III burst are compared. The exciter duration D_e and decay time constant τ of both isolated and associated type III bursts are measured. The observed correlation between D_e and τ for isolated type III bursts and lack of it for type III bursts preceded by type IIIb bursts is explained by the difference in the nature of exciter in the two cases.

In the second chapter the Gauribidanur radio telescope operating at a frequency of 34.5 MHz and an eight channel spectrograph are described. This radio telescope is in the shape of letter "T", with the long arm along the East West direction and short arm along the South direction.The South arm used for the study of solar radio bursts is described. An eight channel filter bank spectral receiver used for the study of fine structure is also described. The frequency resolution of this spectral receiver is 15 KHz and its time resolution is 20 milliseconds.

In the next chapter fine structures observed with the south arm of the Gauribidanur radio telescope are described. Observation on the pulsation pattern in the time profile of short duration solar bursts at decameter wavelengths are presented. The main

characteristics of these pulsations are that they occur predominantly at the saturation phase of the burst. A physical model where the oscillation can be set only during the saturation phase of the burst is given. Spectral observations of spike burst at 34.5 MHz are presented next. These spike bursts are found to have a bandwidth of 200 KHz and slow drift rate of 150 KHz s^{-1}. The exciter of these bursts is shown to be a weak shock. The drift rate and bandwidth of these spikes are used to derive the magnetic field in the outer corona. The time and frequency characteristics of diffuse echo bursts are described next. The exciter is shown to be a proton beam. From the time delay between the primary burst and its echo the distance between the plasma layers corresponding to 17.25 MHz and 34.5 MHz is derived.

In the fifth chapter a broadband array designed and built for the study of solar radio emission in the frequency range of 30 to 70 MHz is described. A four channel receiver system operating at 38, 45.7, 55.5 and 64.25 MHz is also described. The antenna and receiver system are capable of measuring the flux density of both the undisturbed sun and the radio bursts.

In the next chapter the low frequency radio spectra of the continuum emission from the undisturbed sun in the frequency range of 35 to 70 MHz is determined from the observations made using the broadband array. It is found that the spectral index varied from +1.6 to +3.6 during the period when no burst activity was found in our data. It is suggested that the large positive spectral indices are due to the existence of temperature gradient in the outer corona.

In the seventh chapter the time structure and flux density spectra characteristics of microbursts are compared with those of type III radio bursts. It is shown that the characteristics of microbursts are similar to those of type III bursts except for their brightness temperature.

In the last chapter the results are summarized. Future observational work to be done in these lines are presented.

CHAPTER 2

TIME STRUCTURE OF TYPE IIIb, ISOLATED AND ASSOCIATED TYPE III BURSTS

2.1 Time structure of type IIIb bursts

Solar decameter bursts of type IIIb were observed with a multichannel radiometer at wavelength of 12 m. The time and frequency resolution were 10 ms and 100 KHz.Observations of the time structure of these bursts are presented.A theoretical model which accounts for various aspects of these bursts is also presented.

2.1.1 Introduction

Observation of solar radio bursts at meter and decameter wavelengths reveal a great variety of fine structure emissions. These fine structures are mostly observed during periods of noise storm when high sensitivity, time and frequency resolution are used for observations. Ellis and McCulloch (1966,1967) found a new type of fine structure called split pair burst. The split pair burst consists of two parallel short duration narrow band bursts sometimes drifting towards low frequencies. Triple burst consisting of three parallel emission has also been observed by

Ellis and McCulloch (1966,1967). A large number of bursts identical to an individual element of a split pair burst was reported by de la Noe and Boischot (1972). These bursts are called " Striae " bursts. Striae, split pair and triple bursts were often grouped in chains. These chains drift from high to low frequency similar to type III bursts.These chains are called type IIIb bursts.

2.1.2 Characteristics of type IIIb bursts

The type IIIb bursts are most frequently observed at decameter wavelengths, below 50 MHz. De la Noe (1974) observed that the maximum number of type IIIb bursts occur around a frequency of 30 MHz. The frequency at which maximum occurence of type IIIb burst takes place can vary from day to day. Individual striae may drift from high to low frequency at the rate of 250 KHz s^{-1}. But the split pair and triple burst have negligible drift rate. The bandwidth of an individual striae can vary from 15 KHz to 100 KHz. The frequency splitting between the elements of a split pair or a triple bursts is of the order 100 KHz at 30 MHz. The striae bursts show circular polarisation with the degree of polarisation varying from 0% to 100%. The elements in a split pair or triple burst have the same sense of polarisation, but the degree of

polarisation can vary. About 30% of type IIIb bursts were found to be precursor to type III bursts by de la Noe (1972). Detailed analysis of the time delay and frequency ratio between the type IIIb and type III burst favour fundamental- harmonic hypothesis (Bazelyan et al, 1974; Takakura and Yousef,1975; Abranin et al,1980). The coincidence of the position and height of type IIIb and type III bursts at a frequency (Abranin et al 1980) suggests that both type IIIb and type III burst at a fixed frequency are generated at the same plasma level in the corona. The time structure and intensity of type IIIb bursts and their relation to the type III burst which follows the type IIIb burst have not been reported earlier. The time and intensity characteristics of type IIIb burst observed at a frequency of 25 MHz are given here(Krishan et al 1980). The time structure and intensity characteristics of type IIIb bursts are compared with those of type III burst which follows the type IIIb burst. These type III bursts will hereafter be called "associated type III " bursts.

2.1.3 Observations

These observations were made by Sastry (1972) using an antenna system with a collecting area of 3600 m^2. The frequency of operation of the antenna

system was 25 MHz. The antenna system consisted of 104 full wave dipoles. The effective beam width of antenna system was 7 degrees in right ascension and 14 degrees in declination. The beam can be pointed anywhere within 30 degrees of the zenith by manual phasing.

The receiver system consisted of a four channel spectrograph. The bandwidth and time contant were 13 KHz and 10 msec respectively. The channel separation were usually 100 KHz, but can be varied. The data was recorded in an oscillographic recorder. Details of this equipment were given in Sastry (1972). The time profile of radio bursts can be measured accurately with this system . Short duration narrow band decameter solar bursts have been studied using this system and reported by Sastry (1969,1971,1972,1-973)

From the solar burst data obtained during the period January 1971 to March 1972, narrow band bursts which shows time and frequency splitting and occur before the onset of type III burst with a time delay of less than 10 seconds were selected for this study. Fig. 2.1 shows a typical example of the bursts studied. The type IIIb bursts which occur after the type III bursts are rare in our records and are not included in this

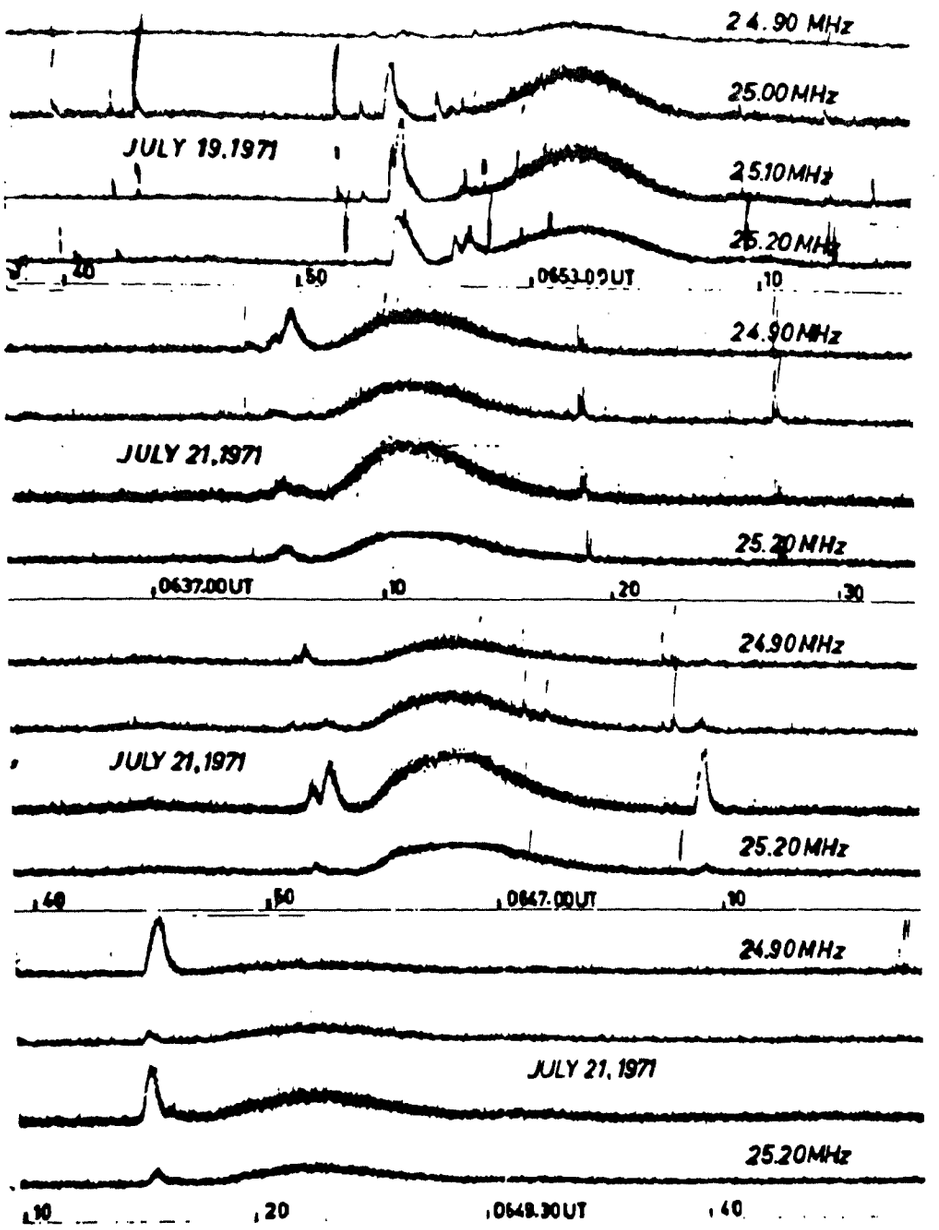

Fig. 2.1. Typical examples of Type IIIb bursts followed by Type III bursts. The vertical spikes are due to atmospherics.

study. 53 numbers of type IIIb - type III association are studied.

2.1.4 Duration

Duration of type IIIb burst at a frequency varies from the time resolution of the receiver (20 msec) to a few seconds. In the frequency range of 20-40 MHz the average duration without discrimination in frequency was found to be 1.00 $\pm$ 04 s and 1.15 $\pm$ 04 s for two separate periods of observation by de la Noe (1974).At a given frequency the duration is shorter when the sources are located near the limb and longer around the meridian of the sun. This variation was found to increase with decrease in frequency. The half power duration at 25 MHz can vary from 0.2 to 1.2 s. Majority of the bursts have half power duration in the range of 0.4 to 0.8 s as shown in Fig. 2.2. The average half power duration is 0.67 s, and the total duration is 1.61 seconds.

2.1.5 Time profile

The time profile of a burst is very interesting to study because it can give some information about the mechanism of generation and physical conditions at the place of generation and propagation. The average time profile of type IIIb

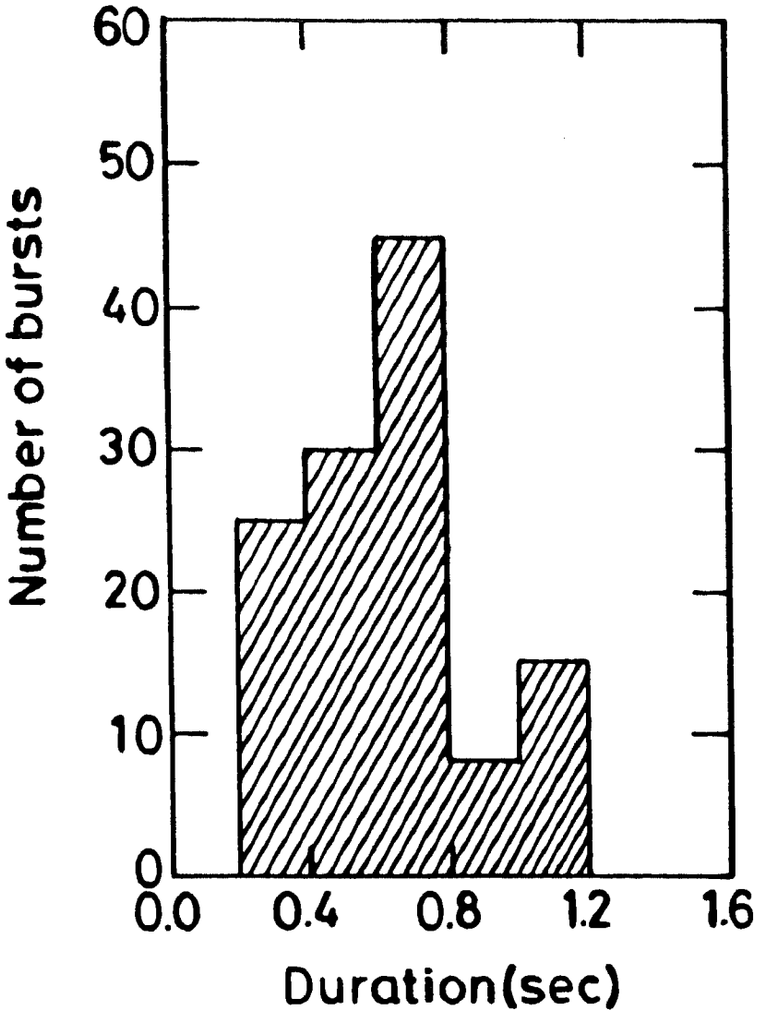

Fig. 2.2. Distribution of the half - power duration of Type IIIb bursts.

burst is shown in Fig. 2.3a. The time profile is very similar to type III burst with a sharp rise and a slow decay. The exciter duration and decay time constant of the average time profile is determined following the method given by Aubier and Boischot (1972). The exciter duration and decay time constant are 0.88 s and 0.31 s respectively. For the associated type III burst the average time profile is shown in Fig. 2.3b. The exciter duration and decay time constant are 6.00 s and 2.11 s respectively. The ratio of exciter duration (D_e type III/D_e type IIIb) and the ratio of damping constant (τ type III/ τ type IIIb) is approximately the same. The ratio is equal to 6.82

The half power duration of type IIIb burst is much smaller than that of the associated type III burst and the ratio of the half power duration of associated type III burst to that of type IIIb burst was found to be 3.5 ± 1.5 at 60 MHz increasing to 6 ± 3 at 29.3 MHz (de la Noe 1974).The ratio is found to be larger (9.83) at 25 MHz. The total duration of type III burst and type IIIb burst are correlated positively with a linear correlation coefficient of + 0.65. Fig. 2.4 shows the scatter diagram of the durations of type III and type IIIb radio bursts.

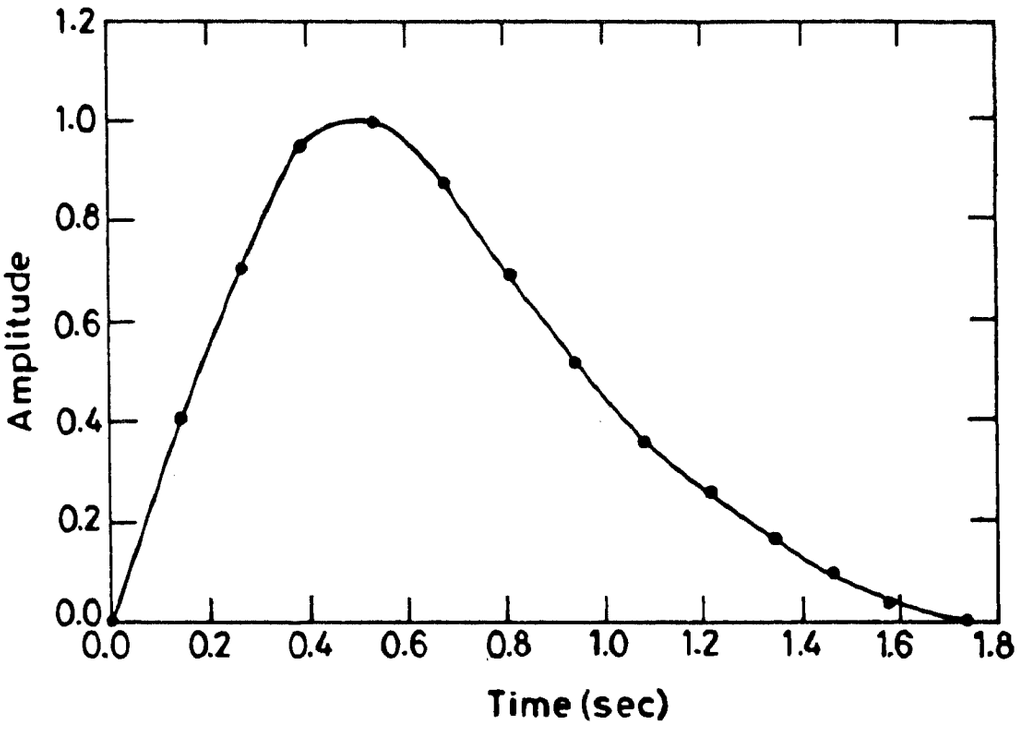

Fig. 2.3a. Time profile of elements of Type IIIb radio bursts.

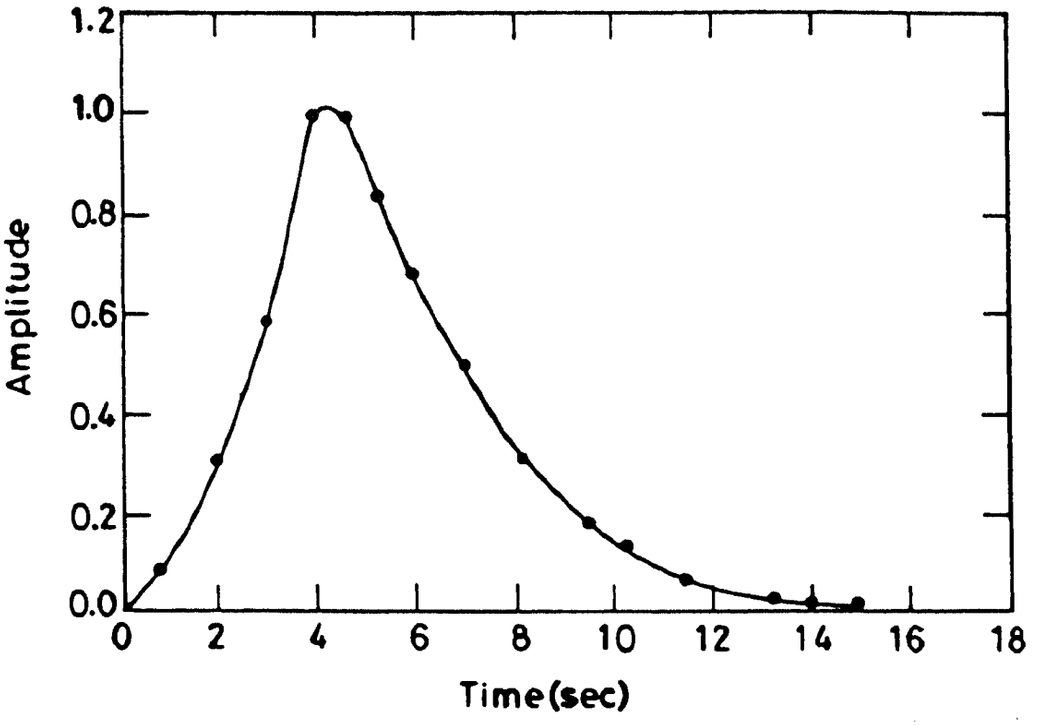

Fig. 2.3b. Time profile of associated Type III radio bursts.

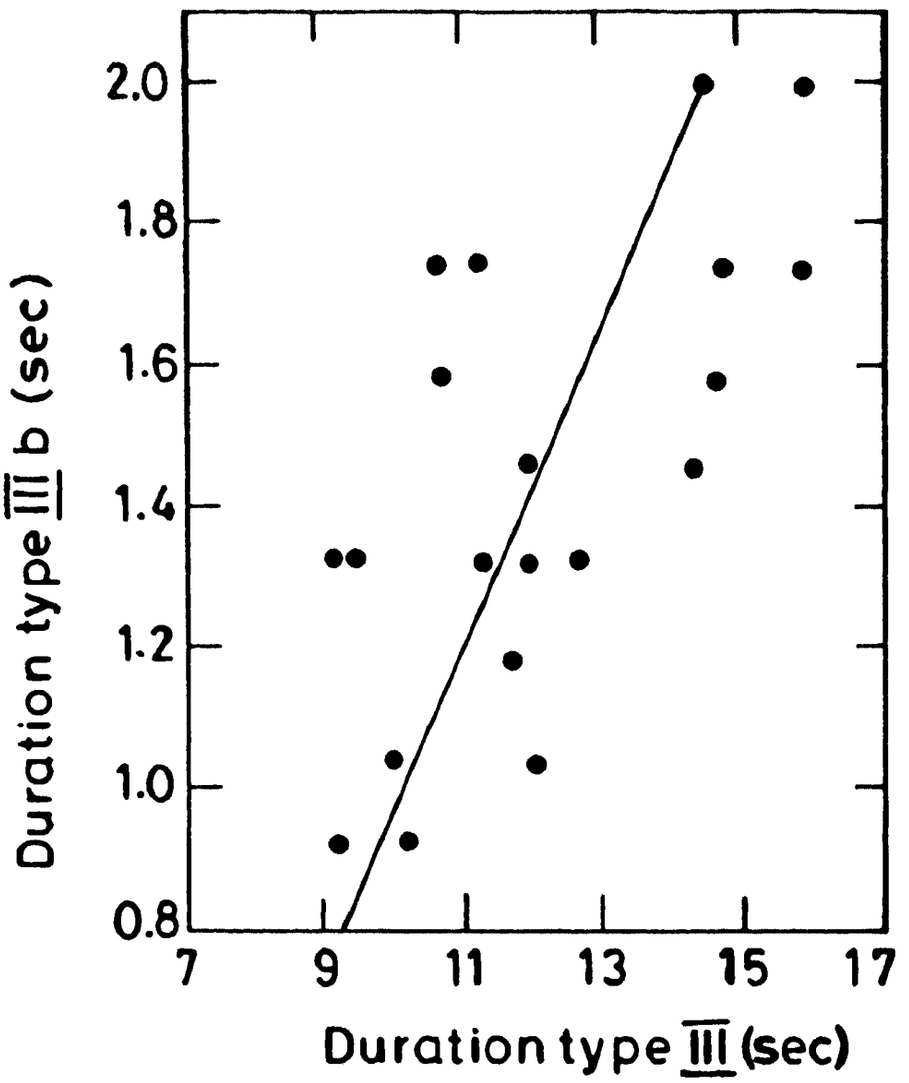

Fig. 2.4. Correlation of the total duration of Type IIIb and accompanying Type III bursts.

2.1.6 Intensity

De la Noe (1974) made a rough estimate of the ratio of the intensity of the components of the split pair and triplet. There are no measurements on the intensity of type IIIb burst in comparison with the that of the associated type III burst. The ratio of amplitude of type IIIb and type III burst is shown in the Fig. 2.5.The amplitude of type IIIb is equal to or greater than that of the associated type III burst.

2.1.7 Discussion

Takakura and Yousef (1975) were the first to present a model for type IIIb bursts. They suggested that the striae in type IIIb burst was due to the existence of filamentary irregularities along the path of the electron stream. These filaments would decrease or increase the gradient of electron density along the path of some electrons. Beam travelling along the path containing normal electron density distribution gives rise to type III bursts. Beams encountering the filamentary structure with a decrease in the electron density gradient gives rise to type IIIb bursts. The reduced gradient of plasma density on the lower edge of the filaments explain the slow drift of the bursts, and also provide a longer effective path length for the

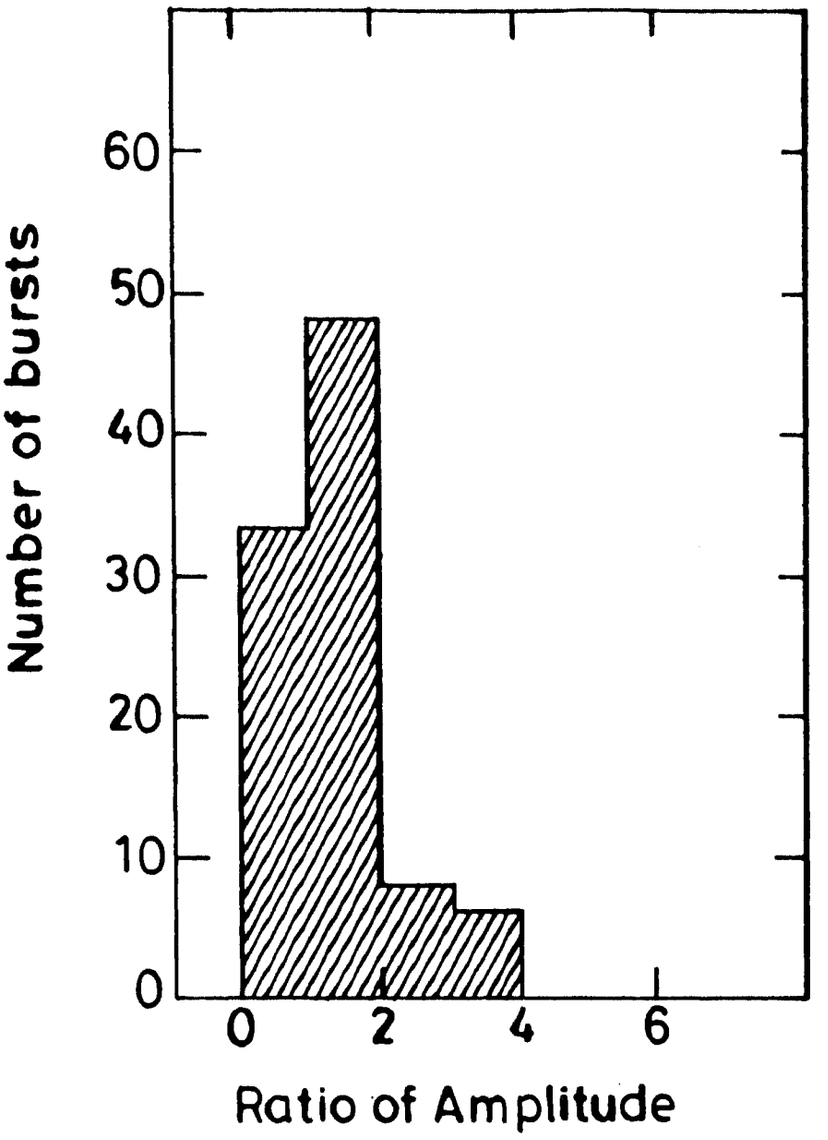

Fig. 2.5. Distribution of the ratio of the amplitude of Type IIIb and associated Type III bursts.

generation of the radiation. The excess density in the filaments was estimated to be approximately 10% higher than the normal electron density. This theory was not able to explain the systematic time delay observed in split and triplets.

Melrose (1983) suggested a mechanism in which frequency splitting occurs during conversion process which was attributed to the coalesence of Langumir waves with lower hybrid waves. Since only a small part of the spectrum of low frequency turbulence is involved in this process two fold coalescence process was suggested in which the broad spectrum of low frequency turbulence produce secondary Langumir waves. These secondary Langumir waves can produce transverse waves by coalescence with a low frequency wave. Double coalescence involving lower hybrid waves was able to explain the observed frequency splitting. This semi quantitative interpretation was unable to explain the kinematics in detail.

A detailed theory for the generation of type IIIb burst was developed by Smith and de la Noe(1976). In this theory it was assumed that Langumir waves are generated by strong beam interaction. Electrons are accelerated in the lower corona forming a beam which is

guided by the magnetic field. The leading edge of such a beam amplify a quasi monochromatic large amplitude plasma wave. The beam is stabilized by trapping of the electrons in the potential well associated with the wave. The trapped electrons oscillate with a bounce frequency ω_c,the gyrofrequency. Frequency modulation of the intial wave with frequency ω by the trapped electron lead to side bands at frequency $\omega_s = \omega \pm \omega_c$. The side bands and the main wave which are electrostatic waves are converted to electromagnetic waves by parametric decay instability. In parametric decay instability some mode of the system is driven unstable by an external imposed oscillation at a different frequency. The externally imposed oscillation is generally a large amplitude wave excited by an external source called pump. This is an approximate way of dealing with the electric field in the sense that the trapped particle instability occurs at a field strength when the electron bounce frequency becomes comparable to the linear growth rate of the beam - plasma instability. Further the particles near the bottom of the trough, executing harmonic motion are included. The effects of anharmonic motion executed by the particles near the top of the potential trough are not taken into account. The parametric decay instability is a threshold effect,and Smith and de la Noe(1976) considered the

interaction of the normal modes of the plasma system with the electric field considered as an external pump. In the treatment given here the plasma is immersed in the electric and magnetic fields and the direct excitation of normal elctromagnetic modes is considered.

2.1.8 Interpretation

An electron beam magneto plasma system where the electron beam generates electrostatic growing oscillation at ω_0 is considered. The electric field associated with this instability grows until the trapped particle effects come into play. i.e., when the bounce frequency of the electron becomes comparable to the linear growth rate of the electric field ,the field saturates and reaches a steady state(Ichimaru 1973).The magneto plasma is under the influence of an electric field which is oscillating at the electron plasma frequency. The beam particles instead of travelling with a uniform speed along the magnetic field execute a gyromotion in a plane perpendicular to the magnetic field and a quivering motion along the magnetic field. The quiver is produced by the electric field E_0 associated with the instability at ω_0. The quivering speed is given by

$$u_e = eE_o/m\omega_o$$

where e is the electric charge

E_o is the electric field

m is the mass of the electron

and ω_o is the frequency at which the instability occurs.

Coupling of gyromotion and quiver motion can generate transverse modes. The electron density and magnetic field are given by the following relation (Lang 1974).

$$Ne(r) = 1.55\times10^{8}\ \rho^{-6}\ cm^{-3}$$

$$B(r) = B_o(\rho)^{-2}$$

where $\rho = r/R_\odot$, $R_\odot$ is the solar radius(6.96×10^{10} cm.).

The function of the electron beam is replaced by the electrostatic field it produces at the frequency ω_o .Then we have a plasma system under the action of an electric field E_o at frequency ω_o acting parallel to the uniform magnetic field B. The dielectric function $\epsilon(q,\omega)$ for such a system was calculated by Krishan(1978a,1978b,) and is given by

$$\epsilon(q,\omega) = 1 - \frac{\omega_{pe}^2}{\omega^2} - \sum_{n,l} \frac{\omega_{pe(eff)}^2 q^2 V_{th}^2 Dl}{\omega^2\{[(r\omega - nk_o) - (q_z - nk_o)u_e]^2 - l^2\omega_{ce}^2\}}$$

$$-\sum_{n,\ell} \frac{\omega_{pe}^2(eff)\, q^2 V_{th}^2 D_\ell}{\omega^2\left\{\left[(\omega - nk_0) - (q_z - nk_0)u_e\right]^2 - \ell^2\omega_{ce}^2\right\}} \quad 2.1$$

where (ω, q) are the frequency and wave vector of the mode to be excited.

$$\omega_{pe}^2(eff) = \frac{\omega_{pe}^2 J_{Ne}^2 - n(Ze)}{2}$$

where $$Ze \sim Ne = \frac{e^2 E_o^2}{m\hbar\omega_0^3}$$

K_0 is the wave vector of E_0.

The value of D_1 for first few value of 1 is given by

$$D_1 = q_\perp^2/4q^2$$

$$D_2 = 4\alpha D_1$$

$$D_3 = 3\alpha^2 D_1/16$$

$$D_4 = \alpha^3 D_1/24$$

$$\text{and} \quad \alpha = q_\perp^2 V_{th}^2/\omega_{ce}^2 < 1$$

Here V_{th} is the thermal velocity of

elctrons and ω_{ce} is the gyrofrequency and α is the ratio of the wavelength to the Larmor radius. Ion dynamics is neglected.

In the dielectric function the integer n stands for the periodic motion introduced by the electric field E_o of the electrostatic beam instability. The integer l signifies the usual cyclotron motion of the particles. In the Bessel function the argument is very large. Therefore the fact has been deployed that the Bessel function is maximum when the argument is equal to the order of the Bessel function.

The electromagnetic modes are found by solving the equation

$$\epsilon(q,\omega) = q^2c^2/\omega^2 \qquad 2.2$$

and finding the real roots.

For each value of n and l equation (2.2) has the following kind of roots (Krishan 1979).

$$\left.\begin{aligned} \omega_1 - nk_o &= (q_z - n_1 k_o)u_e + \sqrt{l_1^2\omega_{ce}^2 - \delta_{n_1}^2 l_1} \\ \omega_2 - nk_o &= (q_z - n_2 k_o)u_e - \sqrt{l_2^2\omega_{ce}^2 - \delta_{n_2}^2 l_2} \end{aligned}\right\}$$

$$\left.\begin{aligned} \omega_3 - n_3\omega_0 &= -(q_z - n_3 k_0)u_e + \sqrt{\ell_3^2\omega_{ce}^2 - \delta^2 n_3 \ell_3} \\ \omega_4 - n_4\omega_0 &= -(q_z - n_4 k_0)u_e - \sqrt{\ell_4^2\omega_{ce}^2 - \delta^2 n_4 \ell_4} \\ \text{where} \quad \delta^2 n\ell &= \frac{q^2\omega_{pe}^2(eff)\,V_{th}^2\,D\ell}{(q^2c^2 - 3k_0^2V_{th}^2)} \end{aligned}\right\} 2.3$$

The sign of the mode (positive or negative) energy is determined by the sign of the quantity

$$F = \frac{1}{2\omega}\frac{\partial}{\partial\omega}(\omega^2\epsilon)$$

which should be + ve for positive energy mode and -ve for negative energy mode.

$$F_1 = \frac{\omega_{pe}^2(eff)\,q^2V_{th}^2\,D\ell}{\omega_1\,\delta^4 n_1\ell_1}\left[\omega_1 - n_1(\omega_0 - k_0u_e) - q_z u_e\right]$$

$$= \frac{\omega_{pe}^2(eff)\,q^2V_{th}^2\,D\ell_1}{\omega_1\,\delta^4 n_1\ell_1}\left[+\sqrt{\ell_1^2\omega_{ce}^2 - \delta^2 n_1\ell_1}\right] \quad 2.4$$

F_1 is + ve for $q < 0$. Therefore ω_1 is a + ve energy mode.

$$F_2 \sim \frac{\omega_{pe}^2(eff)\, q^2 V_{th}^2 D \ell_2}{\omega_2 \delta^4_{n_2 \ell_2}} \left[-\sqrt{\ell_2^2 \omega_{ce}^2 - \delta^2_{n_2 \ell_2}} \right]$$

F_2 is - ve for $q > 0$. Therefore ω_2 is a negative energy mode.

The + ve and - ve energy modes can interact via two mode coupling if the laws of conservation of energy and momentum are satisfied. The interaction of these modes give rise to elctromagnetic radiation. The interaction of ω_1 and ω_2 demands $\omega_1 = \omega_2$.

The mode frequency Ω is given by

$$\omega_1 = \omega_2 = (n_1 + n_2)(\omega_0 - k_0 u_e) + \frac{1}{2}\sqrt{\ell_1^2 \omega_{ce}^2 - \delta^2_{n_1 \ell_1}} - \frac{1}{2}\sqrt{\ell_2^2 \omega_{ce}^2 - \delta^2_{n_2 \ell_2}}$$

$$q_2 u_e = \frac{(n_1 - n_2)}{2}(\omega_0 - k_0 u_e) + \frac{1}{2}\sqrt{\ell_1^2 \omega_{ce}^2 - \delta^2_{n_2 \ell_2}} + \frac{1}{2}\sqrt{\ell_2^2 \omega_{ce}^2 - \delta^2_{n_2 \ell_2}}$$

The growth of these modes can be calculated by the mode - mode coupling (Krishan et al 1978a,b).

The growth rate is given by

$$\gamma = \frac{\omega_{pe}^2}{2\Omega}\frac{1}{\sqrt{F_+F_-}}$$

$$= \frac{\omega_{pe}^2(eff)}{2(q^2c^2 - 3k_0^2V_{th}^2)}\left[\frac{D\ell_1 D\ell_2}{\sqrt{\ell_1^2\omega_{ce}^2 - \delta_{n_1\ell_1}^2}\sqrt{\ell_2^2\omega_{ce}^2 - \delta_{n_2\ell_2}^2}}\right]^{1/2}$$

where q is to be substituted from the equation governing the conservation laws for the respective mode.

Here n_1, n_2, l_1, and l_2 are positive integers. and

$$\delta_{n\ell}^2 = \frac{\omega_{pe}^2(eff)\, q^2 V_{th}^2 D\ell}{(q^2c^2 - 3k_0^2V_{th}^2)}$$

For the case of type IIIb bursts the relevance of the modes for $n_1 = n_2 = l_1 = l_2 = 1$ is pointed here. Modes for higher value of n and l have smaller growth rate.

One finds

$$\omega_\pm = \omega_0 + k_0 u_e$$

$$q_z u_e = \sqrt{\omega_{ce}^2 - \delta_{11}^2}$$

Assuming $q_z u_e \ll \omega_{ce}$ the conservation of energy can be

satisfied if $\omega_{ce} \approx \delta_{11}$

The value of q is calculated by equating $\delta_{11} \sim \omega_{ce}$ given by equation (2.3).

This gives

$$q^2 \sim \frac{3K_0^2 V_{th}^2}{c^2} \left[1 + \omega_{pe}^2 V_{th}^2 D\ell\right] \Big/ \omega_{ce}^2 c^2$$

Substituting in equation (2.6) for the growth rate we get

$$\gamma = \frac{16}{72} \frac{q^2}{K_0^2} \frac{\omega_{ce}^3}{K_0^2 V_{th}^2}$$

at $\omega_{pe} \sim \omega_0 \sim 25\,MHz$

$$V_{th} \sim 10^8\ cm/s$$

$$K_0 \sim \left(\frac{2{\cdot}5}{8{\cdot}0}\right) cm^{-1}, \quad \omega_{ce} \sim 2\,MHz$$

beam plasma density

$$\frac{n_b}{n_0} \sim 10^{-4}$$

and substituting for q^2 from condition $\omega_{ce} \sim \delta_{11}$ the characteristic rise time of the burst is $t \sim \frac{1}{\gamma} \sim \frac{1}{11}$ 0.1 second

Here $q \sim q_\perp$ since $q_z u_e$ has been made vanishingly small by choosing $\delta_{11} \sim w_e$. The total duration of the burst will be much larger than 0.1 seconds because the decay process of the burst is much slower than the growth.

The peak intensity of emission can be found by considering the nonlinear mechanism of the instability. If the saturation is due to the perturbation in the particle orbit then the emission with higher linear growth rate will saturate at higher fields. So the short duration fast rising elements of the type IIIb bursts are expected to be more intense than the type III bursts.

In the model given here the source of type IIIb is the electric field associated with the beam - plasma instabilty. The drift of the type IIIb is due to the drift of the electric field. The group velocity of the electric field is given by

$$V_g = \frac{3 V_{th}^2}{u_0}$$

where u_0 is the speed of the electron beam. The drift rate is given by

$$\frac{\partial \omega}{\partial t} = \frac{\omega(r) - \omega(r+\Delta r)}{\Delta r / v_g}$$

For beam velocity $v_0 \sim 8 \times 10^8$ cm^{-1} the drift rate is $\sim$ 40 KHz s^{-1}. The drift rate can be positive or negative depending on the variation of the plasma density in the underlying medium. Since the bandwidth of the spectrograph is limited the drift rate could not be measured. The predicted value of the drift rate agrees well with the value reported by de la Noe and Boischot (1972). Under the condition $q_\perp > q_z$ the rise time of type IIIb is estimated to propagate at large angle to the magnetic field, which predicts the type IIIb burst is to be circularly polarised as observed by de la Noe and Boischot (1972).

2.2 Time profile of isolated and associated type III bursts

We study the time profile of isolated and associated type III bursts. It is observed that while there exists a strong correlation between the decay

constant and exciter duration for isolated type III bursts,it is absent for those type III bursts which are preceeded by the type IIIb radio bursts. A possible explanation for the presence of correlation in one case and lack of it in the other is proposed.

2.2.1 Type III radio burst

Type III burst was first recognized as a distinct class of solar radio emission from the spectral studies at meter wavelengths (Wild 1950). Type III bursts occur over wide range of frequency from 1 GHz to 10 KHz, corresponding to a height ranging from the lower corona to beyond the orbit of the earth. The dynamic spectra of type III bursts show rapidly drifting bursts. The bursts drift from high to low frequency with a drift rate given by $df/dt = 0.01 f^{1.84}$ (Alvarez & Haddock ,1973) where df/dt is in MHz s^{-1} and f is in MHz. The observed drift rate corresponds to exciter speeds between 0.2 c to 0.6 c (c = velocity of light) and the exciter is electrons which can be directly observed at the orbit of the earth. There is considerable variation between the bursts but on the average they showed a rise time shorter than the decay time. The half power duration at a frequency is given by $D \approx 220/f$ (D in s and f in MHz). The time profile is asymmetric with a sharp rise and an exponential type decay.

It was first pointed out by Aubier and Boischot (1972) that it is possible to derive the exciter duration D_e and decay time constant τ from the time profile of type III radio bursts. They showed that D_e and τ are positively correlated. Barrow and Achong (1975) and Poquerusse (1977) confirmed this result. These authors have studied only isolated type III bursts. The time profile of associated type III bursts (type III bursts which are preceded by type IIIb bursts)have not been studied earlier. Here the time profiles of normal and associated type III bursts are compared (Subramanian et al 1981). The exciter duration and decay time constant for isolated and associated type III bursts have been determined. It is found that the exciter duration and decay constant are strongly correlated for isolated type III bursts and such a correlation does not seem to exist for associated type III bursts. The observed results are explained on the basis of the characteristics of the beam - plasma system responsible for the generation of the type III radio bursts.

2.2.2 Observations

From the solar burst data collected by Sastry during the period January 1971 to March 1972 using the

antenna and receiver system described earlier in this chapter, isolated and associated type III bursts were selected for this study. Most of the data in the present analysis are from the data obtained in the period July - August 1971. Fig. 2.6 shows a typical example of isolated and associated type III bursts. 52 Number of isolated and 32 number of associated type III bursts have been studied.

2.2.3 Theory of time profile

The time profile of Type III burst at a given frequency shows a sharp rise and a slow decay. The rise portion of the the radio burst is directly related to the buildup of the plasma oscillations in the medium as the exciter moves through a particular coronal level; the longer decay phase of the burst is related to the decay of the plasma waves through various possible damping mechanisms. The frequency drift in time reflects the velocity of the exciter as they move outward. The growth in the rise time at low frequency reflects the growth in the physical length of the exciter because of velocity dispersion.

The time profile of type III burst was used for deriving the coronal electron temperature from the observed decay rate of type III bursts. If the decay is

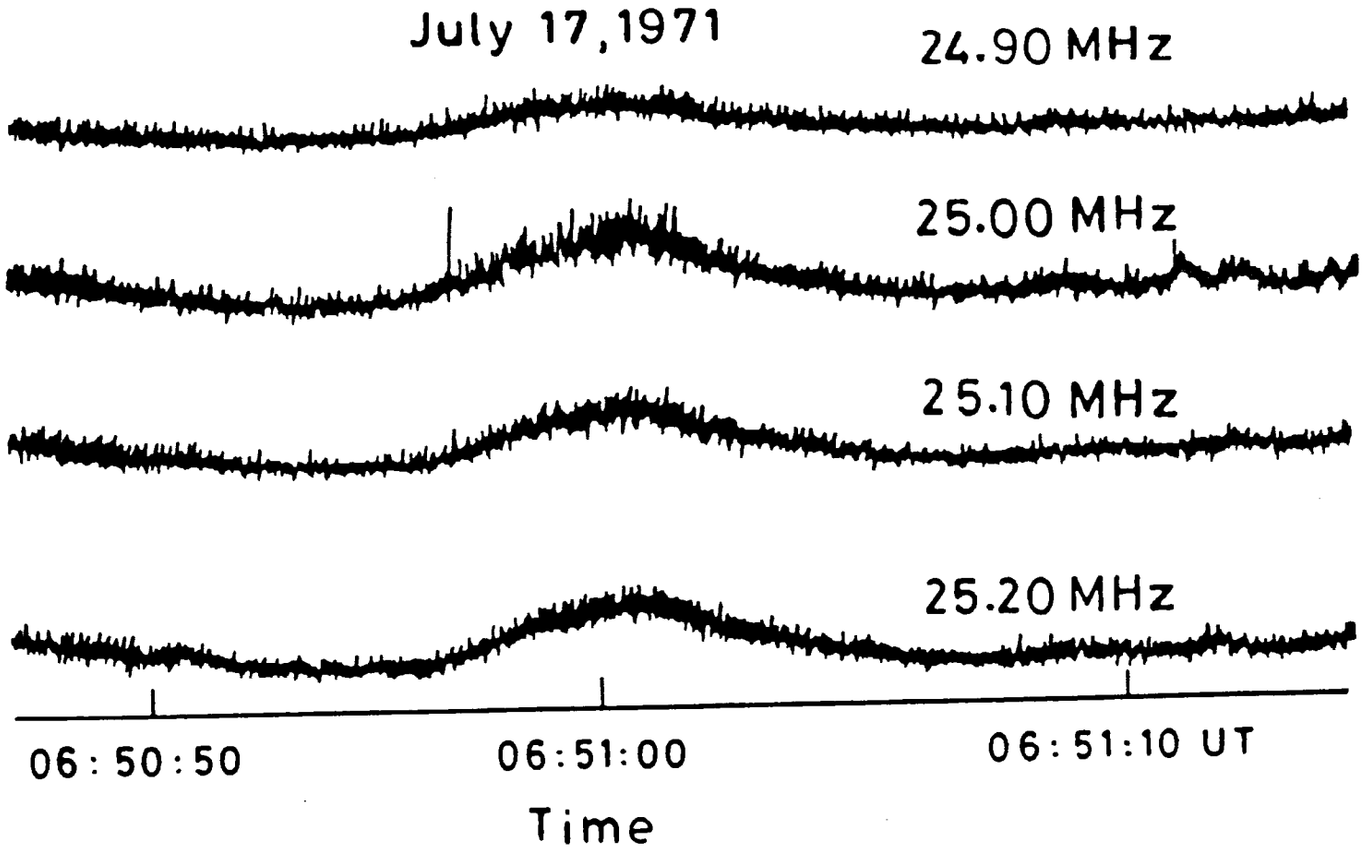

Fig.2.6.Typical example of type III bursts.

due to the damping of the plasma waves by electron-ion collisions (Kundu 1965), the temperature T_e is related to the damping constant by the relation

$$T_e = 0.65 \times 10^{-4} f^{4/3} \tau^{2/3}$$

where f is in Hz and τ is the damping constant in seconds.

The collision damping hypothesis has been questioned (Aubier & Boischot 1972) for several reasons. The collision damping hypothesis leads to a temperature which decreases too quickly as the altitude of emission increases,so that at 1 AU the temperature deduced from type III burst decay constant is much lower than the temperature obtained by insitu measurements. The correlation between the exciter duration and decay constant at a particular frequency and between the decay constant at two freqencies are difficult to explain if the decay constant is a function of temperature only. Landau damping has been suggested by Zaitsev et al (1972) and Harvey & Aubier (1973) for the decay of type III bursts. If the damping is due to electron - ion collisions then the exciter duration and decay constant are linked to different physical systems. The exciter duration is linked to the electron stream and

decay constant to the ambient plasma respectively. If the damping is due to the Landau damping then the exciter duration and decay constant are both linked to the same exciting electron stream.

According to Aubier and Boischot (1972) the observed intensity - time profile of a radio burst at time t is the convolution of the exciter function f(t) by the damping expontial function

$$I(t) = \frac{1}{\tau}\int_{-\infty}^{t} f(x)\, e^{-(t-x)/\tau}\, dx$$

where f(x) represents the exciter function and τ the decay contant.

Differentiating we get

$$\left[\frac{dI}{dt} + \frac{1}{\tau} I(t)\right] e^{t/\tau} = \frac{1}{\tau} f(t)\, e^{t/\tau}$$

therefore

$$f(t) = \tau \frac{dI(t)}{dt} + I(t)$$

f(t) is an exponential function for time larger than $D_\bullet$.

Then $I(t) = \underset{\wedge}{\text{constant}} \times e^{-t/\tau}$ for $t > D_\bullet$.

The exciter duration D_e and decay time constant τ can be measured from a plot of $\log_e(I)$ against t as shown schematically in Fig. 2.7. When the decay is purely exponential the plot is linear and reciprocal of its slope gives the decay constant. The exciter duration is from the onset of burst to the point where the exponential decay starts. The determination of D_e and τ are independent, because an error in determination of beginning or ending of the exciter has no effect on the determination of the slope of the profile which gives τ

2.2.4 D_e and τ for isolated and associated type III bursts

The exciter duration is measured from a semilog plot of the time profile. The uncertainty in locating the beginning of the bursts and the point where the profile becomes exponential is $\pm$ 0.5 s. The average exciter duration in the case of the isolated type III bursts is 4.8 s

The decay constant is the reciprocal of the linear part of the semilog time profile plot. The error in this measurement is determined by the uncertainty of the time at which the time profile of

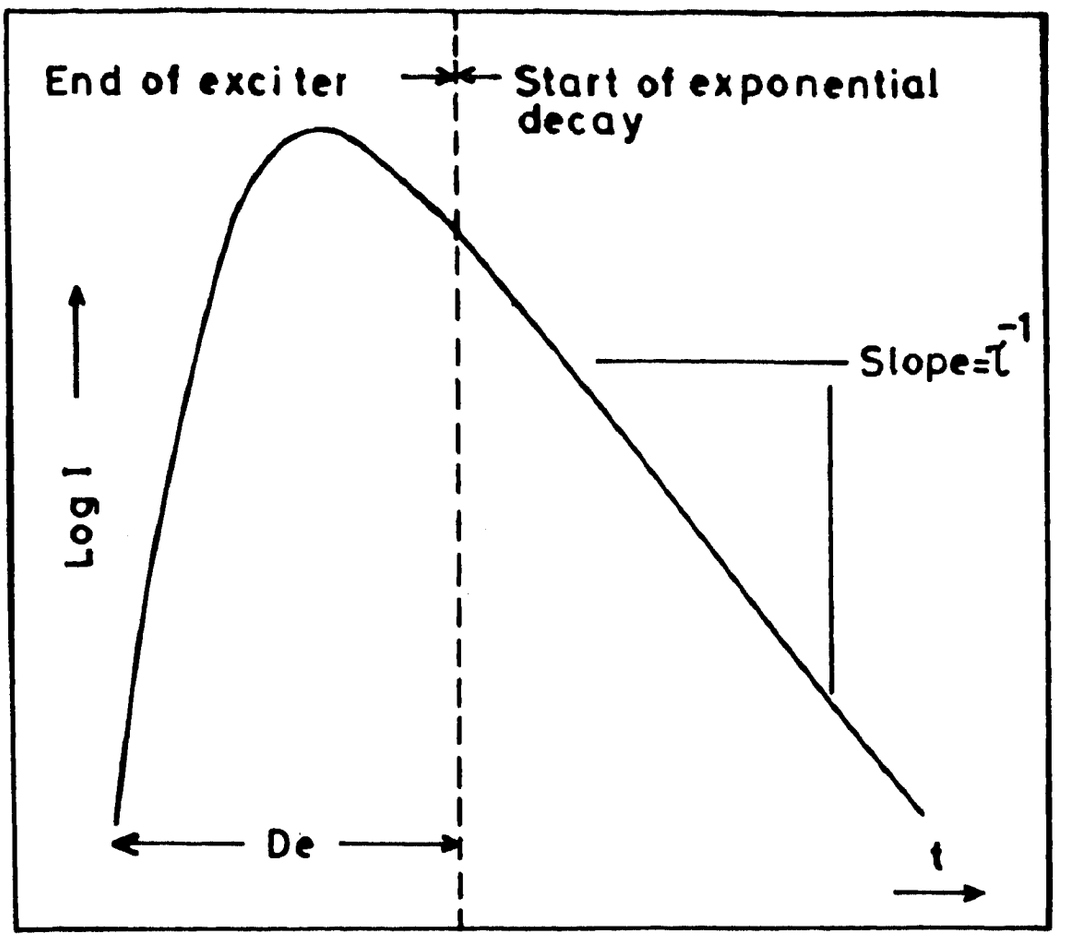

Fig. 2.7. Schematic semi - log plot of a burst profile showing the measurement of the parameters D_e and τ .

bursts becomes exponential and the nonconstancy of the detector laws at different signal levels. The maximum error in the measurement of decay constant is $\pm$ 0.3 s in the case of the isolated type III bursts.

In the case of associated type III bursts the error in the measurement of $D_\bullet$ and τ are the same as in the case of isolated type III bursts. The average value of $D_\bullet$ is 6.5 s and τ is 1.9 s.

The measured value of $D_\bullet$ and τ show variation from burst to burst. Fig. 2.8a shows the scatter diagram of $D_\bullet$ and τ in the case of isolated type III bursts. The relationship between $D_\bullet$ and τ is determined by a least square straight line fit.The two parameters are positively correlated with a linear correlation coefficient of 0.7. Fig. 2.8b shows the scatter diagram of $D_\bullet$ and τ for associated type III bursts. The linear correlation coefficient is 0.2 only in this case.

2.2.5 Discussion

The current ideas on the generation of the type III bursts are based on the plasma hypothesis (Wild 1950) which can be characterised by the

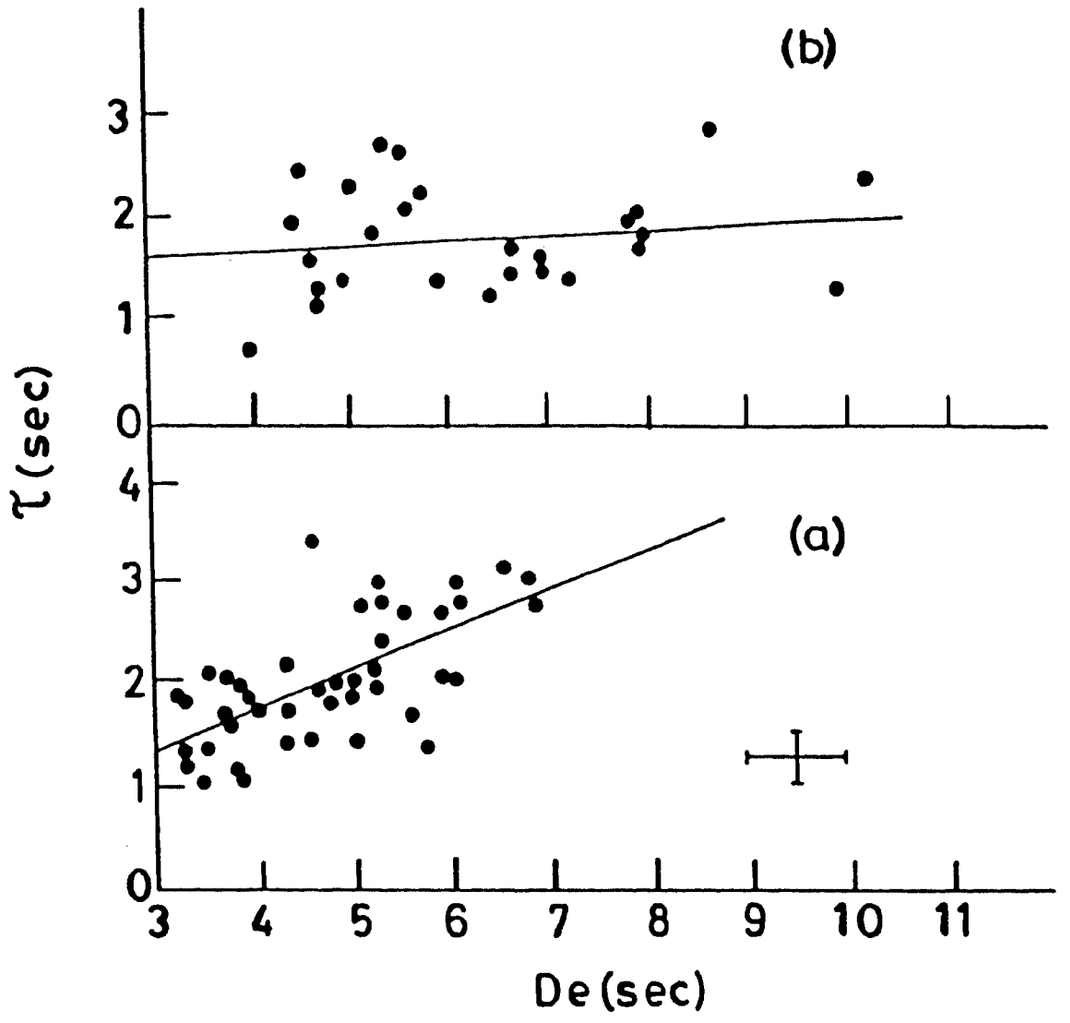

Fig. 2.8.(a) Scatter diagram of D_e and τ for isolated type III solar radio bursts.(b) Scatter diagram of D_e and τ for associated type III radio bursts.

following parts.

(i) A fast moving electron beam called exciter causes plasma waves at the local plasma frequency w_p.

(ii) A certain part of the resulting plasma waves is transformed into electromagnetic waves via scattering at w_p and $2w_p$. The fundamental radiation at w_p is produced by the scattering of the plasma waves on the density fluctuations. The harmonic radiation at $2w_p$ is produced by the coalscence of two waves at w_p.

(iii) So far as propagation is possible the electromagnetic waves can reach the observer.

The type IIIb radio bursts are probably produced when the strength of the electric field of the electrostatic beam - plasma instability exceeds the threshold for the excitation of the side band instability. The duration of the exciter is the time taken by the electron stream to cross any given plasma level in the corona. Aubier and Boischot (1972) have already pointed out that the observed correlation between D_e and is difficult to explain on the basis of collisional damping of plasma waves. Many authors (Zaitsev et al ., 1972 ;Takakura et al 1972) believe that the main damping mechanism is probably non

collisional.The damping of type III burst can be due to the absorption of energy by the particles with velocity smaller than the phase velocity of the wave during induced scattering.

The observed correlation between the exciter duration and decay constant for isolated type III radio bursts and lack of it for type III bursts preceded by type IIIb bursts is believed to result due to the different nature of the exciter in the two cases. The isolated type III bursts have an exciter which is more or less uniform density and speed. The exciter duration and decay constant are both depend on the exciter parameters and hence there is correlation between the two. The asssociated type III bursts have an exciter which is highly nonuniform nature. The decay constant being mainly the function of the front end and the exciter duration being chiefly due to the large rear end, the two are weakly correlated for associated type III bursts. The nonuniformity in the velocity of the electron beam responsible for the excitation of type III solar radio bursts has already been invoked to explain the stabilization of the electron beam (Zaitsev et al 1972). In addition, the density profile could also be nonuniform as pointed out by Svestka (1976).

CHAPTER 3

THE GAURIBIDANUR RADIO TELESCOPE AND FILTER BANK RECEIVER

3.1 Introduction

The Gauribidanur radio telescope is a meridian transit instrument operating at a frequency of 34.5 MHz. This telescope is located at Gauribidanur (Latitude $13^{\circ}\,36'\,12''$ North & Longitude $77^{\circ}\,26'\,07''$ East). This telescope though designed primarily for the study of galatic and extragalatic radio sources was also used for mapping the radio sun and spectral observations of solar radio bursts. A brief description of this telescope is given below.

3.2 Antenna system

The telescope is in the form of letter "T".The dimension of the telescope are 1.38Km along the E - W direction and 0.450 Km along the N - S direction as shown in Fig. 3.1. The short arm of the telescope extending southward from the center of the E - W array here after will be referred to as the South

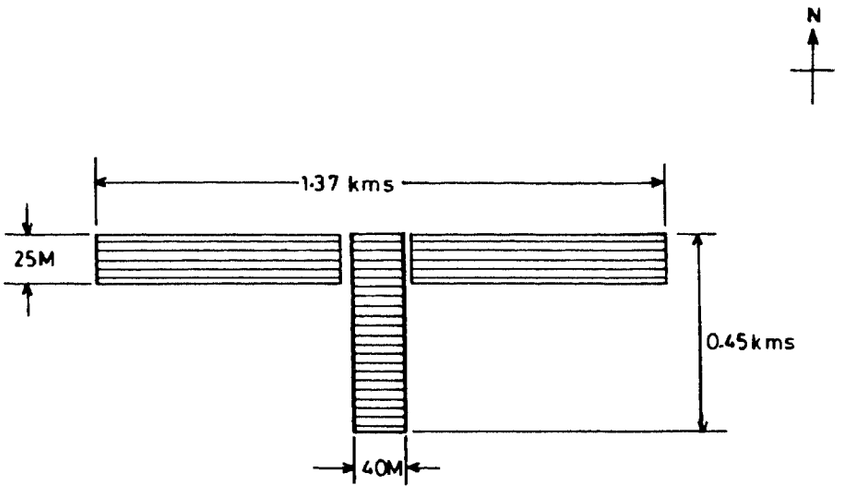

1.E-W Array 4 Rows of 160 elements each
2.South Array 90 Rows of 4 elements each
3.Dipole spacing 8.6 M (E-W) direction
5.0 M (N-S) direction

Fig. 3.1. The Gauribidanur radio telescope operating at 34.5 MHz

array. The telescope consists of one thousand dipoles, 640 in the EW arm and 360 in the South arm. The south array used for the study of solar radio bursts is described here. A complete description of the Gauribidanur radio telescope is given by Sastry (1989).

3.2.1 South array

The physical dimensions of the South array are 40 mts in the E - W direction and 450 mts in the N - S direction. This array consists of 360 dipole elements. The dipole elements are made of 16 gauge copper wires and its measured impedance is 600 ohms. The bandwidth of the dipole is 10 MHz centered around 32 MHz and they accept E - W polarisation. This dipole has a collecting area of $0.25\lambda^2$ where λ is the wavelength. For 34.5 MHz which is the operating frequency of the Gauribidanur radio telescope the collecting area of each dipole is $20m^2$. Fig. 3.2 shows the basic dipole element. The dipoles are mounted on wooden poles. The ground plane consists of galvanised iron wires placed 1.5 mts beneath the dipoles. These wires run in the E - W direction (parallel to the dipoles) and are spaced at intervals of 50cms. The ground plane extends 5 mts beyond the array in all directions. This reflecting screen covers

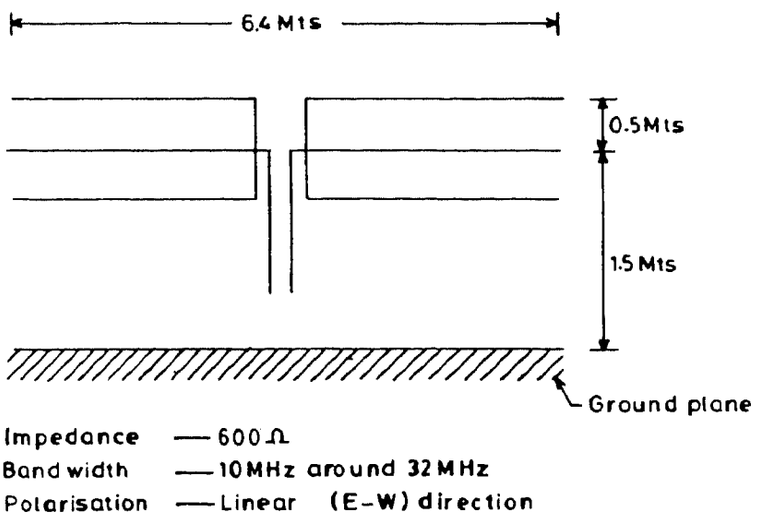

Fig. 3.2. Basic element of the Gauribidanur radio telescope.

a total area of 20,000 m^2

The 360 elements in the south array are arranged in the following way. 4 elements are arranged along the E - W direction with an interelement spacing of 8.4 mts. These four elements are combined in a branched feeder system using 600 ohms open wire transmission lines and 1:2 impedance tranformers as shown in Fig. 3.3. The combined balanced output is converted into an unbalanced output using 300 to 50 ohms balun. The combined output of the 4 elements is terminated in a tuned FET amplifier. The main characteristics of this amplifier are 8 dB gain, 600° K noise temperature, 2 MHz bandwidth and 50 ohms input output impedance. The third order intermodulation product for this amplifier occurs only at input levels greater than - 10 dbm. Since the noise temperature of this FET amplifier is 600° K, the system noise is completely dominated by the sky background temperature which is around $10,000^{\circ}$ K at 34.5 MHz. There are 90 such rows in the south array with a spacing of 5 mts between the rows. The 90 rows are grouped into 6 groups : 5 groups each containing 16 rows and 1 group containing 10 rows. The output from the rows in a group are combined in a branched feeder system using phase shifters $\phi_1, \phi_2, \phi_3, \phi_4$ and power combiners

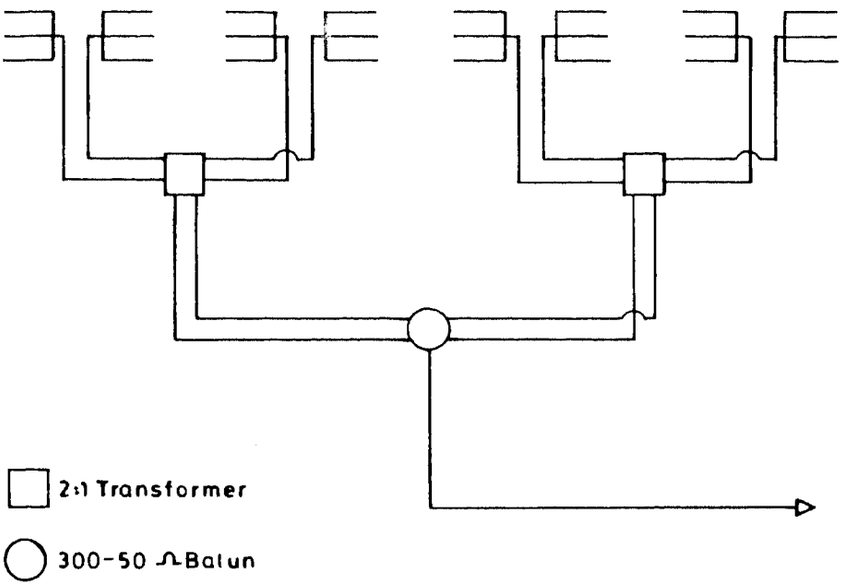

Fig. 3.3. Connection of 4 elements in the EW direction using 600 ohms transmission line, impedance transformer and baluns.

as shown in Fig. 3.4. The position of the beam can be changed without changing the mechanical orientation of the array using these phase shifters. If the phase of the signal from all the elements are same then the relative phase difference between the adjacent elements is zero and the position of the main beam will be broadside (normal) to the plane of the array. The main beam will point in direction other than the broadside if the relative phase difference between the elements is other than zero. If d is the spacing between the elements then the direction of the main beam is at an angle ϕ from the zenith when the phase difference between 2 elements is equal to $2\pi d\sin(\phi)/\lambda$. The phase of the signal at each element in an array with n elements of equal spacing is therefore $n \times 2\pi d\sin(\phi)/\lambda$, where n = 0,1,2,. . . n. Steering the reponse of the array is thus accomplished by introducing a linear phase gradient across the array.

3.2.2 Phase shifters & group connections

The phase shifter ϕ_1 consists of 3 cascaded sections which can introduce phase shifts of 45, 90, and 180 degrees. These phases correspond to different lengths of RF cable. The binary quantisation of cable length makes it convenient to apply digital

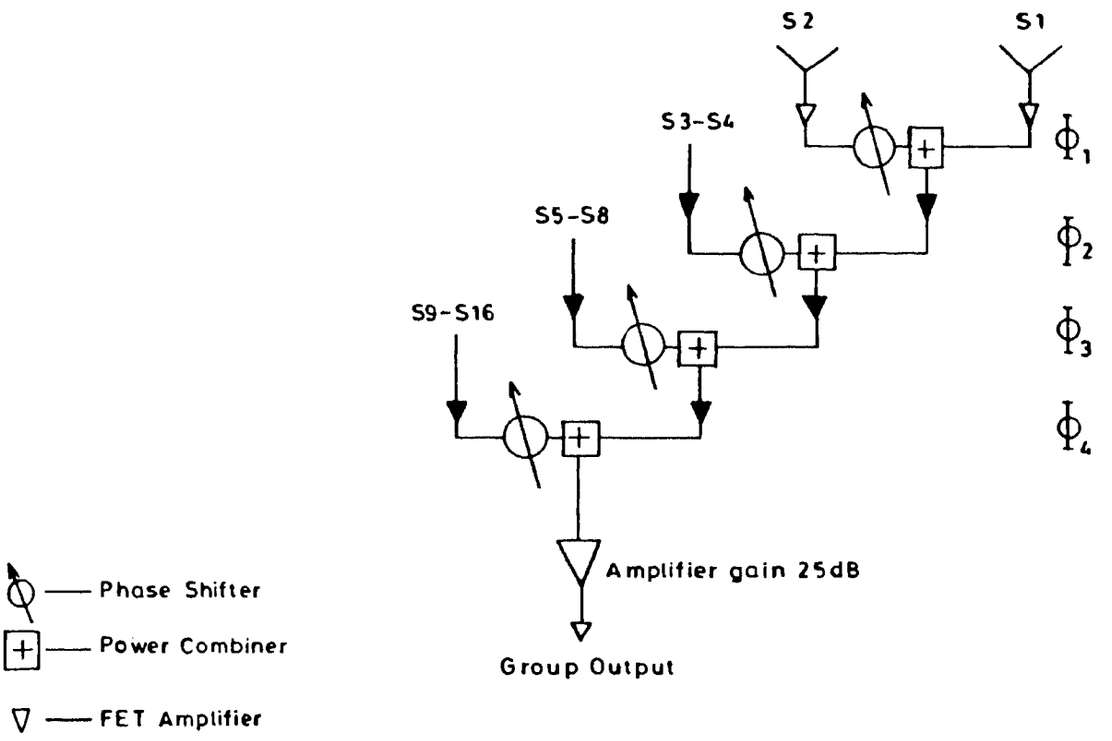

Fig. 3.4. Connection of 16 rows in a group using phase shifters and power combiners.

techniques for activating these phase shifters. Digital control system for these phase shifters are described by Desphande (1987). The appropriate phase can be switched in or out using diodes and matching networks. Fig. 3.5a shows one section of the phase shifter ϕ_1. By control voltages (- V /+ V) phase of either 0 degree or 45 degrees can be set. The other sections of the phase shifter are similar except for the phase cables. Any phase from 0 degree to 360 degrees can be set in step of 45 degrees in the phase shifter ϕ_1. In the zero phase state the input output phase difference is not zero but some "residual" phase. This phase shifter module also has an insertion loss. The values of residual phase and insertion loss are 15 degrees and 0.5 dB respectively. The signal from row 1 which is not phase shifted passes through 0.5 dB attenuator and a cable of length correponding to 15 degrees before being added to the signal from row 2 in a power combiner as shown in Fig. 3.5b. When the phase gradient is not set the signal from row 1 and 2 have the same attenuation and phase at their combined output.

There are 4 stages of phase shifter in a group ϕ_1, ϕ_2, ϕ_3, and ϕ_4. The phase shifter ϕ_2, ϕ_3 and ϕ_4 are similar to ϕ_1 except that

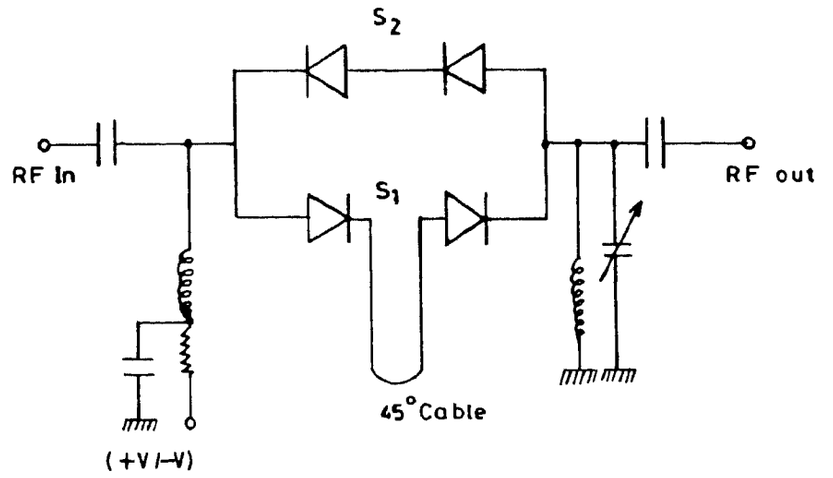

Fig. 3.5a. Phase shifter unit. Only 45 degrees section is shown.

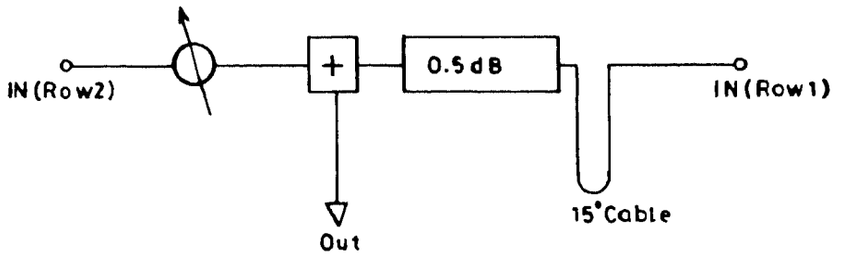

Fig. 3.5b. Connection of 2 rows using phase shifter. Compensating cable and attenuator are introduced in the path from row 1 so that for zero phase gradient signal from row 1 and 2 have the same phase and amplitude at their combined output.

they consist of 4 sections corresponding to 22.5, 45, 90, and 180 degrees. The insertion loss and input output offset phase difference of ϕ_2 are introduced in the corresponding path which is not phase shifted. Similarly in the path which is not phase shifted in the case of ϕ_3 and ϕ_4 the amplitude and phase are compensated. The output of a group is amplified by a tuned amplifier having a gain of 25 dB and bandwidth of 2 MHz. The connections within a group are same for groups 1 to 5. In the sixth group the ten rows are combined as shown in the Fig. 3.6. The combined output of rows 89 - 90 is added to the combined output of rows 81 - 88 after being suitably delayed and amplitude compensated.

The signals from the 6 groups are combined again in a branched feeder system using phase shifters ϕ_5, ϕ_6 and ϕ_7 as shown in the Fig. 3.7. These phase shifters are similar to ϕ_2. The combined output of the six groups passes through an amplifier of 35 dB gain and is carried to the central building by 500 mts of buried RG 8U cable.

The discrete values of phase shift resulting from the use of quantized phase shifter introduces an error in the phase gradient across the

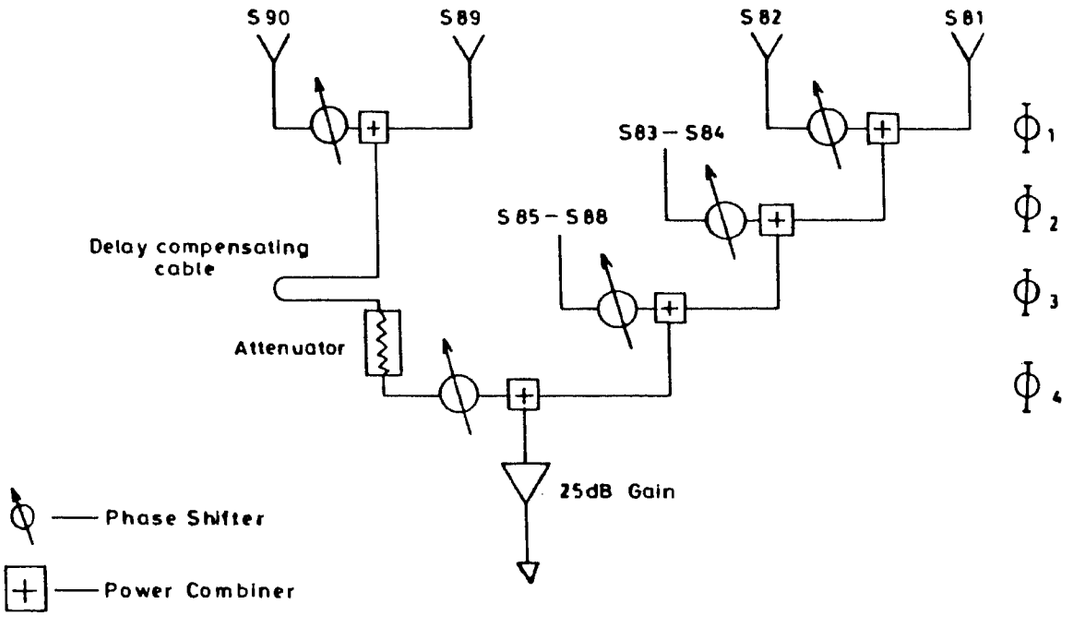

Fig. 3.6. Connection of 10 elements in the 6th group. The combined signal from row 89 and 90 are suitably delayed and attenuated.

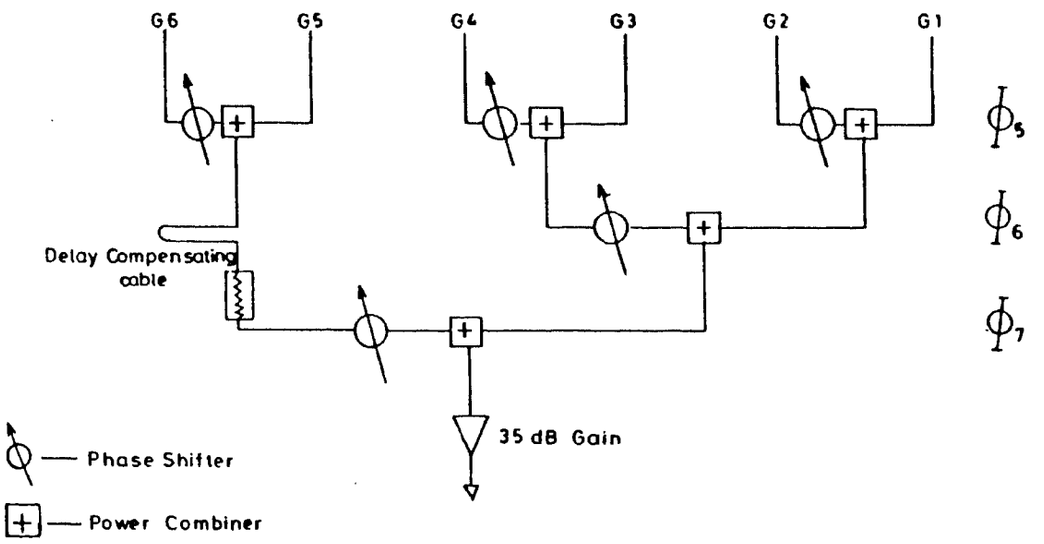

Fig. 3.7. Connection of 6 groups.

array. This phase quantisation can cause a shift in the pointing of the main beam. The maximum phase error of $\pm$ 22.5 degrees would result in an equivalent rms beam pointing error of 3 arc min, which is very small compared to beam width (66 arc min) in the N - S direction. The use of phase shifters instead of delay lines restrict the maximum usable bandwidth to 1 MHz. However this is not a serious disadvantage since terrestrial interference at these wavelengths limit the maximum usable bandwidth to less than 1 MHz.

3.2.3 Parameters of the south array

The South array is tilted 30 arc min with respect to the horizontal due to the terrain. The instrumental zenith is therefore 14.1 degrees, instead of the latitude of the place 13.6 degrees. This array produces a fan beam of 14.5 degrees in Right Ascension and 1.1 degrees in Declination. A source can be observed for an hour using the South array which is essential in the case of sporadic radio emission from sources such as the Sun, Jupiter etc. The effective collecting area of the array is 7200 m^2 because there are 360 dipoles and collecting area of each dipole is 20 m^2. The array can be steered to $\pm$ 60 degrees of the zenith (-45° to $+75^{\circ}$) in step of

12 arc min.

3.2.4 Sensitivity of the south array

The sensitivity is a measure of the weakest source of radio emission that can be detected and for a point source it is given by (Kraus 1966)

$$S_{min} = \frac{2k K_s T_{sys}}{A_e\sqrt{Btn}}$$

where k = Boltzman's contant (1.38×10^{-23}) (joule/kelvin)

A_e = effective collecting area m^2

K_s = receiver constant = 1 for total power receiver

T_{sys} = system temperature (deg K)

B = predetection bandwidth (cps)

t = post detection time constant (sec)

n = no of independent observations

In the case of the solar radio bursts the system temperature T_{sys} is decided by the temperature of the corona which is million degrees. For 15 KHz bandwidth and 10 msec time constant

used for the study of fine structures in the solar radio bursts the sensitivity S_{min} is 3 Solar flux unit (SFU). (1SFU= 10^{-22} watts/m^2/Hz). Therefore the system can detect weak solar bursts.

3.3 Solar radio spectroscopy

Spectrographs are used for two main purposes in radio astronomy. The first is for the study of atomic and molecular line profiles. The second is for the study of sporadic radio emission from the Sun,Jupiter,Saturn etc. In the case of solar bursts the spectrographs must record the dynamic spectrum, the variation of intensity of bursts as a function of time and frequency. There are many ways in which this can be achieved.

The swept frequency spectrograph (Wild & Mc Cready 1950) used for obtaining dynamic spectrum is a superhetrodyne receiver whose pass band is swept continuously over a frequency range which is large compared to the IF bandwidth. A dynamic spectrum is obtained by repeatedly sweeping the pass band of the receiver through the frequency of interest. The data is displayed on a cathode - ray tube and recorded as a series of intensity modulated traces which register

intensity as brightening in the frequency - time plane. Consider the case of a swept frequency spectrograph with IF bandwidth Δf and frequency range f. If Tr is the time in which f is swept then the effective time resolution of the system is given by

$$Tr = (f / \Delta f) (1 / \Delta f)$$

If f is 30 MHz and Δf is 30 KHz then the effective time resolution is larger by a factor of $f / \Delta f$. ie 1000 compared to the time resolution ($1/\Delta f$) in the case where there is no sweeping. Also the signal in a particular bandwidth is sampled only for a fraction $\Delta f/f$ of the total time and therefore the signal to noise ratio is poor compared to system where the signal is sampled continuously.

3.3.1 Filter bank spectrograph

For observing weak solar radio bursts the low sensitivity of a swept frequency spectrograph is a serious limitation. One way to achieve high sensitivity is to use a multichannel receiver (Hays Penfield 1976). Such a receiver uses a superhetrodyne configuration in which the IF band is divided into N number of separate narrow band channels generally spaced in frequency by an amount equal to their bandwidth. The sensitivity of such a

system is $\sqrt{N}$ times greater than that of a swept frequency spectrograph with same frequency range and resolution.

Fig. 3.8 shows the diagram of the 8 channel filter bank receiver used for solar burst observations. The front end amplifier is a tuned amplifier at 34.5 MHz having a bandwidth of 2 MHz and 25 dB gain. The amplified RF signal at 34.5 MHz is mixed with a Crystal oscillator at 85.5 MHz , producing an IF signal at 51.0 MHz. The IF signal passes through a band pass filter of bandwidth 2 MHz before being amplified by an amplifier of 13 dB gain and split up into 8 channels. In the receiver where the splitted IF signal passes through filters at different center frequencies the non uniformity in the bandwidth and filter response shape from channel to channel exists. This nonuniformity distorts the spectral line data. The susceptibility of the receiver to this nonuniformity increases as the number of channels is increased. One way to overcome this is to use crystal filters tuned to the same frequency and Local oscillators of different frequencies to obtain the required channel center frequency distribution. Such a technique is used here. Each one of the 51 MHz IF signal which is split up is mixed

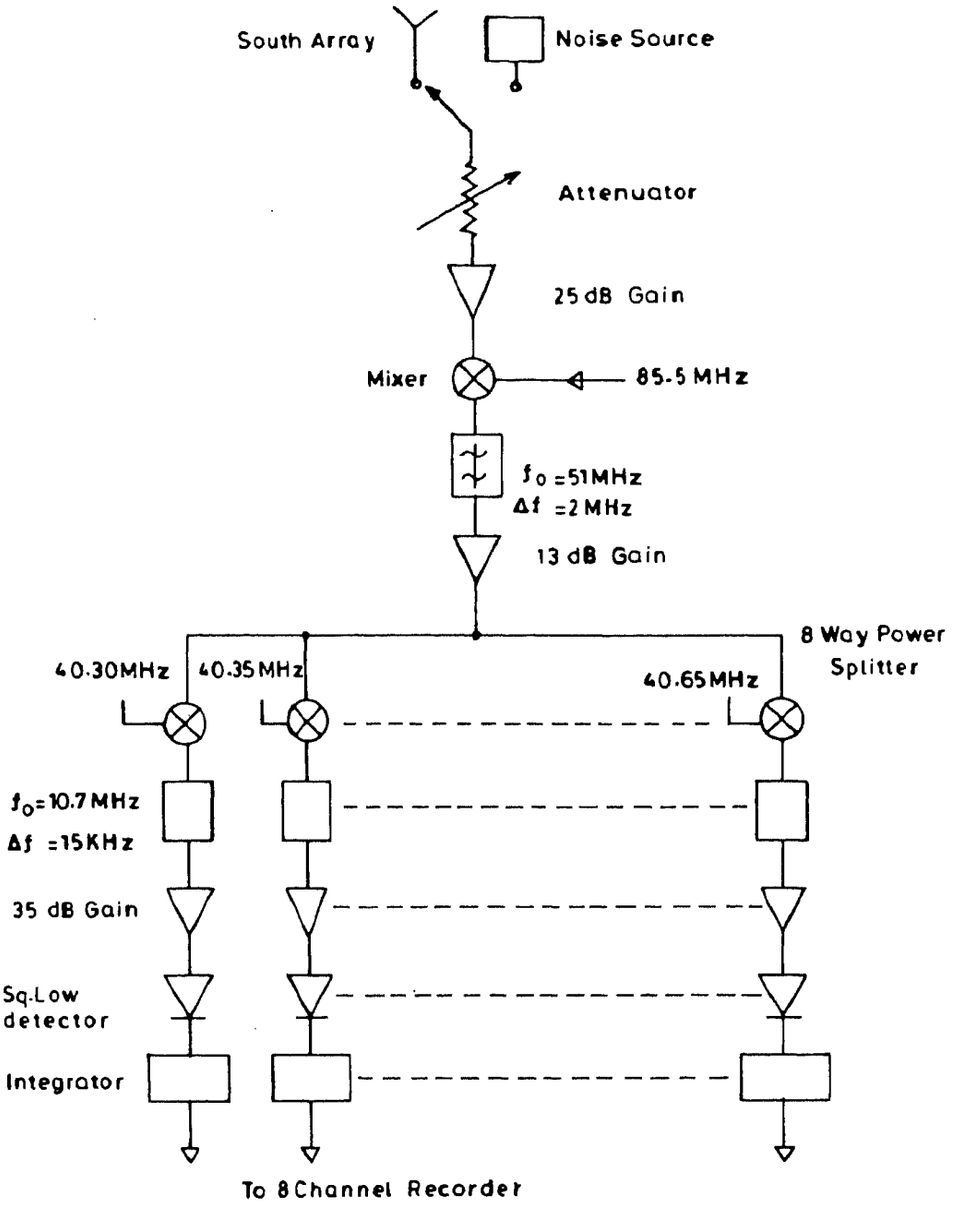

Fig. 3.8. Eight channel filterbank receiver system.

with a crystal oscillator to produce a second IF output at 10.7 MHz and is passed through a crystal filter. These crystal filters have a bandwidth of 15 KHz centered around 10.7 MHz. The crystal oscillators range in frequency from 40.3 MHz to 40.65 MHz at an interval of 50 KHz, corresponding to RF from 34.5 MHz to 34.15 MHz at 50 KHz interval. The filtered output is amplified by an amplifier of 35 dB gain before being detected and integrated. A square law detector is used here which gives an output $\propto$ input ($V_0 \propto V_{in}^2$). The detector output is fed to a low pass filter to reduce fluctuations. The effect of a low pass filter is obtained by a time constant RC integration circuit so that the effective bandwidth of the low pass filter is much smaller than the predetection bandwidth. The time constant used for solar bursts observations is 10 milliseconds. The integrated output is recorded in an eight channel oscillographic recorder. A variable attenuator is used to attenuate the RF signal for the required level at the square law detector. The dynamic range of the system is 15 dB. The receiver is calibrated before and after the observations by injecting noise at the front end amplifier. In the next chapter fine structures observed with the south array and the eight channel filter bank spectrograph are described.

CHAPTER 4

FINE STRUCTURES IN THE RADIO EMISSION OF THE SUN

4.1 Introduction

In this chapter fine structures in the radio emission of the sun observed with the South array of the Gauribidanur radio telescope and an eight channel filter bank spectrograph are described. The fine structures described here are (i) pulsating bursts,(ii) spike bursts, and (iii) diffuse echo bursts.

4.2 Pulsating Bursts

For over two decades radio astronomers have been observing pulsating structures in the solar corona. Pulsations include a wide range of phenomena from strictly sinusoidal oscillations upto rather quasi periodic patterns. Pulsations of the solar radio emission were first detected at decimeter wavelengths. Rosenberg (1970) observed weak broadband fluctuations at 220 MHz superimposed on a background emission. These fluctuations had a period of 1 sec with a bandwidth of 80 MHz. At 150 MHz, McLean et al(1971)

observed pulsating structures which modulated the intensity . These modulations persisted approximately for 1 minute with a period of typically 1 sec. Gotwals (1972) reported pulsating solar emission having a periodicity of 0.5 sec and a bandwidth > 300 MHz, at decimeter wavelengths. Most of these observations were made at wavelengths less than 2 m . Also these pulsations occured during type IV events. These were broad band and were seen at all phases i.e.growth,plateau and decay of that burst.Wild (1973) observed quasi-periodic chains of type III burst with a period in the range of 0.5 sec to 5 sec. Santin (1971) also reported observations of quasioscillatory decay in the case of type III bursts.

At decameter wavelengths Bohm and Kruger (1973) observed pulsations with a period of 5 minutes, pulsating on a time scale of few seconds. Achong (1974) observed pulsations of enhanced continuum in the frequency range of 24 - 26 MHz. These pulsations showed a mean period of 4 s and a sharp low frequency cut off at 24 MHz. Sastry (1969) had reported observations on quasi - periodic variation of enhanced background emission during intense noise storms. Here a different type of pulsation pattern in the intensity time profile of short duration

radio burst at decameter wavelengths is described (Sastry et al 1981).The main characteristics of these pulsations are that these pulsations occur predominantly in the saturation phase of the burst. A tentative physical model to explain the observed characteristics is proposed.

4.2.1 Observations

The sun is observed each day for about an hour centered at local noon during storm period. Since the sensitivity of the system is very high a large number of new and peculiar bursts hither to unclassified were detected. On several occasions we recorded a burst in which there is a smooth growth of intensity to a maximum in a short time and during the maximum phase of intensity the burst exhibits quasi periodic pulsation, and decay with the same smoothness.The basic distinct feature of these profiles is the presence of oscillations or pulsations only during the saturation phase of the radio emission. Typical examples are shown in Fig. 4.1 , in which one can see a rise in intensity starting around $06^h\ 51^m\ 58^s$ UT and then growing into oscillation with an approximate period of 2 seconds. After these oscillations the intensity decays into pre burst level. The total

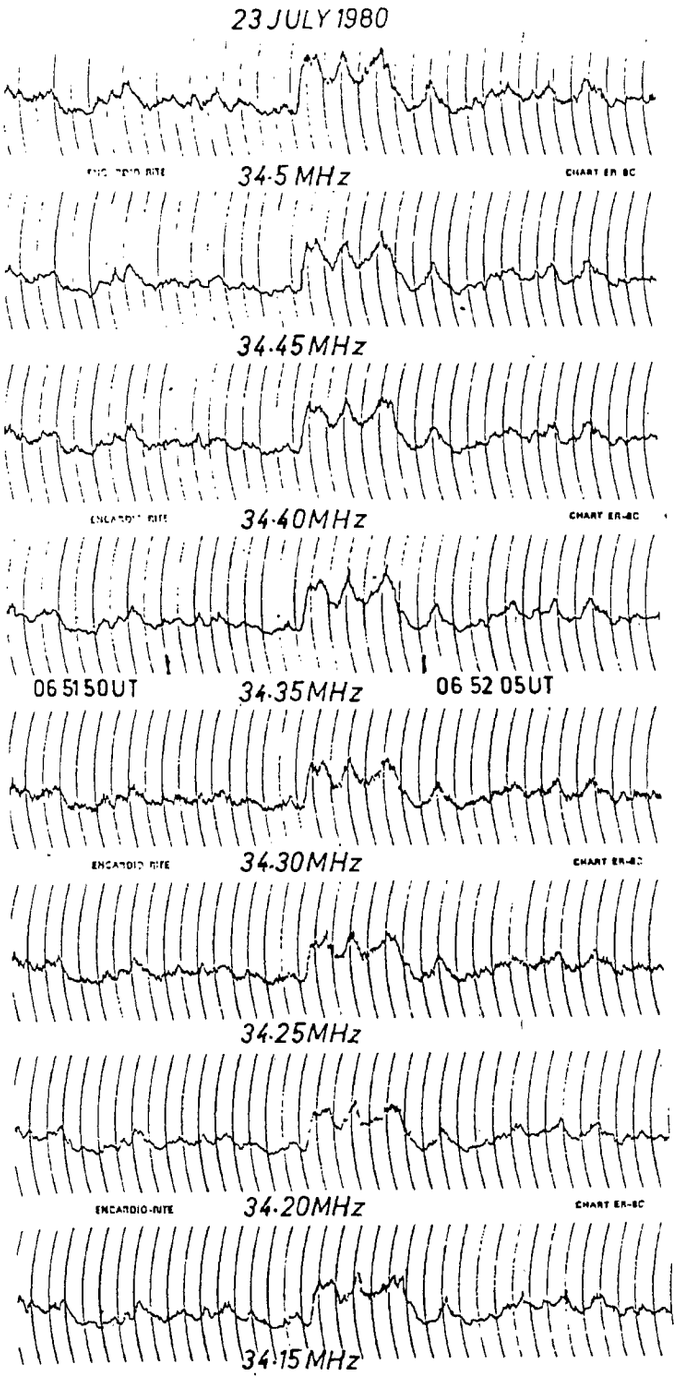

Fig. 4.1. Example of the time profile of the pulsating radio burst.

duration of the burst is about 6 seconds. These pulsating events were observed mostly during the period April - July 1980. These bursts occured during periods of intense noise storm where the base level of emission was very high. Twenty two events observed during the above period have been analysed.

4.2.2 Time structure of pulsating bursts

Several characteristics of these bursts have been derived from the observed time and frequency profiles. The various parameters of the burst measured are shown in Fig. 4.2. The distribution of the pulse repetition rate is shown in Fig. 4.3a. The most common value of the pulse repetition rate is between 0.2 to 0.5 s . Fig. 4.3b shows the distribution of the total durations of these burst. The total duration ranges from 5 to 15 seconds. The average individual pulse profile is found to be symmetric with an equal rise and decay time of 0.9 seconds as shown in Fig. 4.3c.

4.2.3 Intensity characteristics

The modulation index m (Tapping 1978) is defined as

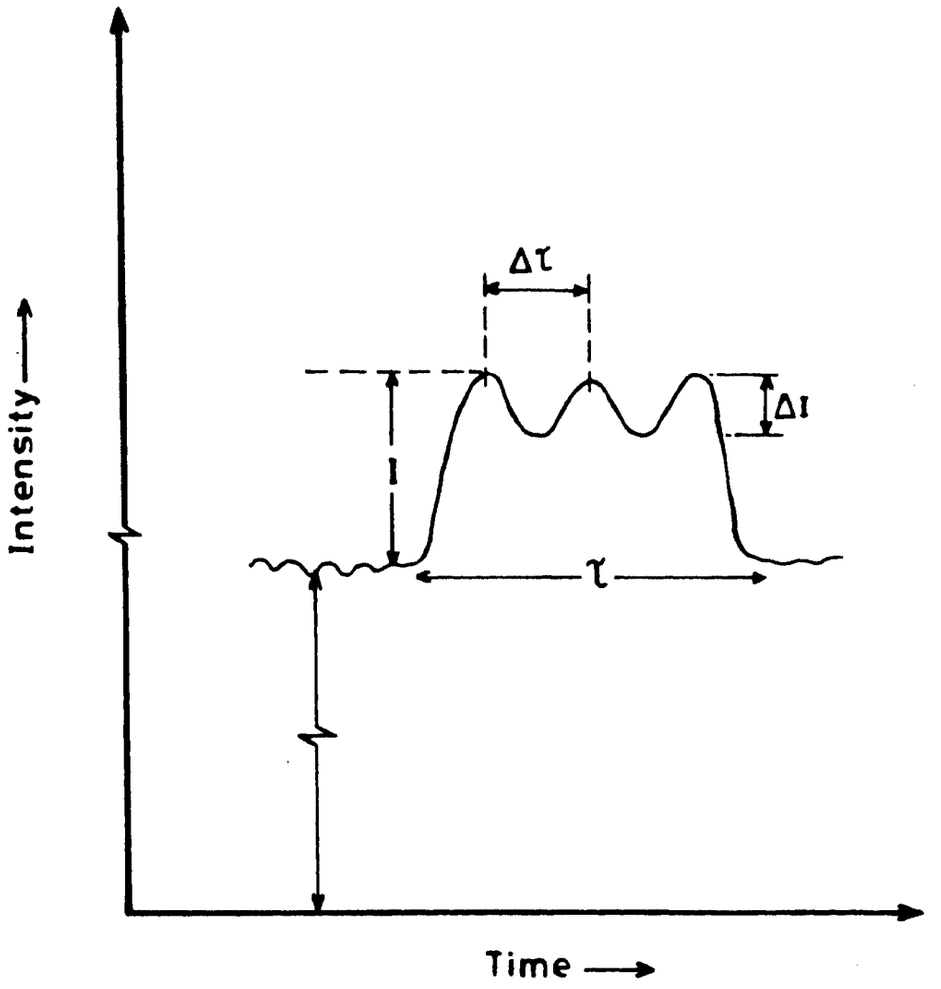

Fig. 4.2. Parameters measured on the time profile of pulsating bursts.

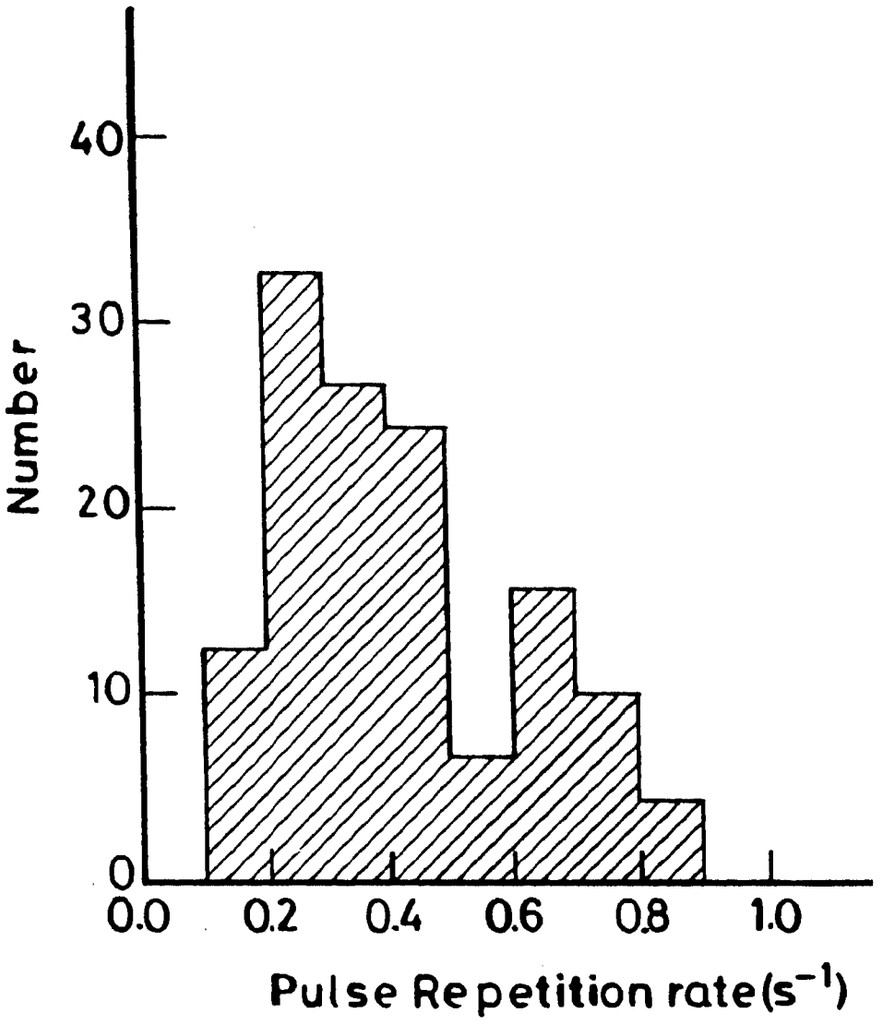

Fig. 4.3a. Distribution of pulse repetition rate.

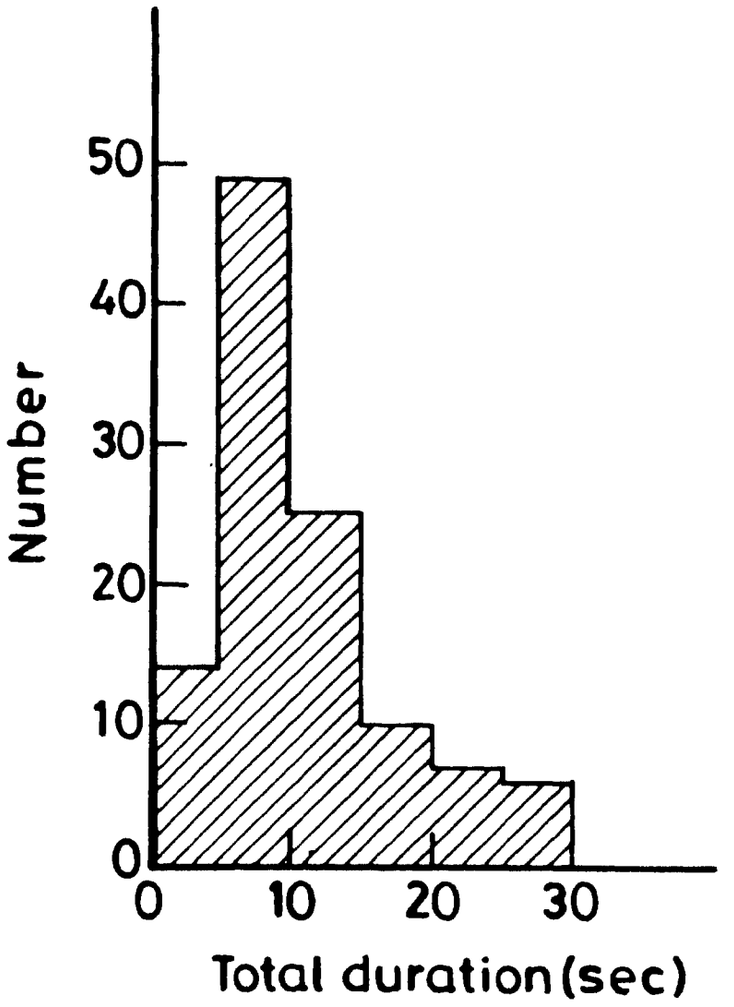

Fig. 4.3b. Distribution of the total duration τ of pulsating bursts.

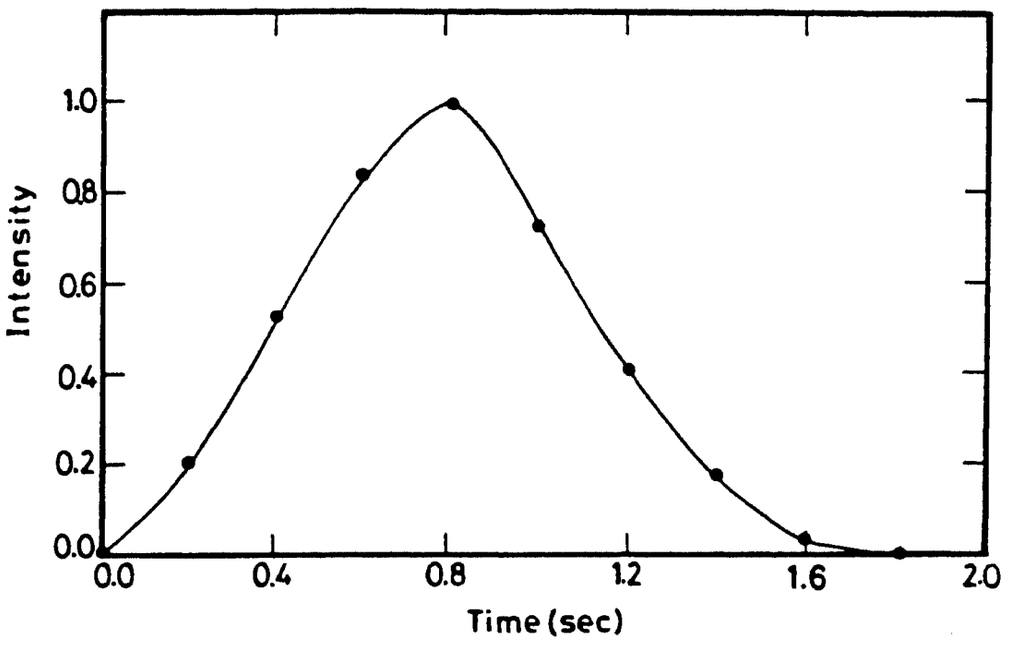

Fig. 4.3c. Average time profile of pulsating bursts.

$$m = (I_{max} - I_{min}) / (I_{max} + I_{min})$$

where I_{max} is the maximum intensity of the pulsating burst, and I_{min} is the minimum intensity. From the Fig. 4.2 the modulation index m can be written in our case as

$$m = \frac{I}{2I - \Delta I}$$

The modulation index is calculated for each burst. From the histogram Fig. 4.4 it can be seen that the value of m lies between 0.2 and 0.4 in a majority of cases. Fig. 4.5 is a scatter plot of the average peak intensity $\langle I \rangle$ and average pulse amplitude $\langle \Delta I \rangle$. The two parameters are positively correlated and the linear correlation coefficient is + 0.7. There is no significant correlation between $\langle I \rangle$ and pulse repetition period $\langle \Delta\tau \rangle$. A similar result is obtained for correlation between the pulse amplitude $\langle \Delta I \rangle$ and pulse repetition period $\langle \Delta\tau \rangle$. No correlation is found between the modulation index m, and the pulse repetition period $\langle \Delta\tau \rangle$. The main characteristics of these bursts are

(i) The pulsations are seen only in the saturation phase of the bursts.

(ii) The pulse repetition period lies within 2 - 5 seconds.

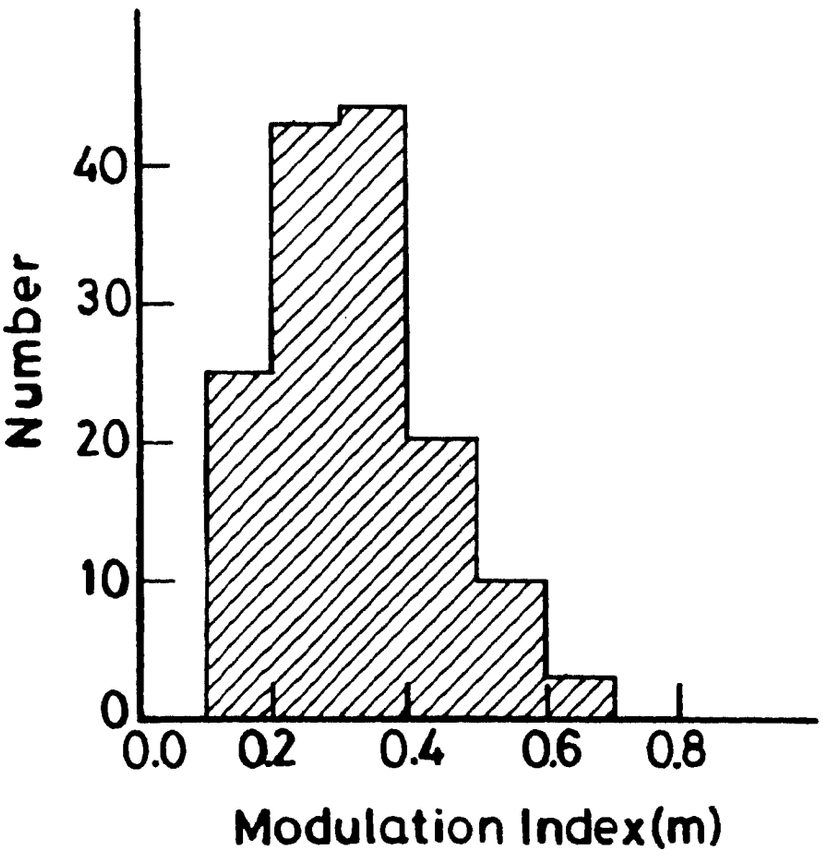

Fig. 4.4. Distribution of the modulation index m.

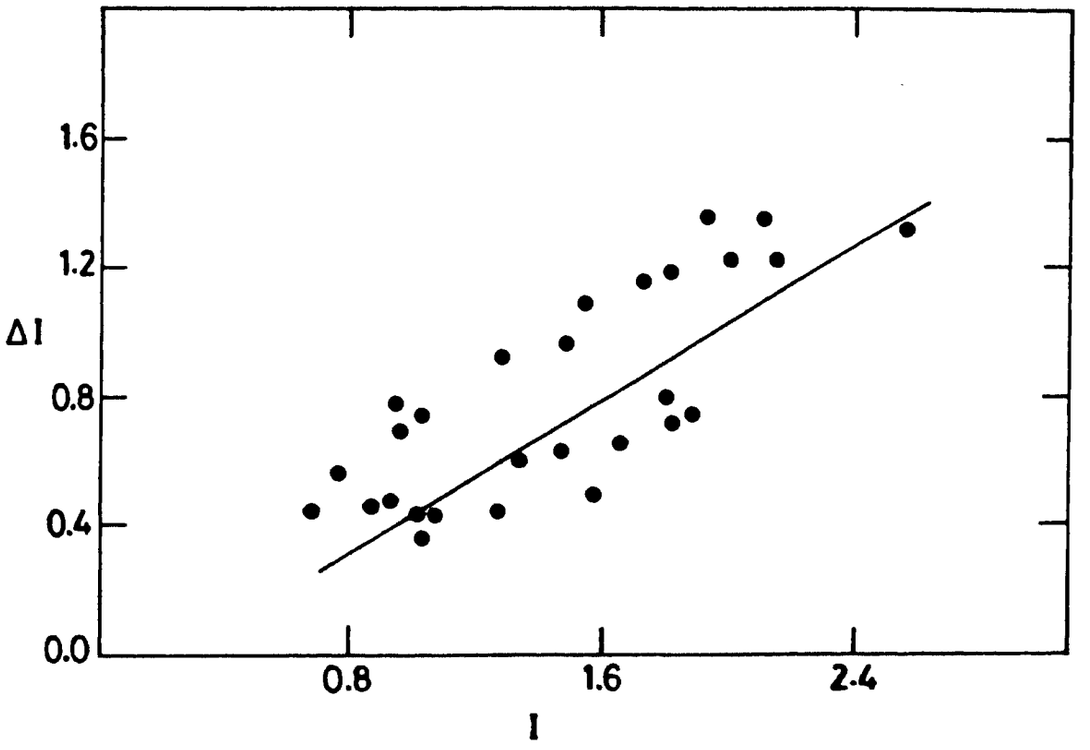

Fig. 4.5. A plot between the average intensity I and average pulse amplitude $\langle \Delta I \rangle$.

and (iii) The amplitude of the individual pulse remains approximately constant during the pulsating phase.

4.2.4 Discussion

Pulsation models can be classified according to their driver mechanism. The three basic mechanism are (i) MHD oscillations (ii) cylic self organizing system and (iii) Modulation of acceleration. There are several attempts to propose a modulation particularly of the magnetic field which then via gyrosynchrotron emission would result in a related modulation of the generated radio continuum. In this model a periodic variation of the magnetic field in a flux tube is attributed to a standing magnetohydrodynamic wave which is triggered by a shock wave. Rosenberg (1970) and McLean et al (1971) proposed a model where magnetic flux tube excutes radial oscillations. The change in the cross sectional area of the flux tube under the condition of conservation of magnetic flux causes cyclic variation of the magnetic field strength in the tube which in turn strongly modulates the synchrotron emission from trapped high energy electrons. In this model the radial oscillations are strongly damped at the boundary of the flux tube due to the radiation of acoustic waves into surrounding plasma

and this inhibits long lived pulsations. Tapping (1983) proposed torsional oscillations instead of radial oscillations in the flux tubes. The synchrotron emission in the flux tube is modulated by the changing orientation of the magnetic field lines with respect to the observer. This model requires high order of torsional harmonic numbers to explain the observed pulse period of 1 s. The derived source size from the pulse period size relation ($\tau \simeq 2.6(a/v_a)$ where a is the source size, v_a is the Alfven velocity and τ is the pulse period) didnot agree with interferometric measurements of pulsating source sizes (Pick & Trottet 1978; Trottet et al 1979). Also the asymmetric pulse shape and narrow bandwidth led to abandon models with synchrotron radiation as emission process and invoke models with plasma emission modulated by MHD waves. Zaitsev (1971) presented a model in which wave - wave interaction in the resonant and nonresonant region driven by two stream instability caused pulsations. This model suggests the pulse period and intensity to be rapidly variable. Aschwanden & Benz (1988) proposed loss cone driven electron cyclotron maser system to explain the pulsating phenomena. None of these models explain the pulsations seen in the saturation phase of the bursts.

A qualitative physical model where the oscillation can be set only during the saturation phase of the burst is presented since it is a new feature of the bursts seen by us. The basic system is a electron beam plasma system. Such a system can support positive as well negative energy waves. The coupling of positive and negative energy waves gives rise to an explosive instability, where the amplitude can become infinite in a finite interval of time, although due to various nonlinear effects, the growth of the amplitude will be arrested. The intial phase of the growing wave is due to the explosive instability,the excitation of which is a threshold effect. Since the pulsating bursts occur when the background level is high, the condition of the explosive interaction of waves is satisfied. The time of expansion is a function of intial amplitude of the interacting waves. The saturation of the explosive instability is due to the non linear complex amplitude dependent frequency shift caused by three wave coupling, two positive energy waves and one negative energy wave. The non linear frequency shift combined with the linear dissipation effects set the saturation stage into an oscillatory mode. The time period of pulsation is a function of the level

of the enhanced background and not the peak intensity I. This would explain the absence of correlation between the pulse repetition rate $\langle \Delta\tau \rangle^{-1}$ and $\langle I \rangle$, $\langle \Delta\tau \rangle$ and pulse amplitude $\langle \Delta I \rangle$ and therefore $\langle \Delta\tau \rangle$ and the modulation index m. Significant correlation between average pulse amplitude $\langle \Delta I \rangle$ and peak intensity is a natural consequence of the mechanism since the pulsations come into play only when $\langle I \rangle$ attain a certain value at which the nonlinear effects are prominent. Fukai, Krishan and Harris (1969) has found the time period of pulsation for such three wave interacting system. The analysis of three wave coupling by Oraevski et al (1973) , Weiland and Wiehelmson (1973,1977) and Fukai , Krishan and Harris (1969) predicts the pulsation to continue throughout the decay phase unlike the observations reported here, where the decay phase is without pulsation. This could be a consequence of the passage of the electron beam out of the interaction region. This decay of the remaining field could be due to collisional or collisionless process.

4.3 Spike Bursts

Spike bursts are the shortest lived bursts observed at radio wavelengths. They are closely

connected with particle acceleration and energy release in solar flares. The duration of the spikes at a particular frequency is less than 500 milliseconds. Radio bursts with duration less than 100 milliseconds were first reported by Drodge and Riemann (1961) and Elgaroy (1961) and studied by de Groot (1962) and Eckhoff (1966). This work was extended by de Groot (1970) and Tanstrom and Philips (1972 a, b). In the first decade of observation of spikes the observing frequencies were in the range of 200 to 350 MHz. This was extended by more than an order of magnitude in the following years. At centimeter wavelengths spike bursts were observed at 1420 MHz by Drodge (1967 and 1977), at 2840 MHz by Slottje (1978) and Zhao and Yin (1982). Stahli and Magun (1986) reported observation of spikes at 5200 MHz. Spike bursts are most abundant in the decimeter wavelengths between 300 to 3000 MHz. Very few observations of spike bursts have been reported at decameter wavelengths. Barrow and Saunders (1972) have found spikes asssociated with type III bursts at decameter wavelengths, but their observations have never been confirmed by spectral measurements. Spectral observations of spike bursts at 34.5 MHz are presented here.

4.3.1 Observations

The observations on spike bursts were made during April 81 and July 82.Most of the spikes appeared during periods of enhanced background continuum. Fig.4.6 shows a typical record of a spike burst.

4.3.2 Time structure

The use of spectrographs with high time and frequency resolution enabled solar radio astronomers to measure the duration of spike bursts. The duration of spike bursts was reported to be around 50 to 100 msec at 250 MHz (Drodge 1967, Benz et al 1982).The duration is found to decrease to 10 -50 msec at 460 MHz and to 3 -7 msec at 1420 MHz (Drodge 1967). The total duration of spike bursts at 34.5 MHz is shown in Fig. 4.7. Most of the bursts have duration around 200 msec. In few cases the total duration is found to increase with decrease in frequency.

4.3.3 Spectral characteristics

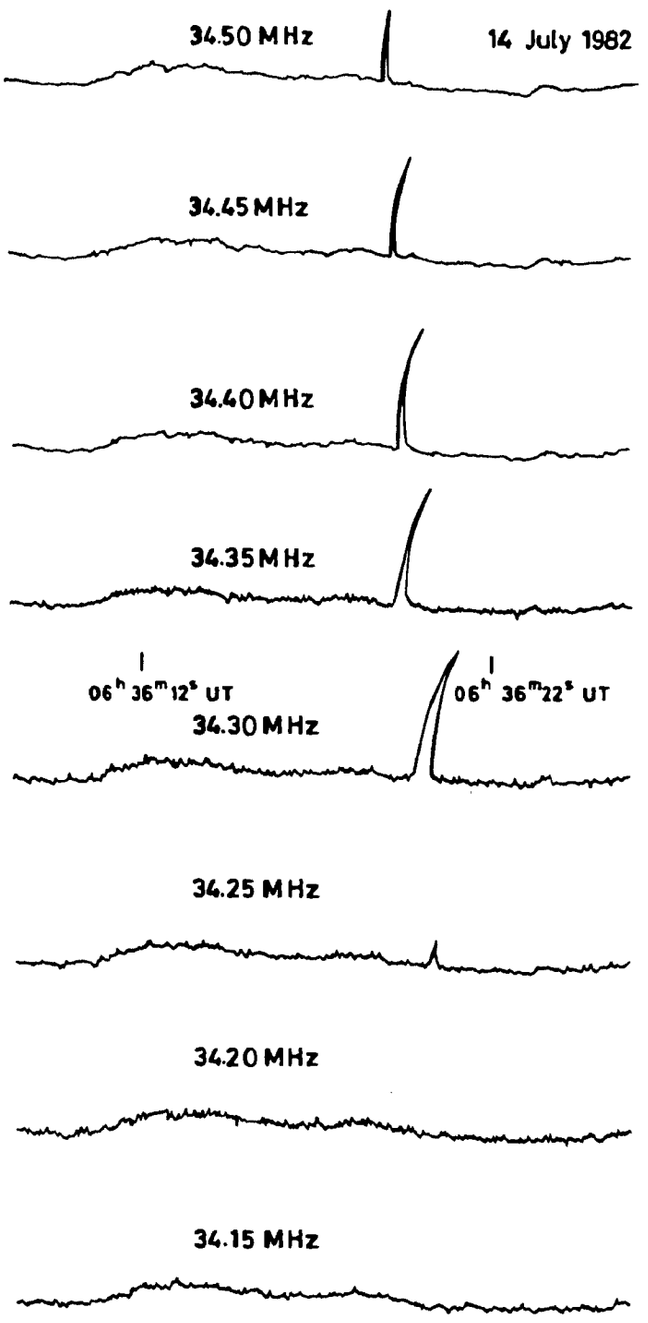

Fig. 4.6. Typical example of spike burst at 34.5 MHz.

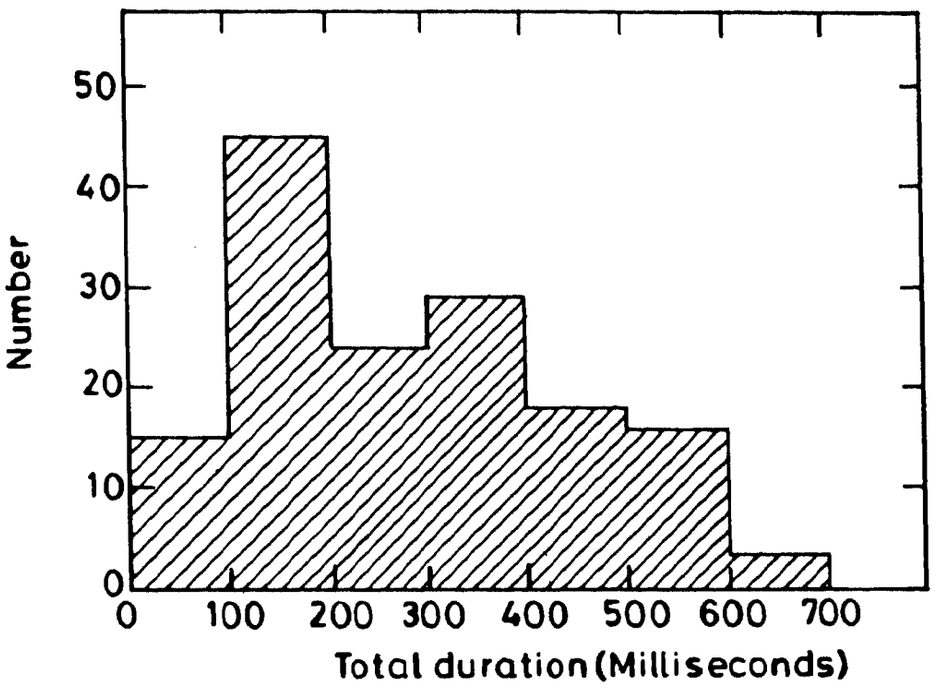

Fig. 4.7. Distribution of the total duration of spike burst.

The drift rate of spike bursts was found to be negative and much higher than type III bursts (Benz et al 1982). Slowly drifting spikes also seem to occur (Tanstrom & Philips 1972a). Barrow et al (1984) reported drift rate of -50 MHz s^{-1} at 263 MHz for spike bursts. Elgaroy & Sven (1979) have published a case with -23 MHz s^{-1} at 525 MHz. The main feature of the spike bursts observed At 34.5 MHz is their slow drift rate. These spike bursts drift from high to low frequencies with a drift rate ranging from 100 to 300 KHz s^{-1} as seen from Fig. 4.8. Most of the bursts have a drift rate between 100 to 200 KHz s^{-1}. These slowly drifting spike bursts also have a narrow bandwidth. Reported observations of the bandwidth of spike bursts vary between 0.5 to 15 MHz. The half power bandwidth at practically instantaneous time is 10 MHz or 1.5% at 600 MHz. The bandwidth at 34.5 MHz is found to range from 100 KHz to 300 KHz as seen from Fig. 4.9. The average bandwidth is 200 KHz or 0.6% at 34.5 MHz. The bandwidth of Slowly drifting spike bursts is is very small similar to most of type I bursts (Elgaroy 1977).

The main characteristics of the spike bursts observed at 34.5 MHz are

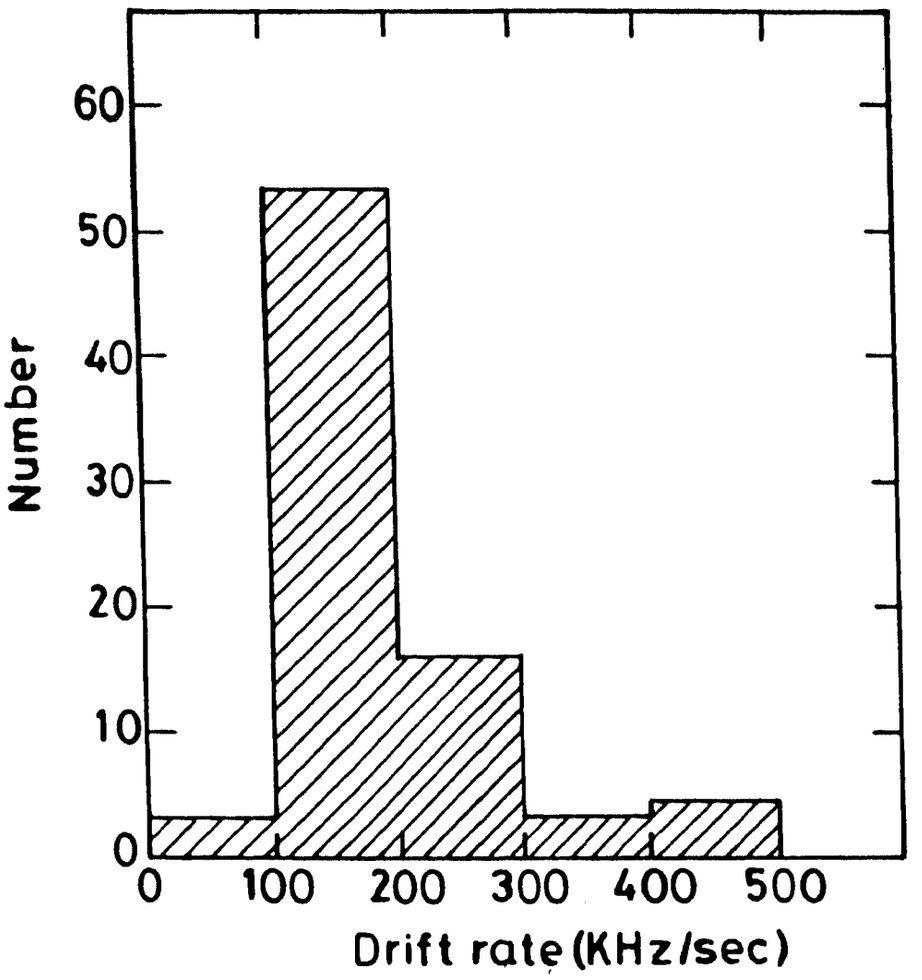

Fig. 4.8. Distribution of the drift rate of spike bursts.

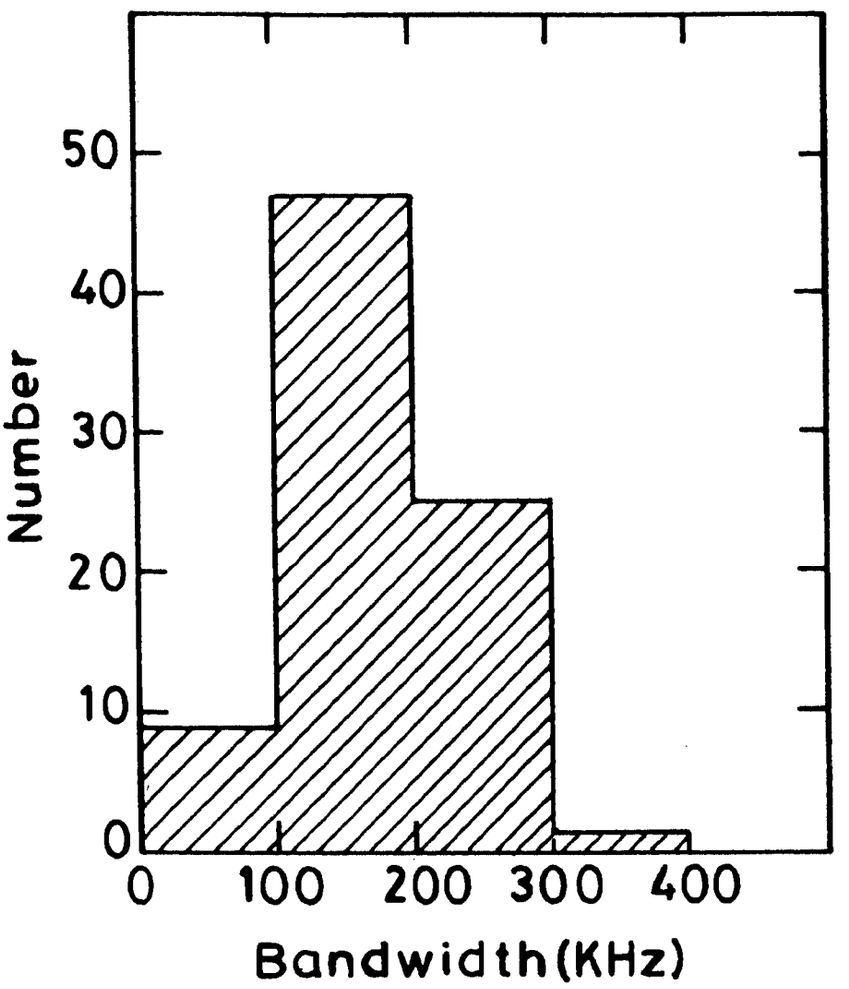

Fig. 4.9. Distribution of the bandwidth of spike bursts.

(i) total duration is 200 msec.

(ii) duration increases with decrease in frequency

(iii) slow drift rate of 150 KHz s^{-1}.

(iv) Narrow bandwidth of 200 KHz.

(v) superimposed on weak continuum.

4.3.4 Discussion

Short duration narrow band bursts called S burst have been reported by McConnell (1981). S bursts have duration of 50 $\pm$ 30 msec, and bandwidth of 120 $\pm$ 100 KHz around 35 MHz. The slowly drifting spike bursts observed at 34.5 MHz,here after called SDS have duration and bandwidth similar to S bursts. The drift rate of S bursts at 35 MHz is 2 MHz s^{-1}. Since the drift rate of SDS is much smaller than 2 MHz these are not S bursts. Also S bursts occur during noise storms whereas SDS occured during periods when storm activity was not found.

The slow drift rate SDS is similar to the type II bursts. But the narrow bandwidth and duration rules out this possibility as type II bursts have bandwidth of 10 MHz and duration of few minutes. Also type II bursts are usually associated with solar flares and no solar flare association is seen in the

case of SDS. Therefore these bursts are probably slowly drifting type I bursts at decameteric level.

The velocity of the exciter of SDS can be calculated from its drift rate. The electron density model given by Newkirk (1961) is used here.

$$n_e(\rho) = M \times 4.2 \times 10^4 \times 10^{4.32/\rho} \text{ cm}^{-3} \quad \ldots 4.1$$

where M is the density enhancement factor and ρ is the distance in solar radii ($R_\odot = 6.9 \times 10^{10}$ cm)

The frequency drift is given by

$$df/dt = (df/dr)(dr/dt) = (df/dt)\, v$$

where $r = \rho R_\odot$ and v is the exciter speed.

The plasma frequency can be expressed numerically as

$$f_p = 9 \times 10^3 \sqrt{n_e} \text{ MHz} \quad \ldots 4.2$$

where n_e is expressed in cm^{-3}.

To allow for the possibility of harmonic radiation we replace eq 4.2 with

$$f = s\, f_p = 9 \times 10^3 \times s \sqrt{n_e} \text{ MHz.} \quad \ldots. 4.3$$

where s is the harmonic number.

Using eq 4.1 plasma frequency f_p can be expressed as

$$f = 9 \times 10^3 \times s \sqrt{M \times 4.2 \times 10^4 \times 10^{4.32/\rho}}$$

$$\therefore \rho = 4.9736 \,/\, (\ln (0.54 \times f/s\sqrt{M}))^2.$$

$$df/d\rho = - \frac{(\ln (0.54 \times f/s \sqrt{M}))^2 \; f \text{ MHz}}{4.9736} \quad \ldots 4.4$$

Expressing in solar radii we get

$$df/dr = -2.9\times10^{-7} \times f \times (\ln(0.54 \times f/s\sqrt{M}))^2 \quad MHz/Km$$

$$\therefore df/dt = -2.9\times10^{-7} \times f \times (\ln(0.54 \times f/s\sqrt{M}))^2 \quad v \quad MHz/sec$$

$$\therefore v=(df/dt)0.35\times10^{7}/f((\ln(0.54f/s\sqrt{M}))^2 Km/sec \quad ..4.5$$

Since the average drift rate of SDS is - 150 KHz s^{-1} the exciter velocity is 1800 Km s^{-1}. Here it is assumed that the emission is at the fundamental (s=1) ,since harmonic emission from type I bursts have not been observed (Benz & Wentzel 1981). The value of M is equal to one because only during noise storms active regions exist and enhanced density (M > 1) is expected. But SDS were seen only during periods when no noise storms are seen. The low velocity of the spike bursts rules out the possibility that the exciter is an electron beam since Langumir waves with phase velocity less than the thermal velocity V_{T_e} are Landau damped. The value of V_{T_e} is$\approx$ 4000 Km/s for the corona with a temperature of million degrees. Therefore the only agency that can generate the SDS is a shock. Since the SDS are not flare associated the shocks may not be strong. Wild and Tlamicha (1964) mentioned that shock waves could generate type I bursts. Zaitsev and Fomichev (1973) had suggested that type I bursts could be caused by perpendicular shocks. Wentzel (1981) proposed that the

radiation mechanism of type I bursts was due to the interaction of Lower Hybrid (LH) and upper hybrid (UH) waves. The UH waves generated by the loss cone distribution of electrons trapped in the closed magnetic fields with the LH waves generated by the shock wave gives rise to type I emission.

Spicer et al (1981) presented a model of type I bursts in which the mode coupling between LH and UH wave gives rise to the radiation. According to this model emerging flux drives a compressional wave at the interface between the emerging flux and ambient plasma. If the Alfvenic Mach no $M_A = V/V_A > 1$ a weak shock will form at the interface boundary. The current density perpendicular to the magnetic field asssociated with the shock will drive cross field elctrostatic instabilities which give rise to enhanced ion density fluctuations. The enhanced ion density fluctuations together with an enhanced level of UH waves due to the loss cone instability of trapped particles excited in the emerging flux as it expands, allows for the generation of meter wave radiation by wave coalescence.

As the observed bandwidth of SDS is very small the shocks travel only a small distance in the corona compared to the coronal scale height. Let us say

that the emission starts at a frequency f_1 corresponding to a plasma layer of density n_1 and stops at a frequency f_2 corresponding to a plasma layer n_2. When the shock reaches the layer n_2 the layer n_1 will be within the shock wave as the shock takes a long time to relax to equilibrium (Lampe & Papadopoulos 1977; Lacombe & Moller - Pederson 1971) compared to the time taken for the shock to travel from layer n_1 to layer n_2. Therefore one can assume that the density remains almost same immediately behind the shock to the starting layer. Therefore one can equate the density jump Δn across the shock to the difference $(n_1 - n_2)$ and hence relate it to the bandwidth $\Delta f = f_1 - f_2$ (Wentzel 1981; Spicer et al 1981; Wenztel 1982). The bandwidth and relative density jump can be related as follows.

Since plasma frequency $f_p = \sqrt{ne^2/m\pi}$

$$\Delta f_p / f_p = \Delta n / 2n$$

where n is the ambient density

m is the mass of the electrons

e is the electric charge

Δn is the density jump

since the observed bandwidth is 250 KHz, $\Delta f/f$ is 0.6%

$\therefore$ $\Delta n/n$ must be 1.2 % .

If we assume strictly perpendicular shock, the velocity of exciter corresponds to the up stream

velocity. The density jump and upstream velocity are related to the Alfven velocity and Ion sound velocity through Rankine - Hugoniot (RH) relation (Tidman & Krall 1971) .This relation or jump conditions give the density,temperature,magnetic field, etc. , behind the shock front in terms of the values ahead of the shock and the shock velocity. The following equation gives this relation.

$$\frac{\Delta n}{n} = \frac{\Delta B}{B} = 1 - \frac{1}{8}\left\{\left(\frac{5C_s^2}{V_1^2} + 1 + \frac{5V_A^2}{2V_1^2}\right) + \left[\left(\frac{5C_s^2}{V_1^2} + 1 + \frac{5V_A^2}{2V_1^2}\right) + \frac{8V_A^2}{V_1^2}\right]^{1/2}\right\} \quad \ldots 4.6$$

where $V_a = B/\sqrt{4\pi n m_i}$ is the Alfven velocity, m_i is the ion mass, C_s is the ion sound velocity, B is the ambient magnetic field, V_1 is the shock velocity and $\Delta B / B$ is the magnetic field jump.

From equation 4.6 we get

$$\frac{V_A^2}{V_1^2} = \frac{8\left(1-\frac{\Delta n}{n}\right)^2 - 2\left(1-\frac{\Delta n}{n}\right)\left(1+\frac{5C_s^2}{V_1^2}\right)}{1+5\left(1-\frac{\Delta n}{n}\right)} \quad \ldots 4.7$$

The value of C_s in the corona having a temperature of 10^6 K is 9×10^6 cm s^{-1}. The shock velocity V_1 is 1.8×10^8 cms^{-1}. For $\Delta n/n = 1.2\%(.012)$, we get from equation 4.7 the value of V_a as 1.7×10^8 cm s^{-1}. Using the relation $V_a = B/\sqrt{4\pi n m_i}$ we get $B \approx 1$ Gauss. This value of magnetic field is in close agreement with other estimates (1G) obtained from frequency splitting and polarization measurements of type I bursts (ter Harr and Tsytovich 1981).

4.4 Diffuse echo bursts

The sporadic radio emission of the sun in some cases reveal features called "Echo " bursts. Echoes have been observed in bursts which occur during decametric solar radio noise storms, such as Drift pairs, split pair and type IIIb bursts. Diffuse striae bursts with an intense core followed by a long weak tail in their time profile was first reported by Bazelyan et al (1974). These bursts differ from the ordinary striae bursts in their duration and frequency splitting. Their total duration is 15 sec and frequency splitting is 0.2 MHz at 25 MHz. In the

diffuse striae bursts, sometimes a pair of narrow band echo type bursts are observed. These echoes are observed at the same frequency with a time delay. Diffuse echo bursts are less intense than the ordinary striae bursts. These bursts are sometimes found in chains similar to type IIIb bursts. But unlike type IIIb burst which is followed by a type III burst, diffuse echo bursts are not followed by a type III burst. The diffuse echo bursts drift from high to low frequency, and were found to have a low frequency cutoff near 16 MHz. The echo bursts are essentially a decameter phenomenon and no observations are reported above 25 MHz. Here observations of echo bursts at 34.5 MHz are presented (Subramanian 1988).

4.4.1 Observations

During the period 11th to 23rd June 1982, noise storm activity was seen at decameter wavelengths. During this period solar activity was maximum with a sunspot number close to that of solar maximum. The number of diffuse echo bursts seen during this period is high, although these bursts have been seen during other periods of activity also. We have studied the time and intensity characteristics of 50 echo bursts. Fig. 4.10. shows a typical record of

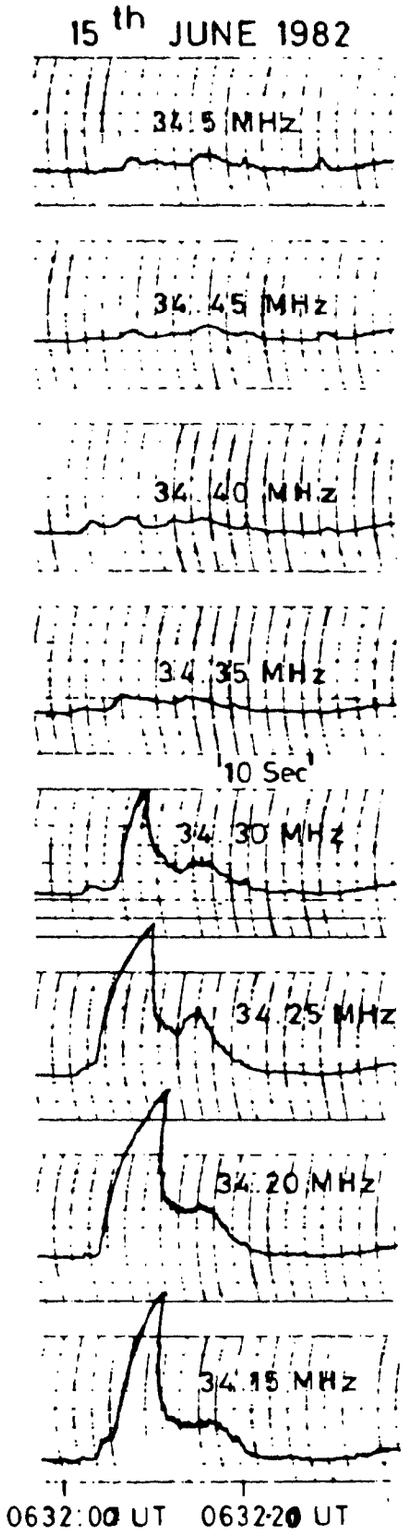

Fig. 4.10. Example of diffuse echo bursts.

diffuse bursts observed at 34.5 MHz.

4.4.2 Spectral characteristics

From the time intensity plots the drift rate (df/dt) of the two elements (primary and echo) were measured. The drift rate can either be positive or negative. The drift rate is of the order of 350 KHz s^{-1} to 1 MHz s^{-1}. The average drift rate is 500 KHz s^{-1}. The drift rate of both the elements are found to be the same. The bandwidth of the primary burst varies from 50 KHz to > 400 KHz . The bandwidth of the echo is always greater than that of the first element. Because of the narrow bandwidth of the spectrograph these values are lower limits.

4.4.3 Time profile

The various parameters of the burst we have measured are shown in Fig. 4.11. The time delay ΔT_1 between the peak of the primary burst and its echo ranges from 4 s to 7 s. The time delay ΔT_1 is found to vary with the heliolongitude of the active region. Since the position information of the noise storm regions at 34.5 MHz are not available,

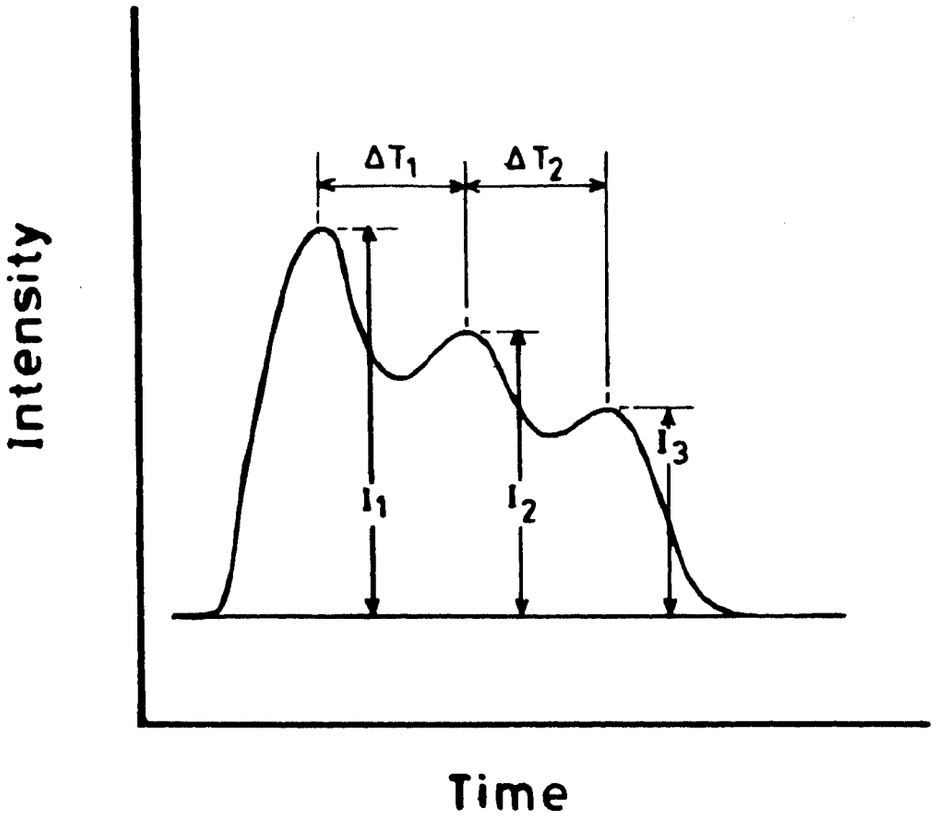

Fig. 4.11. Parameters measured on the time profile of Diffuse echo bursts.

the heliolongitude of the noise storm region observed at 160 MHz were taken from Culgoora measurements reported by Stewart et al (1985). The position of noise storm at 34.5 MHz cannot differ from that at 160 MHz, except at limbs,since the observation of type I storm at 160 and 80 MHz indicate that the sources have a columnar structure (Stewart 1976; McLean 1981). The maximum time delay of 3.8 $\pm$ 0.8 s occured when the active region is at a heliolongitude of 22 degrees and minimum delay of 1.8 s occured when the heliolongitude was < 10 degrees. In the case where there is a second echo the time delay ΔT_2 is found to be well correlated with ΔT_1 with a linear correlation coefficient of 0.86 as shown in Fig. 4.12. The time delay ΔT_2 is given by the following relation

$$\Delta T_2 = 1.64 + 1.62 \ \Delta T_1$$

4.4.4 Intensity

The intensity I_1 of the primary burst is greater than that of the first echo burst. The intensity I_3 of the second echo burst is always less than that of first echo burst. There is no correlation between the intensities of primary ,first echo and second echo bursts .

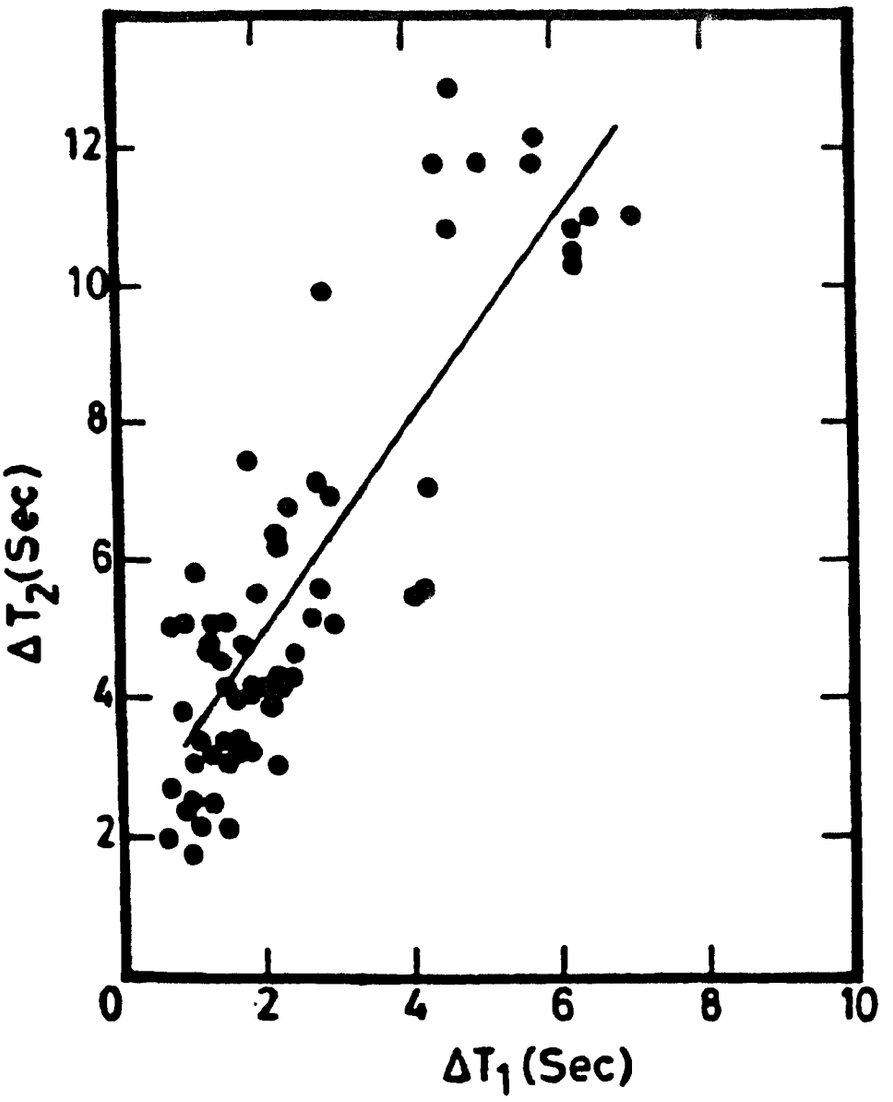

Fig. 4.12. Plot of the time delay ΔT_1 between the primary burst and the first echo versus the time delay ΔT_2 between the first echo and second echo.

4.4.5 Discussion

Tsybko (1984) found that the diffuse echo bursts occur at the second harmonic of the plasma frequency. Therefore the value of s,the harmonic number in equation 4.5 is 2. Also these bursts occur during periods of noise storms when enhanced density is expected. Therefore the density enhancement factor M is greater than unity. From equation 4.5 the velocity velocity of the exciter is found to be 14000 Km/s for diffuse echo bursts with an average drift rate of 500 KHz s^{-1}. Here we have assumed a value of 2 for M, the density enhancement factor. The required velocity of an electron beam to generate longitudinal waves is much higher than 14000 Km/s, since Landau damping inhibits the growth of Langumir waves with velocity below about four times the thermal velocity V_{Te} in the corona. The value of V_{Te} is 4000 Km/s for the corona with temperature of million degrees. In the derivation of drift rate the exciter was assumed to travel perpendicular to the plasma layers in the corona. If the direction of the exciter is inclined at an angle ϕ to the density gradient, the drift is given by

$$\frac{df}{dt} = \frac{df_p}{dr} v \cos \phi$$

With $\phi \sim \pi/2$ and velocity of 14000 Km/s the nearly longitudinal path travelled is $0.2 \times R_{\odot}$ for the diffuse echo burst which has an average duration of 9 s. To keep the density uniform over such large path is very difficult at decameter wavelenghts. Shock waves in the corona have typical velocities of 600 Km s^{-1} and only in exceptional cases can reach velocities of 3000 Km s^{-1} (Robinson 1985). Whistler and Alfven wave soliton move at about the Alfven speed. The Alfven speed is typically 1800 Km s^{-1} for the corona with a magnetic field of 1 Gauss. So the exciter cannot be a whistler or Alfven wave and may be therefore an ion beam.The exciter speed derived from the drift rate corresponds to protons with an energy of 1 Mev. Possibility of ion beams in the energy of 0.1-1 Mev was suggested by Simnett & Strong (1984) for the appearance of nuclear line during impulsive phase and strong plasma turbulence and upflows before the impulsive phases. Benz & Simnett (1986) has proposed proton beam with energies of 0.56 - 3.7 Mev as the exciter for slowly drifting type III bursts. The proton beams are unstable to growing ion acoutic waves. Radio emission may be produced by coupling of the low frequency wave to weak Langumir waves of some other source (Melrose 1980).

The radiation generated at the source region in the corona has to propagate through the over lying ionised medium. During the propagation reflection, refraction,absorption,faraday rotation and scattering will modify the source position,angular structure,brightness-temperature and time profile of radio bursts observed at the earth.

In addition to the smooth variation of electron density,small scale irregularities are present in the corona which give rise to scattering effects. Effects of scattering using isotropic inhomogenities were estimated by Fokker (1965),and Steinberg (1981). Riddle (1972,1974) extended this treatment to anisotropic radially elongated inhomogenities and computed the effect of scattering on the position, size and time profile of solar radio bursts at 80 MHz.

Riddle (1974) has computed the time profile of solar bursts at 1 AU resulting from a short burst of 80 MHz emitted from 78 MHz plasma level followed by the emission of a similar burst of 80 MHz (harmonic of 40 MHz) from the 40 MHz plasma level. The model radio echo is in the form of a longer duration low intensity burst preceded by a short duration burst seen as a direct

ray. One can apply this model in the case of diffuse echo bursts as they occur at the second harmonic of the plasma frequency as found by Tsybko (1984). The echo burst at 80 MHz according to Riddle's calculation has smooth profiles. Such profiles are shaped owing to the propagation of electromagnetic waves down the corona and back through a random scattering medium.

The model applied in our case is shown in Fig. 4.13.The harmonic of 17.25 MHz radiation i.e. 34.5 MHz is emitted towards and away from the observer. The emission toward's the sun gets reflected from the 34.5 MHz plasma level and reaches the observer as an echo. The time delay ΔT_1 between the primary burst and the echo is given by

$$\Delta T_1 = 2(R_2 - R_1)/c + T_g$$

where R_2 and R_1 are the coronal heights corresponding to frequencies 17.25 MHz and 34.5 MHz, respectively and c is the velocity of light, and T_g is the group delay that a radio wave experiences along the path from R_2 to R_1. The value of T_g is 1 s at decameter wavelengths. From the maximum value of ΔT_1 (4 s),the value of $R_2 - R_1$ is $0.64 \times R_\odot$ which agrees well with the distance between the plasma layers at 17.25 MHz and 34.5 MHz in the coronal model given by

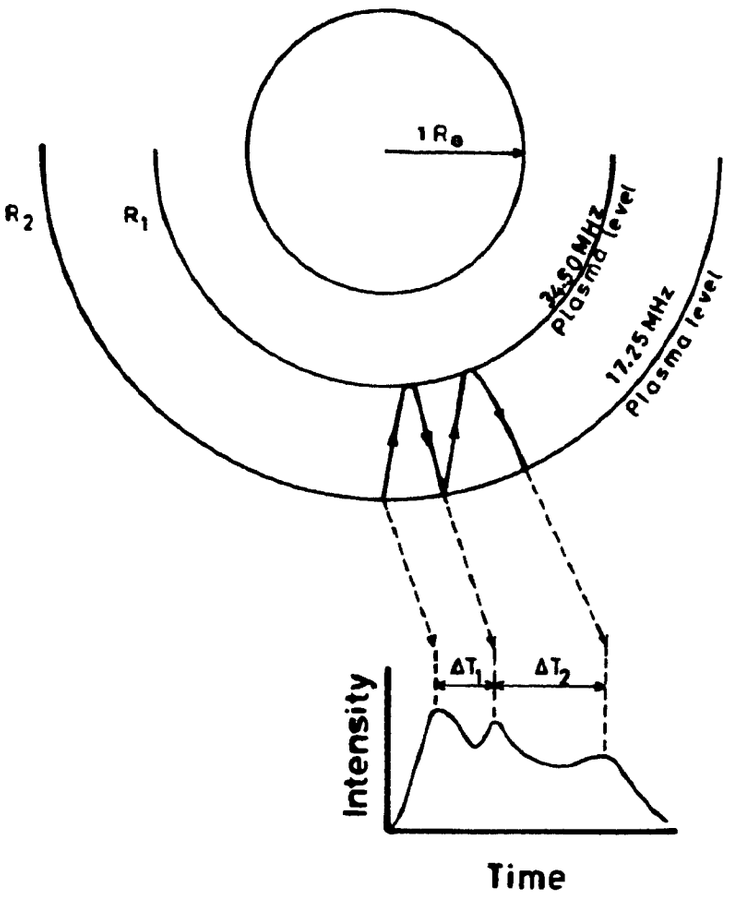

Fig. 4.13. Illustrated interpretation of the intensity - time profile of multiple echo event.

Newkirk (1967). The once reflected 34.5 MHz radio wave on its way towards the earth undergo resonance back scattering of an appropriate part of their power near 17.25 MHz plasma level. This scattered wave again gets reflected from 34.5 MHz plasma level with a time delay of ΔT_2. The resonance scattering of the em wave might be the decay of the elctromagnetic wave $2f_p$ (34.5 MHz) into 2 plasma waves causing the generation of secondary backward radiation. The condition for such conversion require the temperature of em emission to be sufficiently high. Since the echo bursts occur only during noise storms this condition holds good.

CHAPTER 5

BROAD BAND ARRAY

5.1 Introduction

The south array of the Gauribidanur radio telescope used for the study of fine structures in the radio emission of the sun has a maximum usable bandwidth of 1 MHz,centered around 34.5 MHz. The study of dynamic sources such as the Sun,Jupiter and Pulsars using the south array has therefore severe limitations.

(i) In the case of the Sun the spectral features of the burst like frequency drift rate , bandwidth and harmonic structure are related to the physical characteristics of the source. The frequency drift is related to the velocity of the exciter. The bandwidth is related to the source depth Δr($\Delta r < \Delta f (df/dr)^{-1}$,(Δf is the bandwidth of emission and df/dr is the variation of plasma frequency with radial distance),and the harmonic structure is related to the physical processes like plasma or gyroemission.Spectral observations over wide bandwidth are required to obtain the above characteristics of the bursts accurately.

(ii) From the dynamic spectra, the solar

bursts can be classified into three groups . They are

(a) Large scale phenomena (Type I to Type V burst having bandwidth > 10 MHz),

(b) Medium scale phenomena (Band splitting, Type IV pulsating bursts etc having a bandwidth <10 MHz)

and (c) Small scale phenomena (Fine structures like Type IIIb, Drift Pairs, S bursts etc having a bandwith of < 2 MHz).

An attempt to classify the small and medium scale phenomenon without having regard to the entire spectral enviorment leads one easily astray. It is necessary to know which large scale event they belong to,since the narrow band burst may be produced by the local state of the plasma created by the large scale phenomena and therefore wideband observations are required.

(iii) The measurement of the flux density of solar bursts at different frequencies are important to obtain flux density spectra which gives an insight into the generation mechanism of the radio emission of these bursts. In the case of steady sources flux density at different frequencies obtained at different times can be used to determine the flux density spectra. This

method is not applicable in the case of the solar bursts which vary in intensity in time scales of the order of few seconds.Simultaneous measurement of the flux density is required at a number of frequencies over wide bandwidth. Due to the limited bandwidth of the south array such measurements are not possible.

Therefore one of the important requirement of a radio telescope used for the study of solar radio bursts is wide bandwidth. The other requirements are

(i) to observe the Sun for a long period as it is a sporadic radio source

(ii) to operate simultaneously over wide bandwidth

(iii) to have enough sensitivity to oberve radio sources which can be used as calibrators.

A broadband array with the above requirements operating in the frequency range of 30 to 70 MHz was designed and built (Subramanian et al 1986). This telescope is located at Gauribidanur (Longitude $77^{\circ}26^{'}07^{''}$ East, Latitude $13^{\circ}36^{'}12^{''}$ North). The frequency range of 30 to 70 MHz was chosen for the following reasons.

(i) The solar radio bursts at these frequencies are strong ($\approx$10 SFU), and therefore for

their detection a large collecting area is not required

(ii) The spectral characteristics of noise storms change around 50 MHz. Above this frequency mostly type I bursts occur and below this cut off frequency which can change from one storm to another storm type III bursts occur (Aubier et al 1978). Many questions regarding the spectrum of the continuum emission at these wavelengths are not answered. A matter of particular interest is the evolution in time of the continuum spectrum. Also the continuum spectrum shows fluctuations.The spectral characteristics of these fluctuations have not been investigated (Elgaroy,1977).

(iii) A number of fine structures in the radio emission of the Sun occur only at decameter wavelengths. The flux density spectra of these fine structures are important to determine their generation mechanism.

5.2 The array

For the study of dynamic spectra of solar bursts, the response of the antenna system must be uniform over the angular extent of the radio sun.The electron density and therefore the plasma frequency decreases outward from the center of the sun.

From the Newkirk's electron density model we find that the radio emission at 65 MHz originate from a layer at a distance of 1.4 $R_{\odot}$($\simeq$ 22 minutes of arc) from the center of the sun. Therefore the size of the radio sun at 65 MHz is $\simeq$ 44 minutes of arc. Inorder to have uniform response over the radio sun at 65 MHz the half power beamwidth (HPBW) of the array must be greater than 44 minutes of arc. The HPBW of an array is given by the relation

$$HPBW(deg) = 57.3\ \lambda/D$$

where D is the linear dimension of the array and λ is the wavelength

An array having a linear dimension of 360 mts satisfies the requirement of uniform response of the array over the radio sun at 65 MHz. For this dimension of the array,the response is uniform over the radio sun at 35 MHz also because the the size of the radio sun at 35 MHz is $\simeq$ 54 minutes of arc which is less than the HPBW (82 minutes of arc)of the array at 35 MHz. But in order to have more observing time on a sporadic source,the HPBW of the array has to be much larger than these values. To have an observing time of 30 minutes on a source the HPBW has to be 7.5 degrees. To have a HPBW of 7.5 degrees at 65 MHz, the dimension of the array has to be 35 mts along the East West direction.For this dimension of the array the observing

time will be 60 minutes at 35 MHz. Along the North South direction the size of the array should be such to have a HPBW which covers the radio sun at all frequencies. The design of the array is therefore in the form of a rectangular aperture, 40x64 mts along the E-W and the N-S directions respectively. Fig. 5.1 shows the photograph of the array.

5.2.1 Broadband dipole

The antenna system for broadband operation must meet two requirements.

(i) The voltage standing wave ratio (VSWR) of the antenna must not become excessive at any frequency in the band of interest.

(ii) The general behaviour of the directional pattern of the antenna must be maintained over the range of frequencies involved. Though the directivity will increase with frequency, the main lobe should not change materially in direction and split into two lobes over the frequency of interest.

The general principle of frequency independent antennas is given by Rumsey(1966). One technique to obtain wide bandwidth is to use fat dipoles. An effective method of utilizing fat

Fig. 5.1: The broadband array.

dipole principle is to employ biconical antennas. Brown & Woodward (1952) have measured the impedance and power pattern of biconical antennas. The basic design information though obtained an empirical study of biconical antenna was undertaken. The solid biconical structure is so massive for low frequency operation and it is impracticable to fabricate and use them. Realistic variation to its mechanical structure having been sought while retaining as much of the desired electrical features as posssible. The antenna can be simulated by wires along the periphery of its surface which significantly reduce the weight and wind resistance of the structure . The dipole for practical consideration was designed by using wires as bipyramidal instead biconical. Fig. 5.2a. shows the basic element of the broadband array. The elements are made up of 16 gauge copper wires and has a bandwidth of 30 MHz. The impedance of the elements is 600 ohms. The VSWR is less than 2.0 in the frequency of 35 MHz to 65 MHz as shown in Fig. 5.2b. The flare angle α of the element is 32 degrees. For this flare angle α and antenna length A, of 2 mts the HPBW of the field pattern is 100 degrees at 35 MHz and 80 degrees at 65 MHz,both in the XY and XZ plane (Brown & Woodward 1952). The antenna elements are supported on both ends and at center by wooden poles. The elements accept

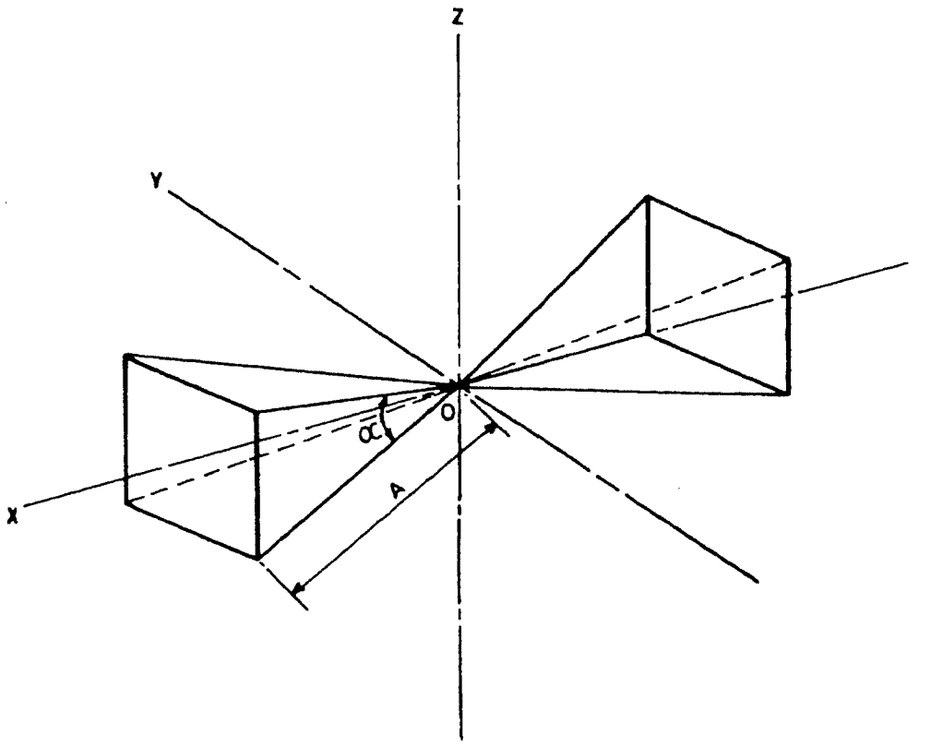

Fig. 5.2a: Geometry of bipyramidal diploe.

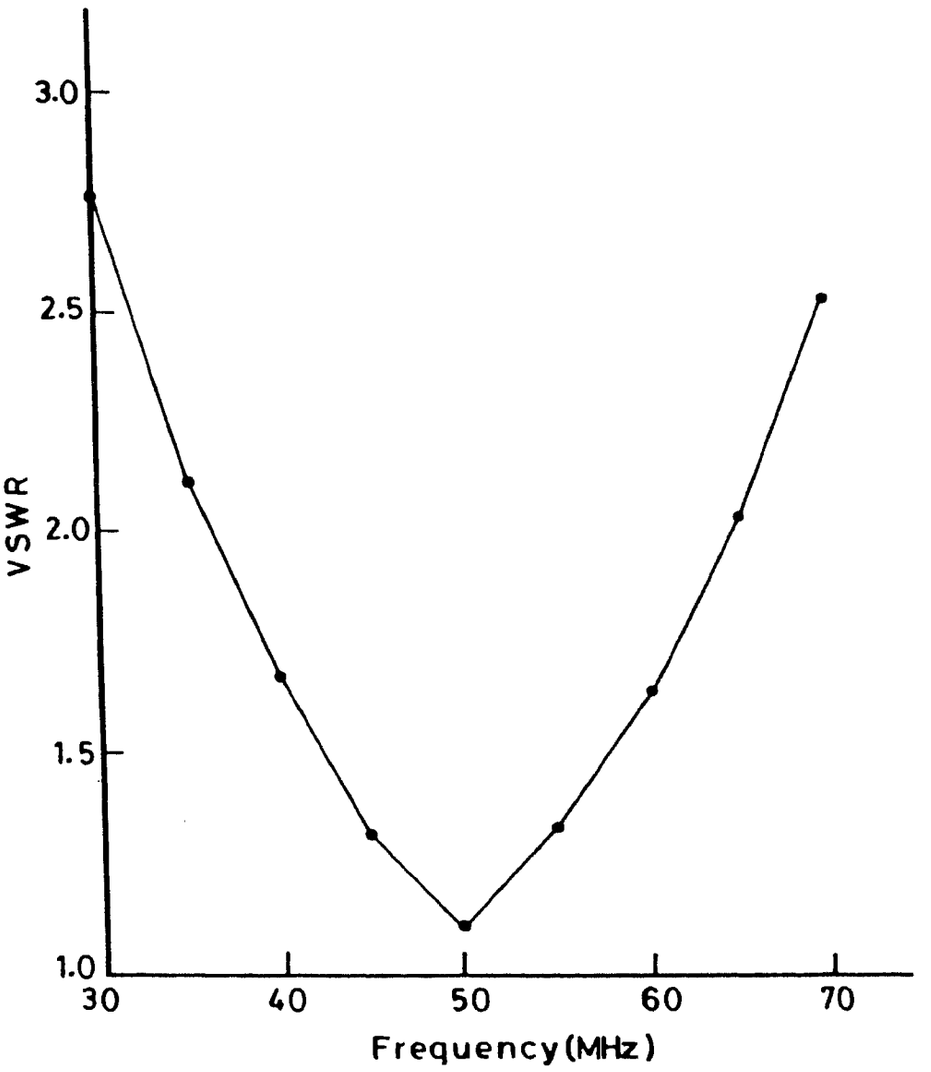

Fig. 5.2b: VSWR of bipyramidal dipole.

linear polarization in the N-S direction.

5.2.2 Array configuration

The array consists of 64 elements arranged in a matrix of 4 x 16 along the E-W and the N-S directions respectively. The four elements in the E-W direction have an interelement spacing of 10 mts. The 600 ohm impedance of the element is converted to 50 ohms by using wideband balun impedance transformer wound on a ferrite core. Four elements along the E-W direction are combined together in a branched feeder system using RG 8U cables and 2:1 transformers as shown in Fig. 5.3. The signal is amplified by a broadband amplifier having a gain of 13 dB and noise temperature of 1000 degrees K. The third order intermodulation intercept for this amplifier occcurs at input levels greater than zero dBm. The amplified signal is brought to the control hut near the array using RG 8U coaxial cable. There are 16 such rows in the N-S direction. The 16 elements in one column are placed in a square corner reflector with an interelement spacing of 4 mts.

5.2.3 Corner reflector

The corner reflectors are antennas of "V"

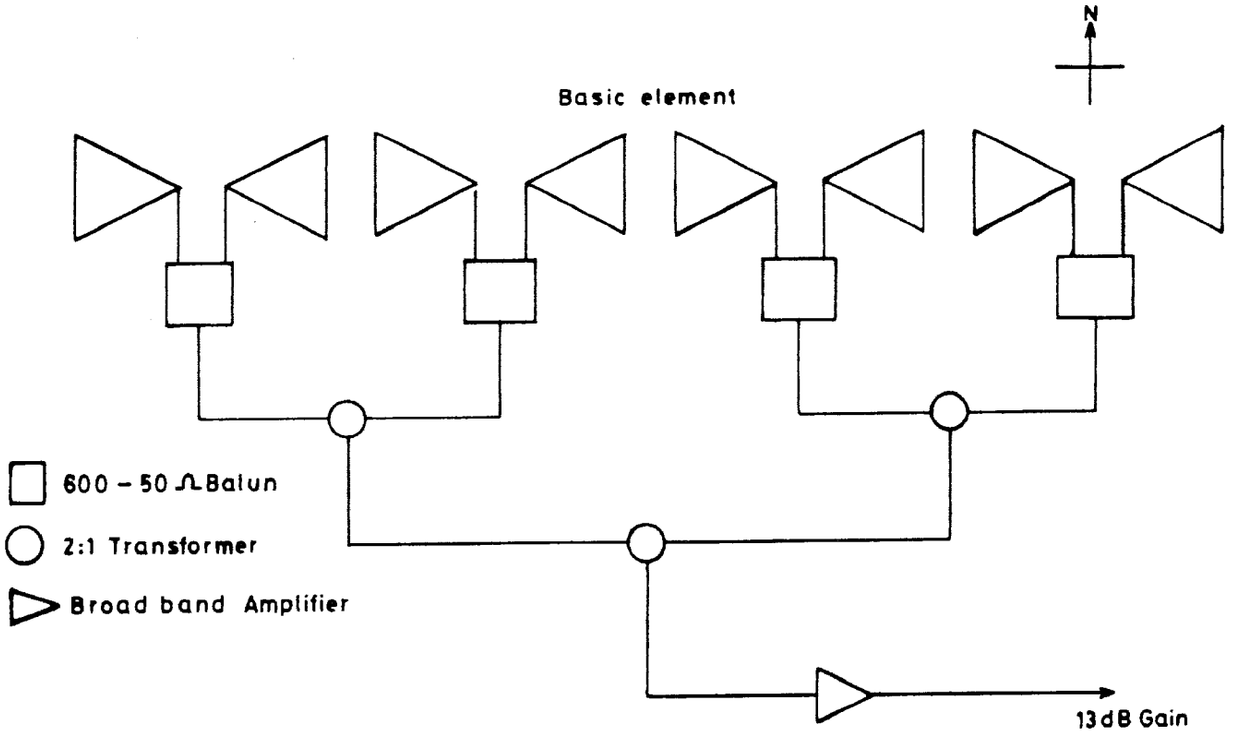

Fig. 5.3: Branched feeder system connecting four diploes in the East West direction.

shaped type, the sides of which are made of two plane reflectors joined together so as to form a corner. The angle between the two plane reflectors is 90 degrees in our case. When the wavelength is large the surface of the corner can be made of grid wires,rather than sheet of metal. The corner reflector in our case is made of galvanised wires spaced 20 cm ($< \lambda/20$ at 65 MHz) apart running in the N-S direction. This design reduces the wind resistance and over all system weight. For wires that are parallel to the dipoles as in our case the reflectivity of the grid wire surface is as good as that of a solid surface. The sides of the corner are 10 mts in length, which is greater than one wavelength at the lowest frequency of operation (35 MHz). This design further increases the bandwidth of the driven element (Kraus 1950). The apex distance between the corner and the element is 2 mts,which is between 0.25λ and 0.7λ in the frequency range of 35 - 70 MHz. Fig. 5.4a shows the antenna element in the corner reflector. The expected gain of the element when placed in a corner reflector of such size and spacing of the driven element is 10 dB over a half wavelength dipole. Also at such a spacing there is no beam splitting (Kraus 1950).

When the spacing between the elements is$> \lambda/2$ there may be more than one main lobe in the visible region,depending on the spacing between the elements.

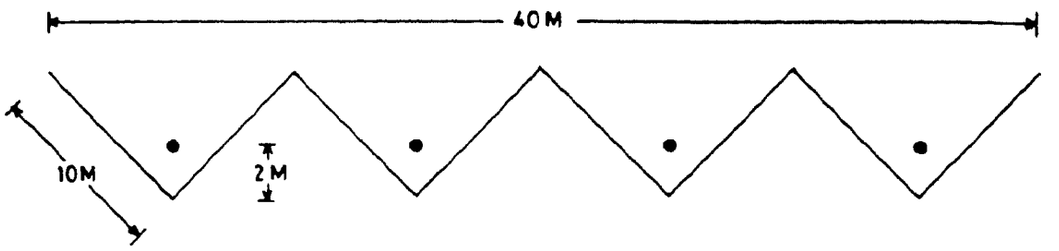

Fig. 5.4a: Antenna elements placed in corner reflectors.

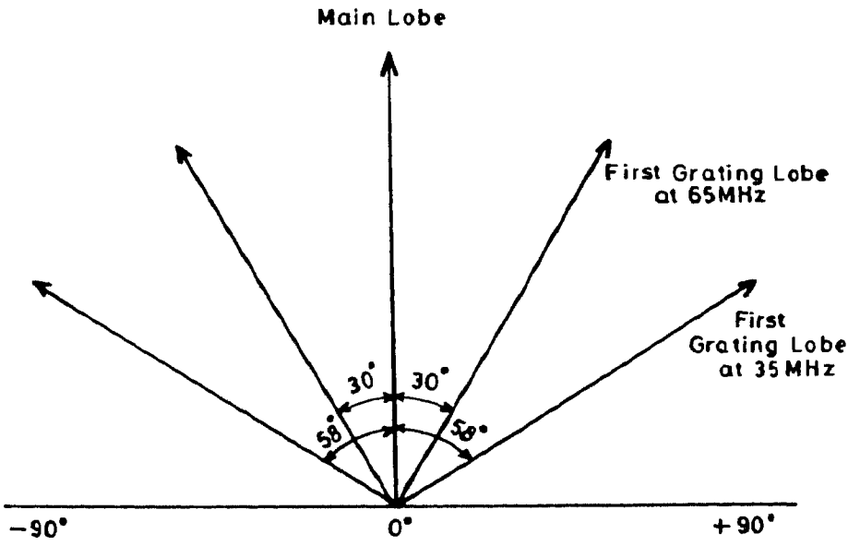

Fig. 5.4b: Grating response in the EW direction. When the main beam is in the zenith first grating lobes appear at ± 30 degrees at 65 MHz and ± 50 degrees at 35 MHz. The grating lobes are attenuated by the primary beam of the bipyramidal dipole when placed in the square corner reflectors.

These addtional major lobes which give rise to an intensity equal to the main lobe at $\phi = 0$ are called grating lobes. In the Broad band array the interelement spacing along the E - W direction being 10 mts grating lobes are present at 30 degrees away at 65 MHz and 50 degrees away at 35 MHz in addition to the main beam at $\phi = 0$ as shown in Fig. 5.4b. The grating lobes caused by the separation of the elements is eliminated with directive elements which radiate little energy in the direction of the undesired lobes. If the beam of the element is less than 60 degrees the grating lobes will be suppressed at 65 MHz. Since the beam of the bipyramidal element is 80 degrees,at 65 MHz,to suppress the grating lobes the elements are placed in the corner reflector. The normalised field pattern of a bipyramidal dipole placed with its axis parallel to the plane of the reflector in a square corner reflector is given by Kraus (1950) as

$$G(\phi) = \frac{E(\phi)(\cos(S_r \cos(\phi)) - \cos(S_r \sin(\phi))}{\cos(S_r) - 1} \quad -- 5.2$$

where $S_r = 2\pi S / \lambda$ (S is the apex distance) and $E(\phi)$ is the field pattern of the biconical dipole given by Brown and Wood (1952). It is assumed here that the field pattern of bipyramidal and

biconical dipoles are similar.

The computed beam is 56 degrees at 65 MHz,better than the requirement for suppression of grating lobe. At 35 MHz the beam of the bipyramidal dipole placed in the square corner reflector is less than 65 degrees and so the grating lobes are suppresed to a greater extent. Since the element spacing is 4 mts along the N-S direction grating lobes are not present.

5.2.4 Beam formation

In the E-W direction the telescope is a meridian transit instrument. To steer the response of the array in the N-S direction,one has to phase the elements. Electrical phasing has the drawback of being monochromatic. A delay in arrival time of waves reaching the two antennas, because of the inclination of the direction of the source, has to be compensated by changing the phase of one of the signals. This compensation can be done accurately only at one frequency or its harmonics. The result is that except in a direction normal to the telescope where all the phases are equal,the direction of the beam will depend on the frequency. This has the effect of decreasing the operational frequency bandwidth in which the array can be used simultaneously. Therefore

delay shifters whose delay time is independent of frequency are to used for steering the beam in wideband arrays. The incorporation of such delays into the circuit offsets the spatial delay of signals in the case of slant incidence of a plane wave.

The broadband array is split up into northern and southern groups of eight rows each. The eight rows of each group are combined in a branched feeder system and delay shifters are introduced at appropriate places as shown in Fig. 5.5a. The broad signal bandwidth of 30 MHz makes coaxial cable the obvious choice for achieving the required delays. The coaxial cable used is RG 174U, a 50 ohm cable having a velocity factor of 0.66. The delay shifters are used to steer the response of the array to $\pm$ 45 degrees of the zenith in the N-S direction.

5.2.5 Delay shifters

To steer the response of the array there are 4 stages of delay shifters ϕ_1, ϕ_2, ϕ_3, and ϕ_4 as shown in Fig. 5.5a. The ϕ_{1s} stage consists of two sections of delay step τ and 2τ. The delay is given by

$$\tau = \beta d \sin(\phi).$$

where β is the velocity factor of the cable used

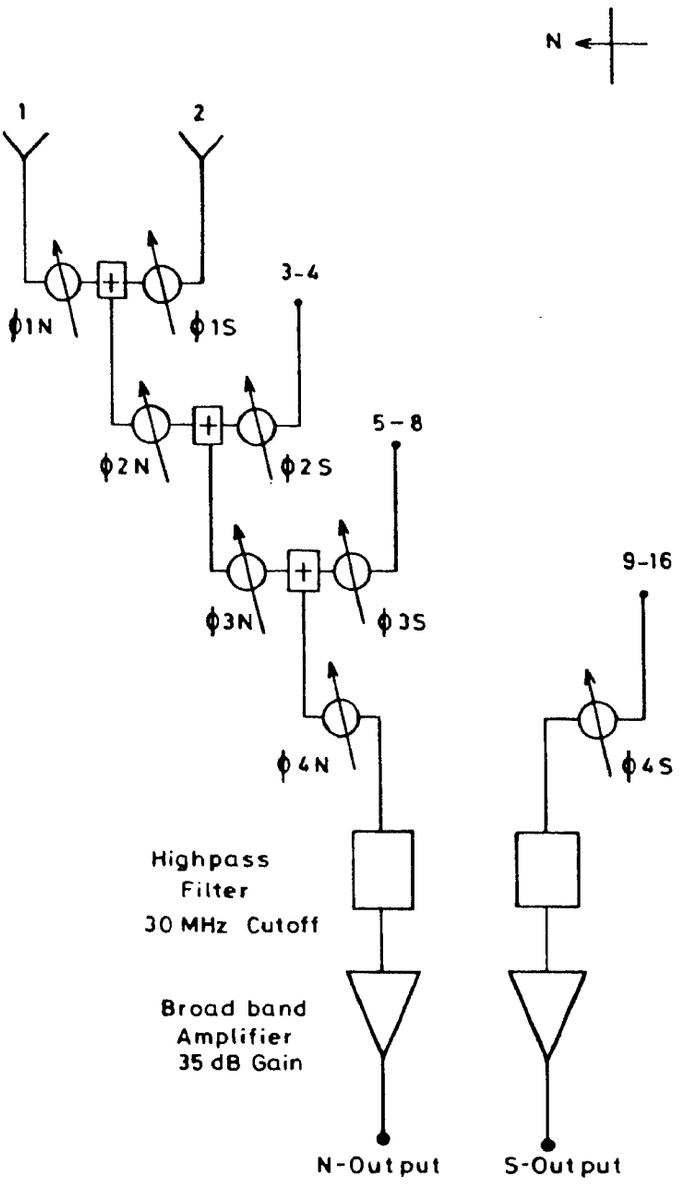

Fig. 5.5a: Branched feeder system in North South direction. Delay shifters are introduced at appropriate places to steer the beam in NS direction to $\pm$ 45 degrees.

= 0.66 for RG174U cable

d is the spacing between two elements

= 4 mts

and ϕ is the angular step by which the beam is changed in the first stage, such that the sequential beams at 65 MHz overlap at better than HPBW.

The spacing between the 2 elements in the N-S direction in the first stage being 4 mts the HPBW is equal to 66 degrees at 65 MHz. An overlap of 85 % was chosen to minimise the no of delay stages. The value of ϕ is 12 degrees.

and therefore $\tau = 0.66 \times 4 \times \sin(12^\circ)$ mts

= 0.55 mts

Each section of delay shifter consists of 2 coupled RF diode switches S1 and S2 as shown in Fig. 5.5b. When the control voltage is + ve, S1 is open and S2 is closed and the RF signal passes through additional length of cable corresponding to the required delay. When the control voltage is - ve, S2 is open and S1 is closed and no delay is introduced. The isolation between the delay on and off position is > 40 dB. Using τ and 2τ delay cables and by control voltage any delay from 0τ to 3τ can be set

The variable capacitors are used to match the input output impedance to 50 ohms. Over the frequency

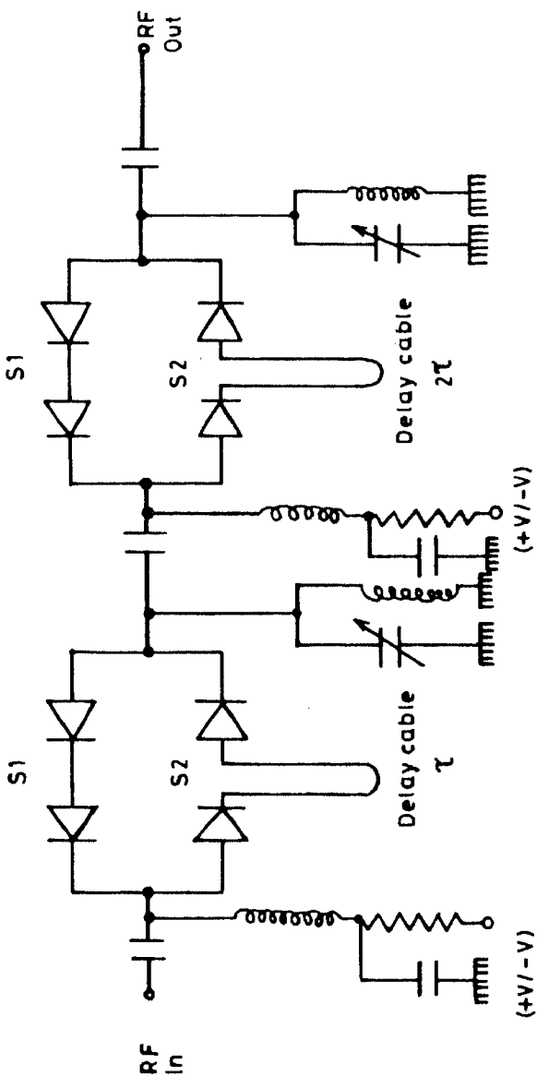

Fig. 5.5b: Delay shifter unit

range 35 - 70 MHz the input/output VSWR is better than 1.3 for any delay setting. The insertion loss of the delay shifter varies by not more than 0.5 dB as a function of the delay over the whole frequency range.

The delay shifter ϕ_{1s} can steer the response of row 1 & 2 to southern direction from the zenith. To steer the beam to northern direction delay has to be introduced in the row 1 which is accomplished by ϕ_{1n}. In this module either 0τ or 3τ delay can be set. By the combination of delays in ϕ_{1s} and ϕ_{1n} any delay from 0τ to 3τ can be set either in row 1 or 2 with respect to the other. The response time of these delay shifters are of the order of 1 msec. For zero delay setting in ϕ_{1s}, the input output offset delay is 1.3×10^{-9} s. The insertion loss is 0.5 dB at 35 MHz and 0.7 dB at 65 MHz. An attenuation of 0.6 dB is taken as the average insertion loss of this delay shifter. For ϕ_{1n} the input out offset delay is 0.4×10^{-9} s and average insertion loss is 0.4 dB. Because the number of sections in ϕ_{1s} is more than that of ϕ_{1n}, there is an extra delay and insertion loss in ϕ_{1s} compared ϕ_{1n} which are compensated in ϕ_{1n}, as shown in Fig. 5.5c.

The delay shifters ϕ_{2s}, ϕ_{3s} and

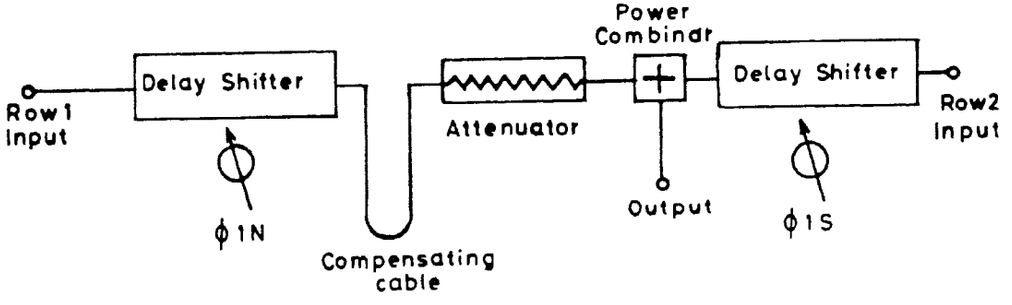

Fig. 5.5c: Connection of two rows using delay shifters.

ϕ_{4s} similar to ϕ_{1s} except that it consists of more number of sections. Table 5.1 gives details of all the delay shifters used in the system. In ϕ_{2n}, ϕ_{3n}, and ϕ_{4n} the compensatory delay and insertion loss corresponding to ϕ_{2s}, ϕ_{3s} and ϕ_{4s} are introduced. Each delay network is housed in a separate metal box. The DC control lines are well filtered. These precautions minimize the cross talk between the delay networks connected to different rows.

The output from the northern and southern groups pass through high pass filters and broad band amplifiers. The filter has a cut off frequency of 30 MHz and the amplifier has a gain of 35 dB. The amplified signal from the north and south groups are separately brought to the main receiver room by open wire transmission line of length 0.8 Km. For such an interferometer when the baseline between the interferometer is equal to the linear dimension (in the same direction as the baseline) of each of the element of interferometer, the power pattern is given by Kraus (1966)

$$P(\phi) = \frac{\sin (n\psi/2) \cos (x)}{n \sin (\psi/2)}$$

Delay shifter	No of stages	Delay
ϕ_{1S}	2	$\tau, 2\tau$
ϕ_{1N}	1	3τ
ϕ_{2S}	3	$\tau, 2\tau, 4\tau$
ϕ_{2N}	1	7τ
ϕ_{3S}	4	$\tau, 2\tau, 4\tau, 8\tau$
ϕ_{3N}	1	15τ
ϕ_{4S}	6	$\tau/2, \tau, 2\tau, 4\tau, 8\tau, 16\tau$
ϕ_{4N}	1	$31\frac{1}{2}\tau$

Table 5.1. Details of Delay shifters.

where $\psi = 2\pi d \sin(\phi)/\lambda$

and $x = 2\pi s \sin(\phi)/\lambda$

In the case of broadband array n = 8 and d, the spacing between the rows is 4 mts, and s the baseline between the N and S group is 32 mts.

The theoretical power pattern in the NS direction at four frequencies are shown in the fig 5.6. The power pattern shows a single maximum and no fringes at all frequencies. The beam width and observing time at various frequencies are given in Table 5.2

5.2.6 Bandwidth decorrelation

The discrete values of delay that result from the use of quantised delay shifters causes a difference between the true delay required to compensate for the path length difference and the actual delay introduced. This introduces bandwidth decorrelation, pointing errors, and gain variations when pointed in different directions.

If L is the baseline of an interferometer and θ is the zenith angle, then the time delay between the signals arriving at the two antennas is given by

$$t = L \sin(\theta)/c$$

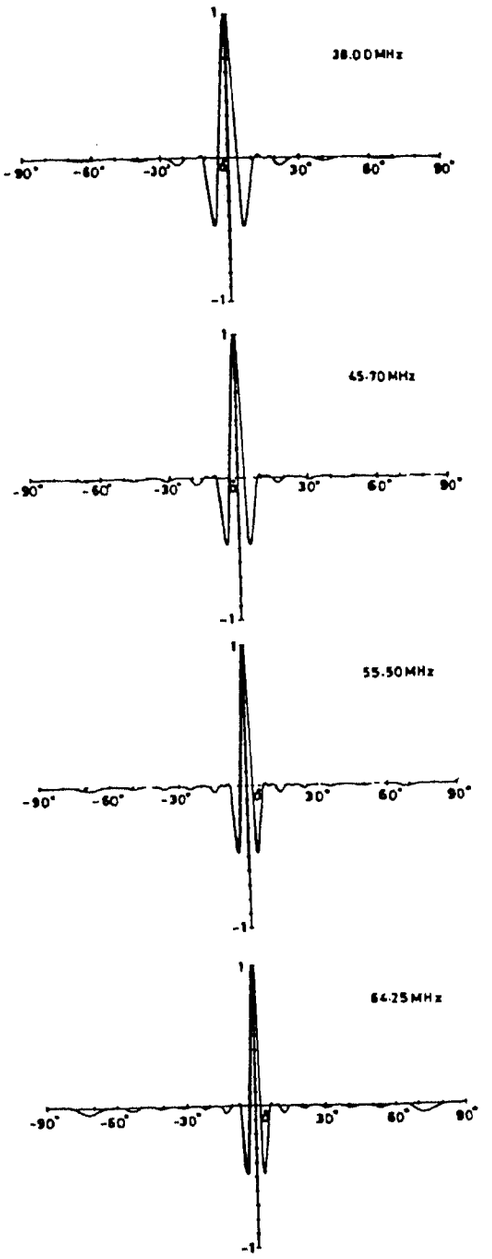

Fig. 5.6: Theoretical power pattern of the Broad band array used as a multiplying interfermeter, in the North South directions.

Frequency (MHz)	HPBW (deg)		Observing time (min)
	EW	NS	
36.25	12.27	7.60	50
45.70	9.55	5.96	38
55.50	7.85	4.88	31
64.25	6.61	4.13	26

Table 5.2. Beamwidth at different frequencies.

where c = velocity of light

If τ is the delay introduced to compensate the path length then the error in delay is given by

$$\Delta\tau = (t - \tau) \text{ sec.}$$

The decorrelation factor R over system bandwidth is given by Christiansen & Hogbom (1969)

$$R = \sin(\pi B \Delta\tau) / (\pi B \Delta\tau)$$

For B = 30 MHz and $\Delta\tau = 0.77 \times 10^{-8}$ (the maximum possible time delay error in the broadband array) the value of R is 0.91. We can neglect this effect of small decorrelation.

5.2.7 Sensitivity

Sensitivity is a measure of the weakest signal a radio telescope can detect . Even in the absence of any radio source in the beam of the radio telescope the output of the receiver will not be steady and will have fluctuations. This fluctuations are produced by the noise inherent in the system. The amount of fluctuation is given by

$$T = M \frac{T_{sys}}{\sqrt{Bt}}$$

where T_{sys} is the system temperature (deg K)

$$T_{sys} = T_{sky} + T_{Rcvr}$$

T_{sky} is the noise cortibuted by the radio sky

T_{Rcvr} is the noise contributed by the receiver system,

B is the predetection bandwidth (cps)

t is the post detection integration time (sec)

and M is a multplication factor which depend on the receiver

At meter wavelengths the T_{sys} is mainly due to the sky noise, which is due to the synchrotron radiation produced by the relativistic electrons gyrating in the magnetic field of our galaxy. One can associate an equivalent black body temperature with this radiation and this value varies depending on the frequency of observation and direction in the sky.

With a flux density spectral density index α the sky temperature at low frequency can be expressed as

$$T(f)_{sky} = 20\ (408/f)^{2+\alpha}$$ (Perley & Erickson 1984)

where f is the frequency in MHz and α is the spectral index.

For α= 0.75,the value of T_{sky} is 3100^{o}K at 65 MHz and 17000^{o} K at 35 MHz. Since the receiver

temperature is much less than these values it is clear that system temperature will be dominated by the continuum radiation from the galatic background.

The minimum detectable flux density for a point source is given by (Christiansen & Hogbom 1969)

$$S_{min} = \frac{5\ Ks\ 2k\ Tsys}{Ae\ \sqrt{Btn}}$$

T_{sys} = 3100° K at 65 MHz

= 17000° K at 35 MHz

B = 1 MHz

t = 100 msec

Ks = 2 for phase switching receiver

k = 1.38×10^{-23} joule /Kelvin

Ae = 2000 m^2

S_{min} = 150 Jy at 65 MHz

= 800 Jy at 35 MHz.

5.3 Receiver system

The signal output from the N and S groups are split into four channels,centered around 35,45,55, and 65 MHz with a bandwidth of 2 MHz. These bands were found to be interference free most of the time. The signals at the corresponding frequencies are correlated

using phase switched receivers. Fig. 5.7 shows the block diagram of the receiver. The receiver at 35 MHz is described here. The signal from the N and S groups pass through front end filters centered around 35 MHz with a bandwidth of 3 MHz. The signal is then amplified by a broad band amplifier of 28 dB gain. The amplified signal from the N group is phase switched and added to the amplified signal from the S group. The added signal is mixed with strong Local oscillator signal at 65 MHz. The IF signal at 30 MHz is passed through a filter centered around 30 MHz with 1 MHz bandwith and is further amplified by a tuned amplifier. The amplified IF signal is detected in a square law detector and is passed through a phase sensitive detector and integrator. The intergated signal is recorded both in analog and digital form. The other channels are similar except for the front end filter and local oscillator. The switching frequencies of the four channels are made different to avoid cross talk between the channels. The post detection time constant can be varied from 100 msec to 1 sec.

The digital form of recording is done using a microprocessor based system which can acquire signals upto a bandwidth of 30 KHz with programmable sampling interval from 1 msec to 500 msec in step of 1

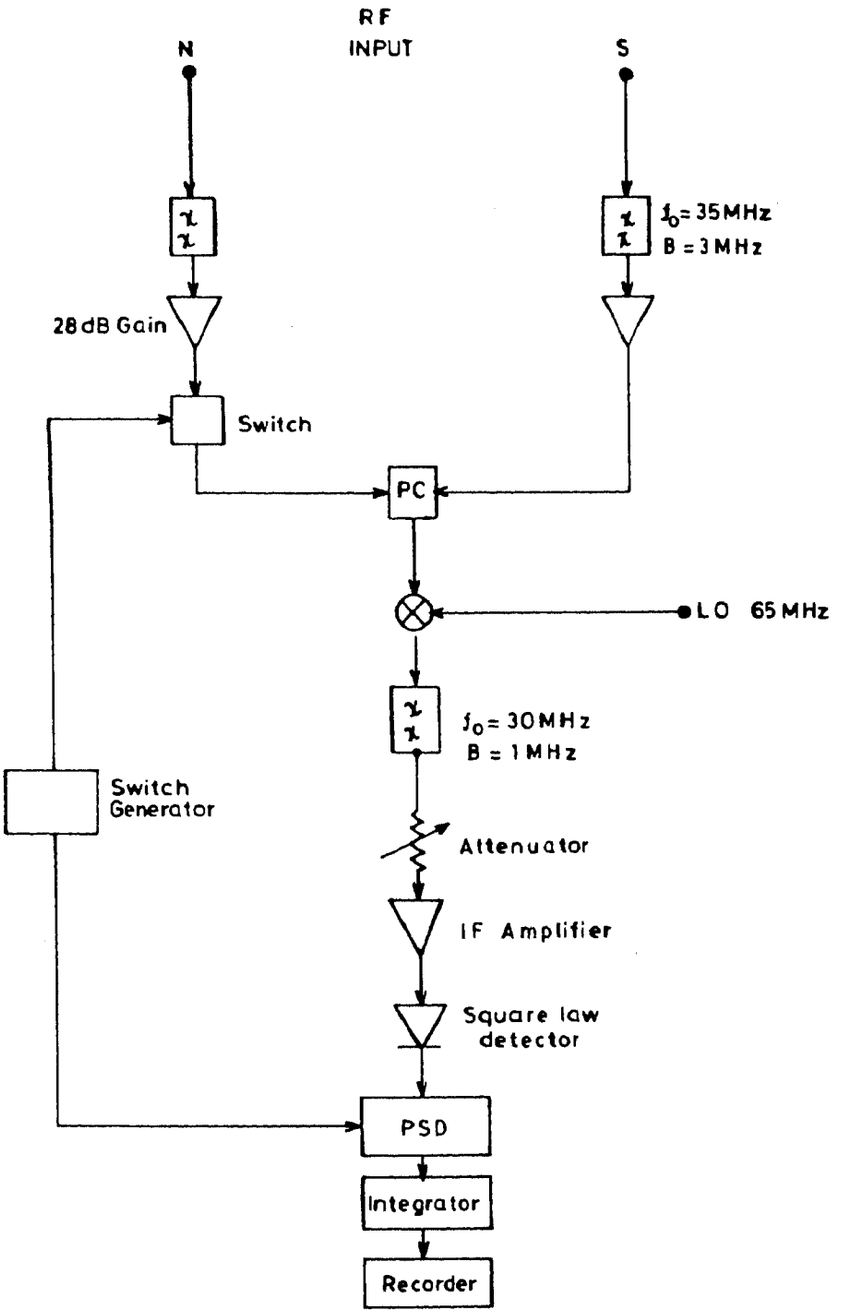

Fig. 5.7: Block diagram of receiver system operating at 35 MHz.

msec. This system is interfaced to a magtape unit. A maximum of 32 channels can be recorded a with sampling of 30 microsec/channel.

5.4 Performance

The system described above is used for the study of

(i) Continuum emission from the undisturbed sun

(ii) Fine structure of solar bursts

(iii) Scintillation of radio sources

and (iv) pulsars

Fig. 5.8 shows a typical scan of the continuum emission from the radio source 3C 218 at four frequencies. The scans of undisturbed sun at four frequencies are calibrated using the responses from point sources of known flux densities which lies close to the position of sun,and will be discussed in the next chapter. Fig. 5.9 shows a typical analog record of solar burst. Type III burst is seen at all four channels with type IIIb only at 36.25 MHz. An acousto optic spectrograph will be used for high resolution study of these fine structures in future.

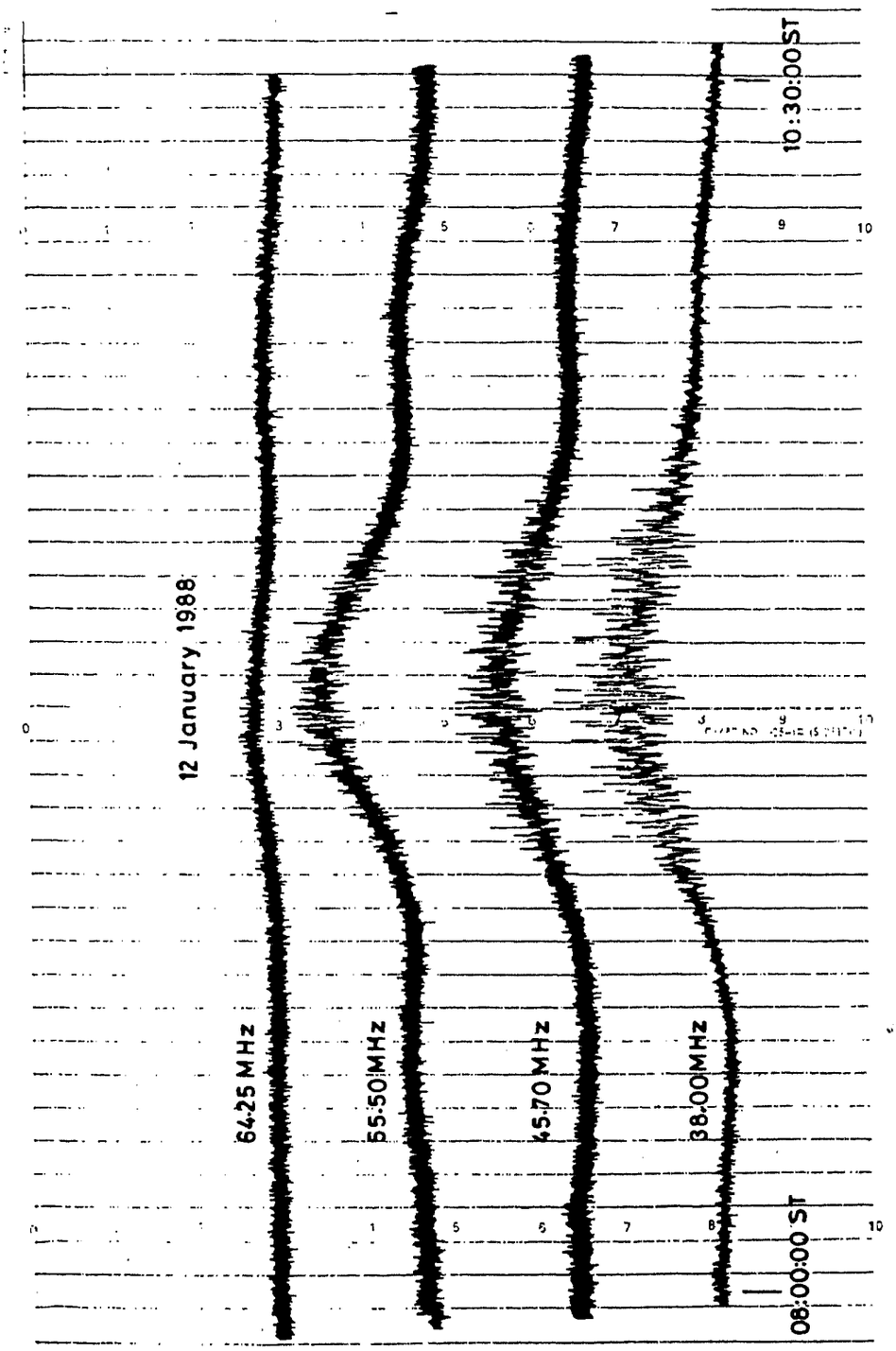

Fig. 5.8: Analog records of the Radio emission from 3C 218 at four frequencies.

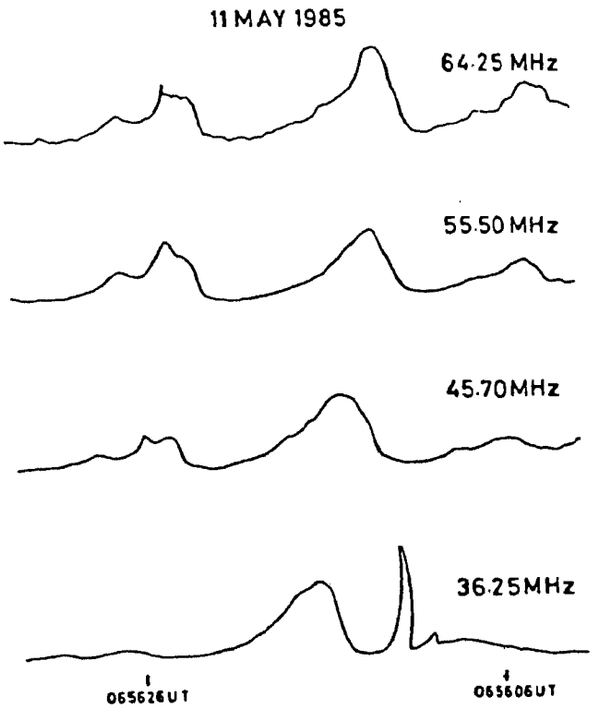

Fig. 5.9: Analog record of radio bursts from the sun at various frequencies.

CHAPTER 6

SPECTRUM OF THE CONTINUUM EMISSION FROM THE UNDISTURBED SUN

6.1 Introduction

The solar corona being a hot body at million degrees temperature is expected to emit thermal emission. It is expected to emit waves at radio wavelengths with an intensity depending on the temperature according to black body radiation laws. The radiation from the quiet sun is the radiation when there are no active regions on the sun. The identification of the base level of the quiet sun at centimeter and decimeter wavelengths is straightforward near the solar minimum when there are no active regions on the sun. The solar flux density at these wavelengths are large relative to the background sky. From a series of daily measurement of the solar flux, minimum baselevel can be determined. At meter, decameter wavelengths the measurement of quiet sun flux is difficult since most of the time intense radio bursts of nonthermal origin occur and are superimposed on the

quiet sun radio emission . Also the sky background temperature is large compared to quiet sun emission. However few decameter wavelength measurements of the solar brightness temperature were done in past years.

(i) Aubier et al (1971) have measured the flux density of the radio sun at 60,36.9 and 29.3 MHz using the Arecibo radio telescope during solar maximum. The flux density measured was 0.33,0.40 and 1.03 solar flux units (1 solar flux unit = $10^{-22} Wm^{-2}Hz^{-1}$) at 29.3,36.9 and 60 MHz. The coronal temperature deduced from these flux densities are of the order of $0.5 \times 10^{6} K$. The low temperature values obtained are explained due to the effect of scattering by an irregular corona.

(ii) Erickson (1977) has determined at decameter wavelengths the spectrum of quiet sun in the frequency range of 109 -19 MHz. The flux density of the quiet sun has been compared with that of strong radio sources such as Taurus A and Virgo A. The spectral index of the quiet sun at solar minimum was found to be about + 2.3 in the frequency range of 109 - 19 MHz.

(iii) Kundu et al (1977) have made use of the meter and decameter observations of the quiet sun on a few days in 1975 and 1976 using the Clark Lake radio telescope to obtain the solar brightness distribution. The slowly varying component (SVC) was first identified

in the decameter wavelengths range.

(iv) Sastry et al (1981,1983) have observed SVC at 34.5 MHz using the Gauribidanur radio telescope. It was observed that the brightness temperature varied between 0.3×10^6 to 1.5×10^6 K in a time scale of few days.

Measurements of the quiet sun emission are of considerable importance since they provide information on the kinetic temperature and shape of the corona. By using different frequencies in the cm,decimeter and meter wavelengths one can obtain densities and temperature in different layers of the solar atmosphere. Multi frequency observations at decameter wavelengths are important, since these radiation originate in the outer corona, where optical observations are difficult because of the very small optical luminosity of these regions.

Very few measurements of the flux densities and spectra of the low frequency (<100 MHz) radio emission from the undisturbed sun have been made on a synoptic basis. The radio emission from the undisturbed sun is defined as the emission from the sun when no burst activity is seen. The difficulties in making low frequency measurements are

(i) At low frequencies the sky background temperature rises, whereas the solar brightness temperature decreases.

(ii) Few calibrator sources with accurately determined spectra are available.

(iii) The calibrator source generally differ in declination from the sun. Accurate determination of the gain vs zenith distance relation for the system employed is required. The determination of this relation is often difficult.

At decameter wavelengths the only measurements available are due to (i) Aubier,Leblanc & Boischot (1971) who published only one set of data at three low frequencies in the range of 60 to 29 MHz and (ii) Erickson et al (1977) who reported two sets of flux densities in the frequency range of 109 to 19 MHz and computed the spectral index. The variation of the spectral index were not investigated.

6.2 Observations

The broad band array described in the

last chapter was used to measure the flux densities of the undisturbed sun at four low frequencies in the range of 64 to 36 MHz (Subramanian & Sastry 1988). During the solar minimum period (1985 May - Sept) measurements which were made are described here. The time constant used was 1 sec for these observations. Since the sensitivity of the system is better than $\simeq$ 200 Jy at 65 MHz it is possible to detect extremely weak radio bursts from the sun. The sun was monitored continuously during the period 1985 May - Sept and for 24 days no transient burst activity was found on the sun. Fig. 6.1 shows a typical record of the undisturbed sun observed using the broadband array.

Radio sources Tau A and Virgo A were used as calibrators since their spectra are accurately known (Viner 1973) and their position is close to the sun during the above period. A least square fit was made to the flux densities given by Viner(1973) to obtain the low frequency spectra and is given by

$$\mathrm{Log}S_{144} = 3.9283 - 0.3307 \times \log f_{MHz}$$

$$\mathrm{Log}S_{274} = 5.0148 - 0.9465 \times \log f_{MHz}$$

where S is in Janskys

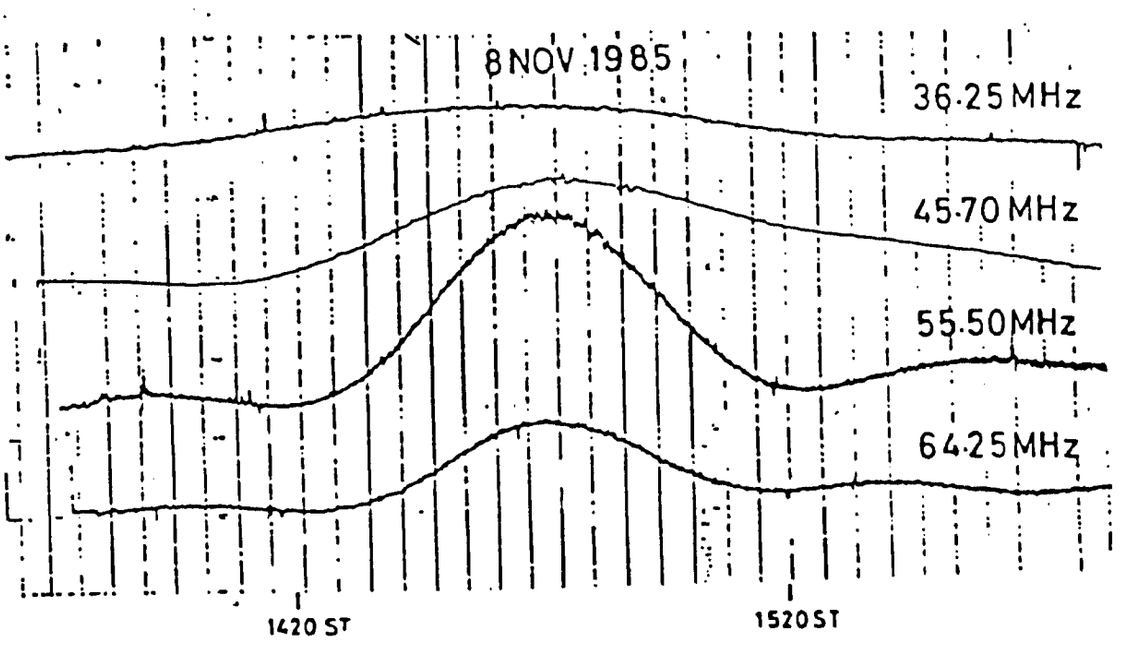

Fig. 6.1: Typical record of undisturbed sun.

The following corrections were made to the measured flux densities of the sun at various frequencies.

(i) During the entire period of observations the declination of the sun was within 5 degrees of the calibrating sources. On a majority of days the difference between the declination of the sun and the calibrator was less than 2 degrees. Corrections were applied to the change in the gain of the antenna with declination.

(ii) Due to the incremental nature of the delay shifters there was in general a difference between the setting of the beam and actual position of the source in the sky. The maximum difference is about 0.25 degrees, and correction due to this < 2 percent.

(iii) The distance between the two phase centers of the antenna in the North South direction is 32 meters and sun is slightly resolved. Visibility correction for this effect is applied and is given by

$$V_S(\lambda) = \frac{\sin 2\pi S_\lambda(\alpha/2)}{2\pi S_\lambda(\alpha/2)}$$ (Kraus 1966)

where α is the source size in radians,

and S_λ is the baseline in wavelengths.

The sun's brightness distribution is assumed to be represented by a disk of uniform temperature. Although this does not realistically represent the shape of the sun at decameter wavelengths it gives the highest value for the visibility function. The correction factor are given in Table 6.1

(iv) The major factor contributing to the error in the flux density measurement is the baseline determination in the data. The uncertainty due to this amounts to about $\simeq$ 5 percent at 65 MHz and $\simeq$ 10 percent at 38 MHz.

After taking into account all the above individual errors the total error in the measurement of the flux density is to be about $\simeq$ + 15 percent. The maximum and minimum values of the measured flux densities are given in Table 6.2. The minimum values agrees well with the spectrum given by Erickson et al (1977)

The spectral index η (defined as in the expression $S \propto f^{\eta}$) is calculated for each day using the observed values of the flux densities at four

Frequency (MHz)	Assumed solar diameter (arc min)	Visibility correction uniform disk
36.25	55	0.9937
45.70	50	0.9912
55.50	48	0.9880
64.25	45	0.9868

Table 6.1 Assumed solar diameter and visibility correction for solar disk of uniform temperature .

Frequency (MHz)	Flux density (Jy)		
	Maximum	Minimum	Average
36.25	4212	1011	2436
45.70	6135	2402	3615
55.50	10616	3598	5818
64.25	18686	5513	11784

Table 6.2 Measured maximum,minimum and average flux densities at various frequencies during the period 1985 May -Sept.

frequencies. It is found that spectral index varied from 1.6 $\pm$ 0.4 to 3.9 $\pm$ 0.7. Out of total 24 days for which the spectral index measurements are available on 18 days its value was greater than + 2.5 and on 6 days the value is less than 2.3. Fig. 6.2 shows the distribution of spectral index of the undisturbed sun during the period 1985 May - September.

6.3 Discussion

The solar radio emission in the frequency range of 35 to 65 MHz originates entirely in the corona. The total flux density of the undisturbed sun is the sum of the flux densities due to the quiet sun and the contribution due to the bright regions. Kundu,Gergely & Erickson (1977) measured the peak brightness temperature of the quiet sun and some source of slowly varying component (SVC). According to Sastry et al (1981) the continuum emission from bright regions identified as SVC at 34.5 MHz can be explained on the basis of thermal emission from regions of enhanced electron density and temperature. Erickson et al (1977) derived a spectral index + 2.3 based on observed flux densities of the quiet sun in the frequency range of 109 to 19 MHz. We have computed the total flux of the quiet sun at several frequencies in the range of 35 to

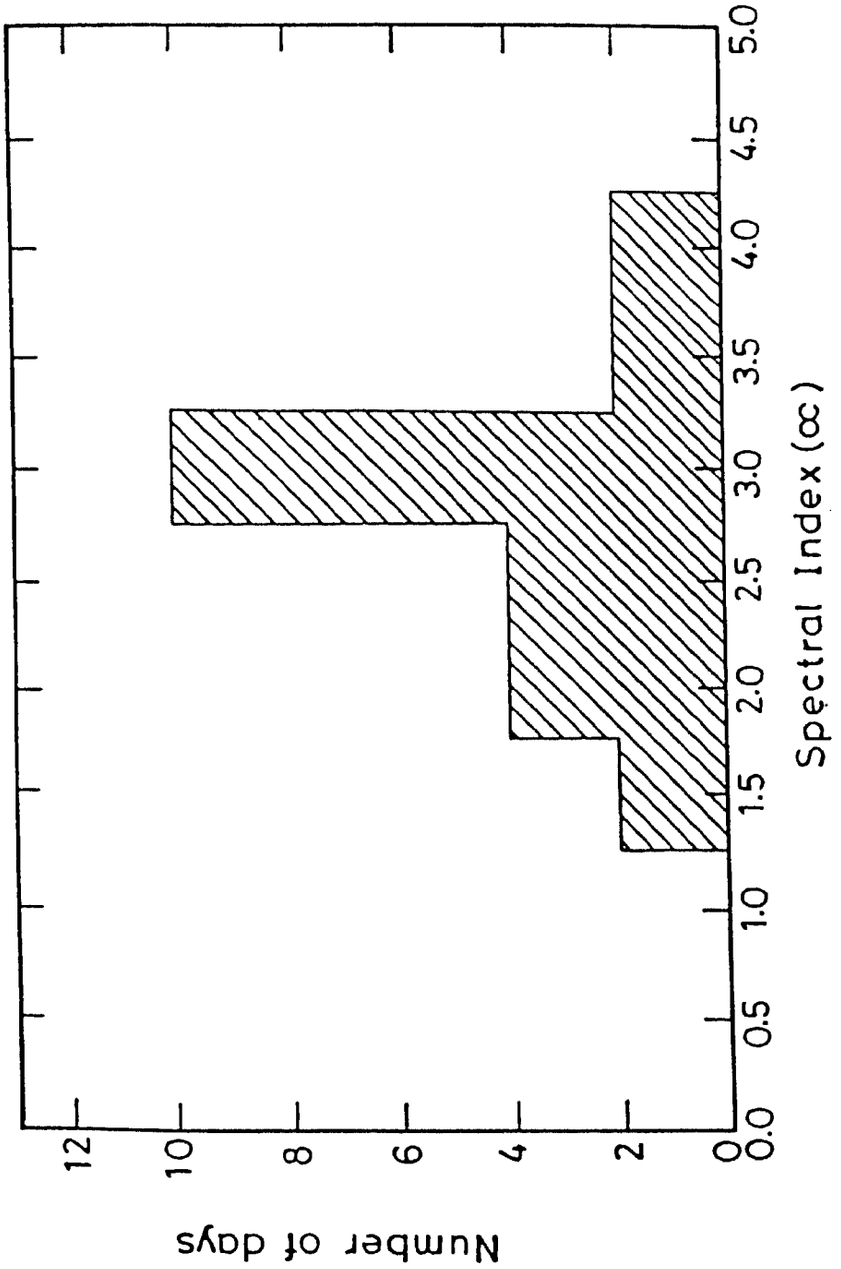

Fig. 6.2: Distribution of spectral index of the undisturbed sun during the period 1985 May - September.

65 MHz,by determining the brightness temperature T_B distribution using the equation

$$T_B(f) = T_e(1 - e^{-\tau(f)})$$

and integrated over the solid angle subtended by the sun at each frequency. Here $\tau(f)$ is the optical depth at any frequency. A spherically symmetric corona with uniform temperature $T_e(k)$ of 10^6K and density distribution of Newkirk (1961) is assumed.

The electron density distribution is given by

$$N_e(\rho) = M \times 4.2 \times 10^4 \times 10^{D_g/\rho}$$

where M is the density enhancememt factor

ρ is the distance measured from the center of the sun in solar radius

and D_g is the density gradient

= 4.32 for Newkirk's density model

The possibility of nonthermal contribution to the observed flux densities is considered. This contribution at any frequency must originate at the corresponding plasma level or above that. If it originate at the plasma level then one can consider to a first approximation that the thermal and nonthermal

contribution are mixed along the line sight. This is because the major contribution to the optical depth comes from a thin region located near the plasma level.

The equation of transfer can be written as

$$\frac{dI}{d\tau} = -I + \frac{j_T}{k} + \frac{j_N}{k} \qquad \text{-------(6.1)}$$

where j_T is the emissivity per unit volume of the synchrotron sources,

j_N is the emissivity per unit volume of thermal sources

and k is the absorption coefficient. Equation (6.1) can be written as

$$\left[\frac{dI}{d\tau} + I\right] = \left[\frac{j_T}{k} + \frac{j_N}{k}\right]$$

multiplying both sides by e^{τ}

$$\left[\frac{dI}{d\tau} + I\right] e^{\tau} = \left[\frac{j_T}{k} + \frac{j_N}{k}\right] e^{\tau}$$

$$\left[\frac{d}{d\tau} I e^{\tau}\right] = \left[\frac{j_T}{k} + \frac{j_N}{k}\right] e^{\tau}$$

$$\therefore I = e^{-\tau}\int e^{+\tau}\left[\frac{j_T}{k} + \frac{j_N}{k}\right]d\tau + Ce^{-\tau} \qquad \text{------(6.2)}$$

where C is a constant

The above integral can be integrated if $\frac{j_T}{k}$ and $\frac{j_N}{k}$ are constant. The equation (6.2) can be written as

$$I = \left[\frac{j_T}{k} + \frac{j_N}{k}\right] + Ce^{-\tau}$$

$$= \left[B(T_e) + \frac{j_N}{k}\right] + Ce^{-\tau} \qquad \text{------ (6.3)}$$

where $B(T_e)$ is Planck's radiation formulae.

Applying the boundary condition $I = 0$ at $\tau = 0$ for equation (6.3) we get

$$I = \left[B(T_e) + \frac{j_N}{k}\right]\left[1 - e^{-\tau}\right] \qquad \text{------ (6.4)}$$

If J_N is the synchrotron emission in the absence of thermal emission

$$J_N = \int j_N ds = \int \frac{j_N}{k} k ds = \frac{j_N}{k}\tau$$

Therefore $\frac{j_N}{k} = \frac{J_N}{\tau}$

$$\therefore I = \left[B(T_e) + \frac{J_N}{\tau}\right]\left[1 - e^{-\tau}\right] \quad \text{------} \quad (6.5)$$

Interms of equivalent brightness temperature using Raleigh Jean's law equation (6.5) can be written as

$$T_B = \left[T_e + \frac{T_N}{\tau}\right]\left[1 - e^{-\tau}\right] \quad \text{-------} \quad (6.6)$$

The frequency dependence of T_N and τ is given by

$$T_N = T_N f^{\beta}$$

and $\tau = \tau(f)$ respectively.

$$\therefore T_B(f) = \left[T_e + \frac{T_N f^{\beta}}{\tau(f)}\right]\left[1 - e^{-\tau(f)}\right] \text{-----} \quad (6.7)$$

Here T_N is the nonthermal brightness temperature and β is the spectral index. The above equation describes the solution of transfer equation for uniform mixing.

If the nonthermal radiation originates in front of the region of thermal radiation then the equation describing the frequency dependence of the

brightness temperature is

$$T_B(f) = T_e\left(1 - e^{-\tau(f)}\right) + \frac{T_N f^{\beta}}{\tau(f)}\left(1 - e^{-\tau(f)}\right)$$

$$= T_e\left(1 - e^{-\tau(f)}\right) + T_N f^{\beta}, \text{ for nonthermal}$$

radiation originating in front of region of thermal radiation.

In the direction of the center of the sun, the corona is optically thick ($\tau >> 1$) in the frequency range of 65 to 35 MHz for an uniform temperature of 10^6K and Newkirk's (1961) electron density distribution. Therefore the factor ($1 - e^{-\tau(f)}$) is approximately equal to unity in the above equation. The nonthermal spectral index is less than zero and can be -3 for some process like plasma emission (Kaplan & Tsytovitch 1968). It can be seen from these equation that the observed flux density should increase with decreasing frquency in the presence of nonthermal emission for both cases described above. The spectral index is not likely to attain value greater than + 2.3 positive values. This will not be the case if the nonthermal emission is confined to frequency around 65 MHz only either due to bandwidth of the emission process or the radial extent of the source. However such a situation is most unlikely since the measured sizes of bright regions are $\simeq$ 20 arc min and the bandwidth of emission is > 100 MHz (Kundu, Gergely &

Erickson 1977).

Another possibility is the existence of temperature gradient in the corona. We have assumed a temperature of 10^6K at 65 MHz plasma level and decreasing to 0.5×10^6K at 35 MHz plasma level and compute the expected flux densities from the quiet sun. In this case the spectral index turns out to be $\simeq$ + 3.0. The existence of such gradient in the coronal temperature distribution can be infered from the arguments based on the constancy of conducted energy flux. According to Athay (1976) the gradient would be about - 0.4° K / km at 1.5 $R_{\odot}$ in the case of a hydrostatic conduction model and - 0.8°K /km if coronal expansion is taken into account. Aubier, Leblanc & Boischot (1971) measured brightness temperature of 0.60, 0.50 and 0.36 ($\times 10^6$K) at 60, 37 and 29 MHz respectively and Erickson et al (1977) measured brightness temperature of 0.7 and 0.2 ($\times 10^6$K) at 74 and 26 MHz. Sastry et al measured the peak brighrness temperature in the range of 0.2 to 0.5 ($\times 10^6$ K) at 34.5 MHz. These measurements also imply the existence of temperature gradient if the corona is optically thick at these frequencies. Then the measured brightness temperatures are equal to the electron kinetic temperature. It is therefore possible that

temperature gradients of the order of -1° K /km do exist at distance of the order of 1.5 $R_{\odot}$ in the solar corona on some ocassions.

It should be also pointed out that the density model of Newkirk (1961) and others may not be applicable to the corona on some occasions. The corona could become optically thin if the density gradient is much steeper than in Newkirk's model. This would also lead to steep positive spectral indices. The variations in the spectral indices in this case would mean variations in density by a factors of 2 to 3 or more.

Another possibility is the scattering of radiation by density inhomogenities in the corona, (Aubier, Leblanc & Boischot 1971). The effect of scattering, if it exists is to raise the level of reflection above the plasma level leading to smaller optical depth at lower frequencies. The resulting decrease in the brightness temperature of the order of twenty to thirty percent, is not sufficient to explain temperatures of about 0.2×10^{6}K sometimes observed at 34.5 MHz by Sastry, Shevgaonkar & Ramanuja (1983). Also according to McLean & Melrose (1985) the scattering hypothesis fails to account for the observed sizes and directivity of Type I solar radio

bursts although it should offer a plausible explanation for these features. On this basis, the effect of scattering to explain coronal phenomena, is not favoured by many authors.

CHAPTER 7

MICROBURSTS AT DECAMETER WAVELENGTHS

7.1 Introduction

The nature of the energy releases observed on the Sun remains an outstanding problem in solar physics. The energy release from the Sun was investigated theoretically by Parker (1983). He showed that dissipation of twisted magnetic flux tubes in the photosphere lead to impulsive nonthermal energy releases which are responsible for coronal heating. Lin et al (1984) using balloon borne instrumentation of high sensitivity have detected weak hard X-rays bursts with a flux of about $7X10^{-3}$ $cm^2 s$ Kev^{-1} at 20 Kev. But solar radio bursts were reported only for a few of these hard X-ray bursts. These hard X-ray bursts are attributed to small energy releases from the Sun. These energy releases which are nonthermal and impulsive and occur at low level were investigated at radio wavelengths by Kundu et al (1986). Microbursts which appear as brief enhancement above the Quiet Sun emission and have

brightness temperature in the range of 10^6K to 10^7K were first reported by Kundu et al (1986). White et al (1986),Kundu et al (1986) and Gopalswamy et al (1987) have assumed that these microbursts are weak type III bursts. Following these investigations involving small number of events, Thejappa(1990) took up a statistical study of microbursts and compared them with those of normal type III bursts. It was found that the drift rate is somewhat lower than normal type III bursts,and source size is similar to normal type III bursts. It is required to compare all the characteristics of microbursts with those of normal type III bursts in order to identify characteristics peculiar to microbursts. Difference between the properties of microbursts and normal type III bursts should allow us to study the role of strong turbulence effects of type III bursts. The time profile of microbursts were not investigated due to the poor time resolution (1 s) of the Clark Lake system. Also the observed brightness temperature may be underestimated due to 1 s time resolution. In this chapter statistical investigation of microbursts in the frequency range of 38 to 65 MHz with 100 milliseconds time resolution are presented. The temporal, spectral and flux density characteristics of microbursts are compared with those of normal type III bursts. In

addition to confirming earlier results, new characteristics of microbursts are presented.

7.2 Observations

The present observations were made using the broad band array described in Chapter 5. The radio bursts data used in the present analysis were obtained during the period April - September 1988. About 50 microbursts used in this study were observed on March 18th,April 20th,July 14th & 15th,Aug 19th and Oct 10th 1988. Only bursts which occured within $\pm$ 5 minutes of the transit of the sun were used in the present analysis to minimise the effects of East West beam gain correction at all frequencies. Antenna gain may change with declination, and due to the difference between the setting of the beam and actual position of the source in the sky. Proper corrections were applied to counter these effects. The radio sources Tau A, Virgo A, Hydra A and Hercules A were used as calibrators since their positions were very close to the sun during the above period. Table 7.1. shows the period in which the above calibrators were used. The Sun's declination was within

Period	Calibrator used	Flux density at 38 MHz in Jy	Spectral index
Mar 28 - Apr 18 Sept 4 - Sept14	3C 348	1690	- 0.3±0.1
Apr 17 - Apr 29 Aug 14 - Aug 26	3C 274	3570	- 0.79
May 16 - Jul 23	3C 144	2430	- 1.0±0.1

Table 7.1. Calibrators used in different periods during April - Sept 1988. Their flux density at 38 MHz and spectral index between 38 and 178 MHz is also given.

2 degrees of the calibrating sources in the above period . The flux density of the calibrators at 38,45.7 ,55.5 and 64.25 MHz were calculated using their 38 MHz flux densities and a spectral index given by Kellermann et al (1969) between 38 and 178 MHz, which are also shown in Table 7.1. The spectral type of the bursts could be easlily recognised as type III from the oberved drift rates. The solar Geophysical data (SGD) were examined and found that these were not storm type III bursts. Only on oneday (Oct 20th) there was a noise storm but it occured outside the time range of our observations (06:30 UT - 07:30 UT).No H_{α} flares were present during any of our type III events.

Fig. 7.1 shows a typical drift scan of the sun. Quiescent emission with superposed bursts can be seen at all frequencies. The broad time profile is due to quiet sun (Subramanian & Sastry,1988) which is also observed ocassionally without bursts. As can be seen in the Fig.7.1 the bursts are a few times brighter than the undisturbed Sun. Since the sensitivity is better than 200 Jy at 65 MHz it is possible to detect even weak radio bursts from the sun.

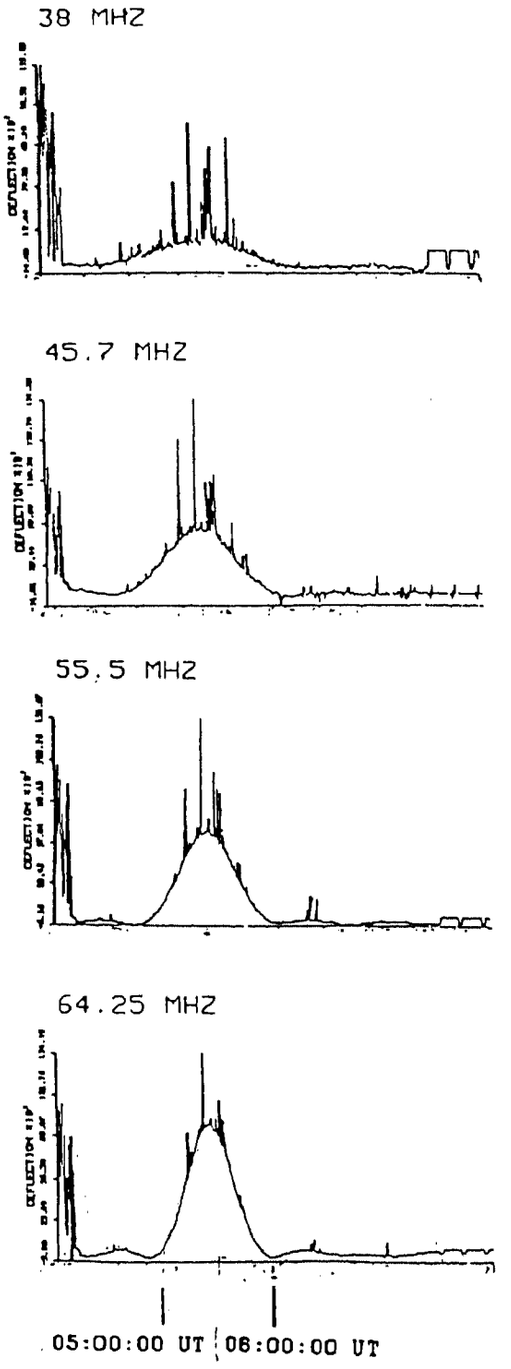

Fig. 7.1.Typical example of drift scan showing both continuum and burst emission.

7.3 Characteristics of microbursts

Fig.7.2 shows the time profile of a typical microbursts observed,with a time constant of 100 milliseconds. The time profiles of the burst are arranged in such a way that the figure mimics a dynamic spectrum. Note that at the highest frequency, the burst starts first and duration increases with decrease of frequency. Using these time profiles some of the observational characteristics of the microbursts are derived.

7.3.1 Frequency drift

The drift rate is estimated by comparing the times of peak flux density at different frequencies. The drift rate is measured only for bursts which appeared at all frequencies. From the distribution of the drift rate shown in Fig.7.3, it can be seen that most of the bursts have a drift rate in the range of - 4.5 MHz s^{-1} to - 6.5 MHz s^{-1}, with an average value around - 5.8 MHz s^{-1}.

The microbursts were found to be stationary at any given frequency (Kundu et al 1986), which

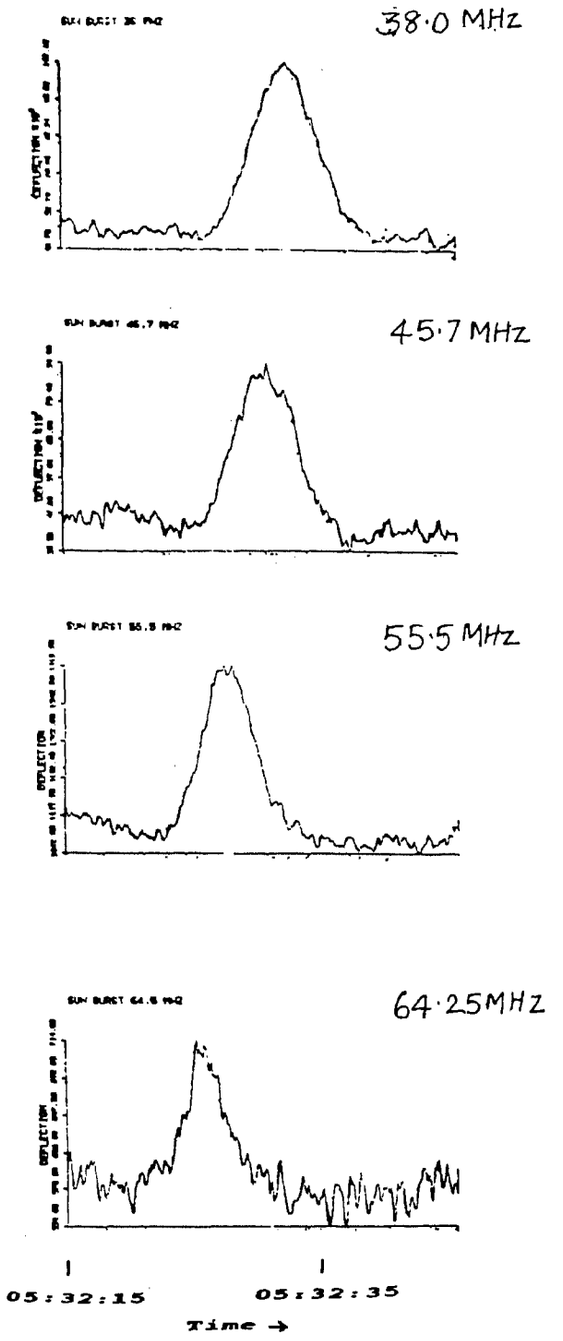

Fig. 7.2.Typical example of microburst observed on 16th September 1988, at 38, 45.7, 55.5 and 64.25 MHz.

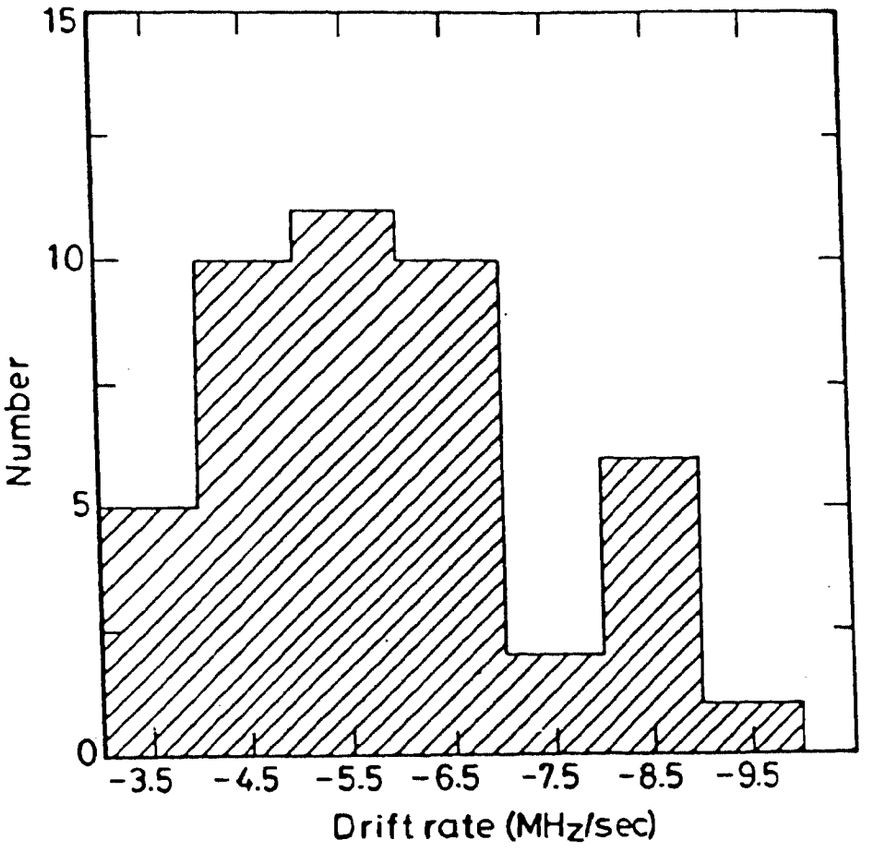

Fig. 7.3.Distribution of frequency drift in MHz/sec.

suggests that they are due to plasma emission from the layers of the corona in which w_p or $2w_p$ equals the observing frequency. The occurence of similar bursts over a wide frequency range approximately at the same time, suggests that microbursts are like type III bursts. The drift from high to low frequency is consistent with an electron beam propagating out through the corona, exciting plasma oscillations at low frequencies as the beam propagates towards outer corona.

The electron density in the corona is given by

$$N_e(\rho) = M \times 4{\cdot}2 \times 10^4 \times 10^{4{\cdot}32/\rho}$$

where M is the density enhancement factor (1-5) and ρ is the radial distance in units of solar radii. The radial velocity of the beam is related to the drift rate by the following relation given in McConnell (1981).

$df/dt = - 8.7 \times 10^2 (v/c) f (\ln(0.54f/s\sqrt{M}))^2$ MHz s^{-1}.

where s is the harmonic number (s = 1 for fundamental emission and s = 2 for harmonic emission).

Plasma emission at the second harmonic w = $2w_p$ involves coalescence of two Langumir waves to produce an observable electromagnetic wave. Because of

the large wave number of the Langumir waves they must be antiparallel or else coalescence is kinematically forbidden. The antiparallel nature of the Langumir waves are assumed to be produced by scattering of beam resonant waves off ions. This process is efficient only if scattering is induced which implies brightness temperature, greater than 10^7K (Melrose 1980). Since the brightness temperature of microbursts are less than 10^7K the emission should be fundamental (s = 1).

Kundu et al (1986) and Gopalswamy et al (1987) showed that weak type III bursts occur within or close to the edge of the dense coronal streamers where the electron density is higher than that in the corona and therefore in the electron density model given above M > 2. Table 7.2 shows the drift rate calculated at 50 MHz which is the center frequency of our observations for different values of M. The measured value of drift rate corresponds to a beam velocity of 0.2 c (c= velocity of light) which is lower than the beam velocity of type III bursts. Of course actual values of df/dt in the case of normal type III bursts have a larger dispersion and our value is within the observed scatter. Similar values were obtained for Clark Lake microbursts (Thejappa et al 1990).Moreover

v/c	drift rate (MHz s^{-1})			
	Value of M			
	2	3	4	5
0.1	3.78	3.3	2.95	2.6
0.2	7.56	6.61	5.89	5.40
0.3	11.35	9.9	8.84	8.09
0.4	15.13	13.23	11.78	10.80

Table 7.2. Drift rate of microbursts calculated for different value of exciter velocity and density enhancement factor M.

Dulk et al (1987) have estimated velocities as low as 0.14 c for type III exciters in the interplanetary medium. Hence it can be concluded that the drift rates of microbursts are similar to those of normal type III bursts.

7.3.2 Half power duration

The half power duration (hpd) of microbursts was measured from the time profile at four frequencies, with an error bar of $\pm$ 0.25 s. One can see from Fig. 7.4 that the hpd decreases with increase in frequency. The average values of hpd at 38,45.7, 55.5 and 64.25 MHz are shown in Table 7.3. For comparison the duration obtained from the relation for normal type III bursts is also given. The hpd (seconds) of type III burst scales with frequency f(MHz) as (220/f) (Suzuki & Dulk 1985). It can be seen that the hpd of microbursts agrees with that of type III bursts at 55.5 and 64.25 MHz. At lower frequencies the hpd of microbursts is somewhat smaller than that given by the empirical relation. The actual observed values of hpd used to obtain the empirical relation had considerable scatter,in the case of normal type III bursts.

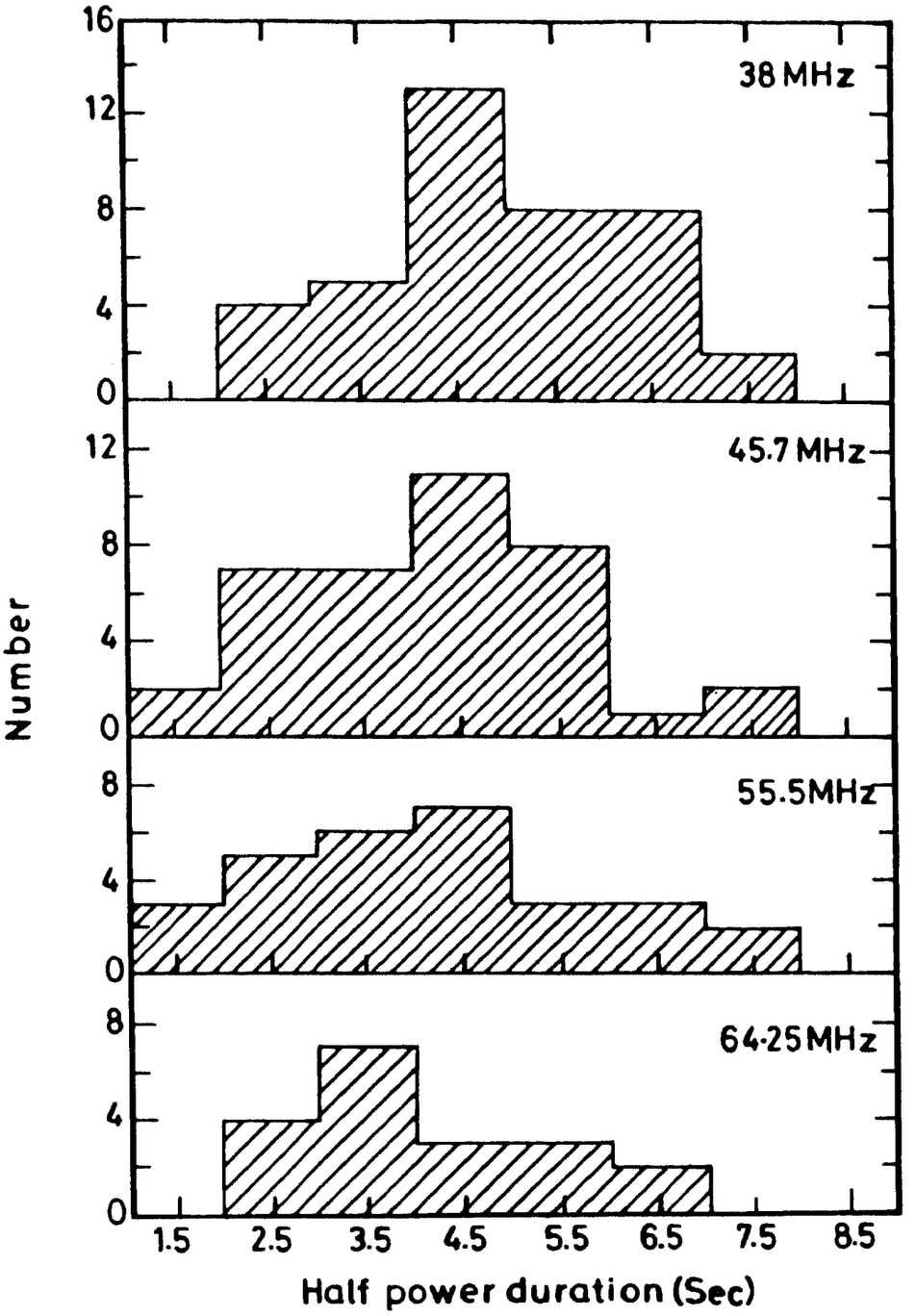

Fig. 7.4.Distribution of half power duration of microbursts at 38,45.7,55.5 and 64.25 MHz.

Frequency (MHz)	Measured flux density (Jy)			Half power duration (sec)	hpd of type III $(220/f_{MHz})$s
	Maximum	Minimum	Average		
38.00	88500	10765	31300	4.93	5.79
45.70	79090	7161	28800	4.18	4.82
55.50	58980	3311	20200	3.95	3.96
64.25	26770	1230	10069	3.69	3.43

Table 7.3 Measured maximum, minimum and average flux densities of microbursts, their half power duration,and half power duration of type III bursts, at four frequencies.

7.3.3 Time profile

Following the procedure of Aubier and Boischot (1972) the exciter duration D_e and decay time constant τ were measured for 43 microbursts. The errors in the measurement of D_e and τ were $\pm$ 0.5 s, and 0.2 s respectively. The value of D_e and τ vary from burst to burst. The average value of D_e is about 7.95 s at 38 MHz decreasing to about 6.84 s at 45.7 MHz. The average value of decay time constant is about 1.89 s at 38 MHz decreasing to about 1.4 s at 45.7 MHz. The number of good time profiles at 55.5 and 64.25 MHz were small and so statistical analysis was not made. The average value of D_e and τ of microbursts are plotted against frequency along with the corresponding plots for normal Type III bursts as given by Aubier and Boischot (1972) and Barrow and Achong (1975) and is shown in the Fig 7.5. The value of D_e and τ of microbursts lie close to that of type III bursts. All of the .values of D_e and τ for four frequencies are plotted in a single diagram and is shown in Fig. 7.6., together with the least squares fit for these points. The correlation coefficient between D_e and τ is 0.56 for which 95% confidence limits are 0.32 and 0.72. In the case of

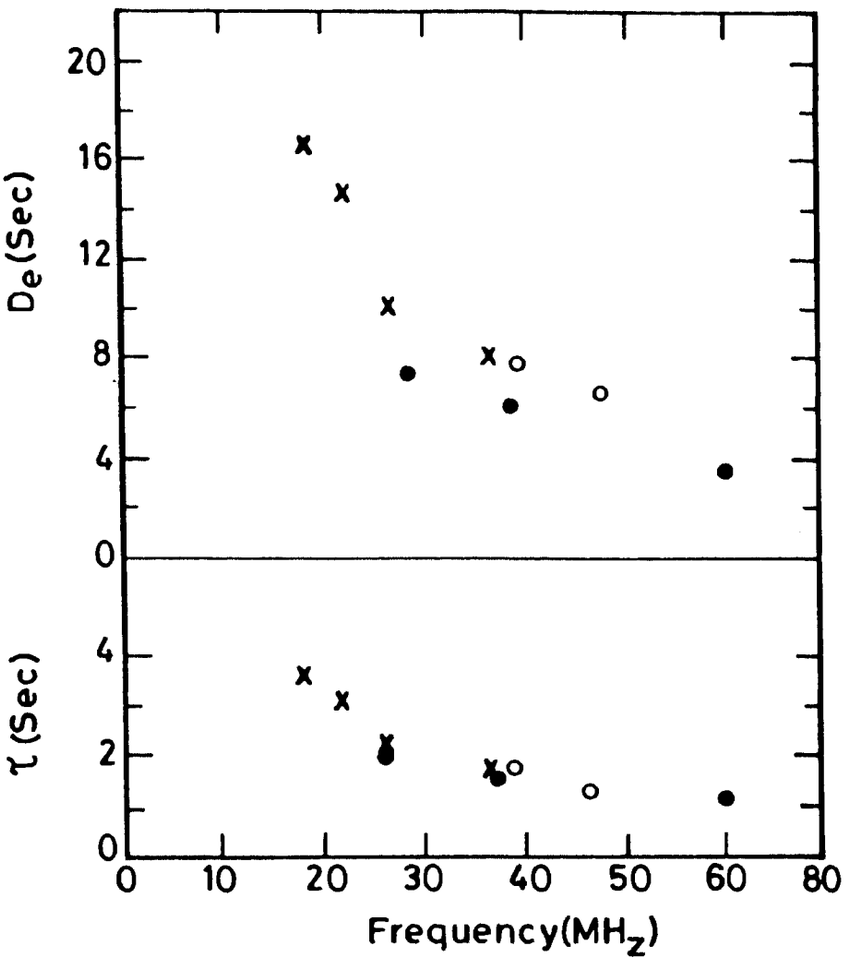

Fig. 7.5. Plot of average values of D_e and τ of microbursts against frequency (open circles) compared with value of D_e and τ for type III bursts given by Aubier and Boischot (1972)(Dark circles) and Barrow and Achong (1975) (crosses).

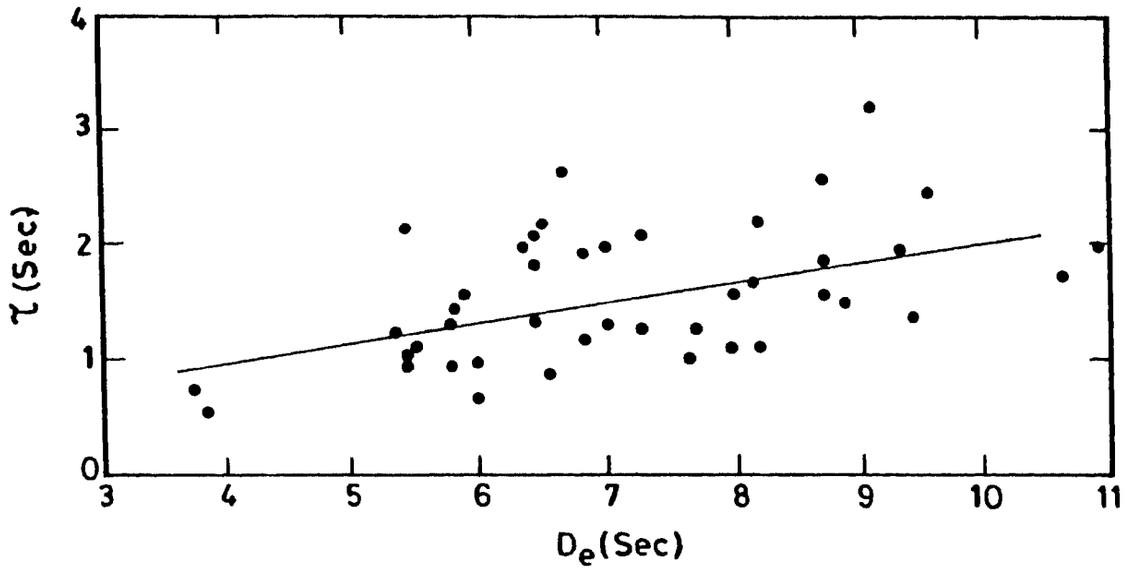

Fig. 7.6. Correlation between D_e and $\bar{\tau}$ (all frequencies combined) and least square fit.

normal type III bursts Barrow and Achong (1975) have found that $D_\bullet$ and τ are correlated with a linear correlation coefficient of 0.63. Subramanian et al (1981) have also found that in the case of normal type III bursts $D_\bullet$ and τ are correlated with a linear correlation coefficient of 0.7. We find that the correlation coefficient is slightly smaller for microbursts. These characteristics are determined by the collision frequency in the coronal plasma and the extent of the exciting beam. Hence It can be concluded that the electron beam responsible for microbursts are similar to those exciting normal type III bursts.

7.3.4 Peak flux density

At meter and decameter wavelengths Culgoora and Clark lake radio telescope were used to measure the brightness temperature and size of the solar radio bursts. From the observed brightness temperature and size the flux density can be calculated. The observed size may not be the true size due to scattering and wave ducting (Duncan 1979;Kundu & Gopalswamy, 1990) so that the flux density calculated may not be the true flux density. Since most of the type III characteristics were obtained using non-imaging telescopes , it is important to

obtain accurate flux density measurements for a better comparison. Accurate values for the peak flux density of 50 microbursts at 38,45.7,55.5 and 64.25 MHz were obtained by calibrating their peak amplitude with that of radio sources which lie close to the sun. Fig. 7.7 shows the distribution of peak flux density at different frequencies. The peak flux varied by a factor of $\simeq 10$ at any frequency. The error in the measurements are 10% at 38 MHz and 15% at 64.25 MHz. Table 7.3 shows the maximum , minimum and average values of the measured flux densities at different frequencies . Since spatial information were not obtained for these bursts, the peak brightness temperatures were calculated indirectly using the observed peak flux densities and assuming source size. The size of microbursts were shown to be the same as that of type III bursts (Thejappa et al 1990). Assuming the size of microbursts as 7 arc min at 65 MHz and 18 arc min at 38 MHz , We obtain brightness temperatures of the order of 10^7K, agreeing with Clark Lake values. Thus the microbursts seem to be low frequency extension of the brightness temperature spectrum of type III bursts.

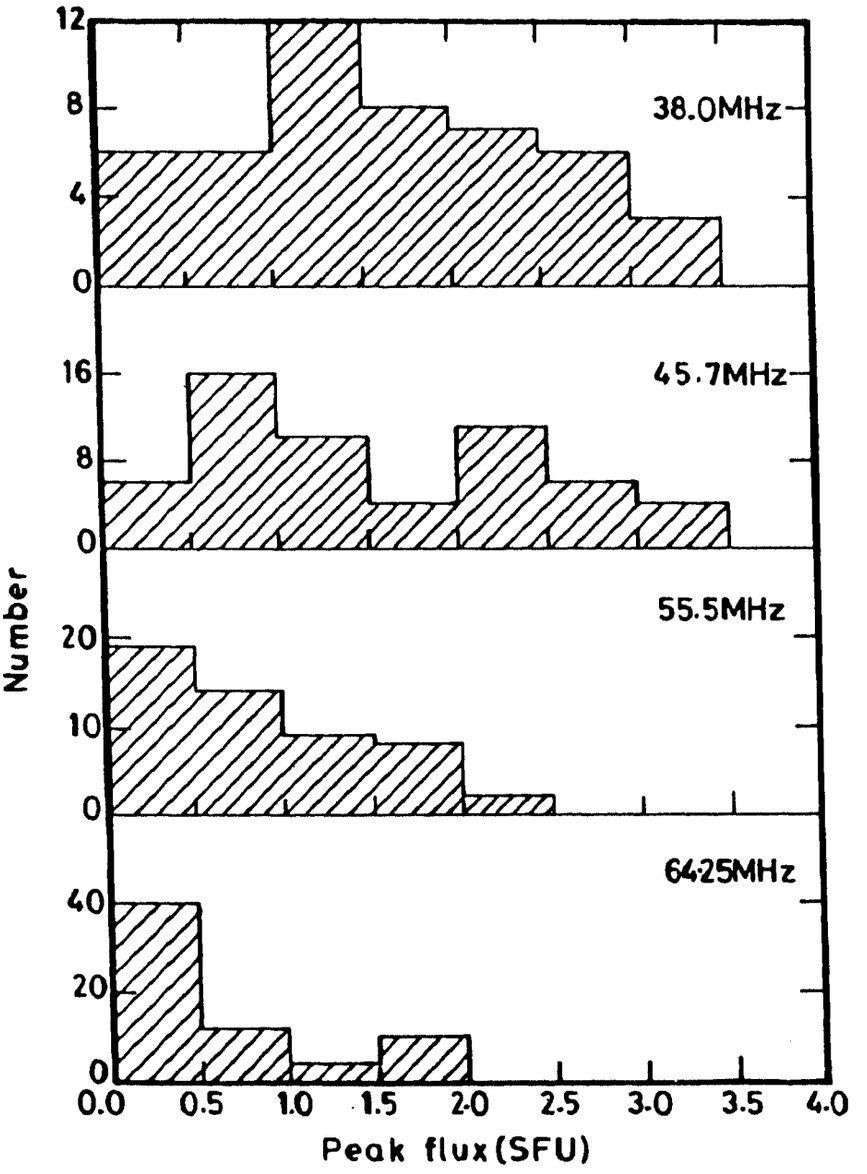

Fig. 7.7. Distribution of the peak flux density of microbursts at 38,45.7,55.5 and 64.25 MHz.

7.3.5 Peak flux density spectra

From the observed flux densities at four frequencies two major types of spectra were found. (i) Straight spectra and (ii) Curved spectra.In the case of straight spectra the spectrum over the whole frequency range can be described by a simple power law so that log(S_f) plotted against log(f), the data lie on a straight line. Fig. 7.8 shows a typical spectrum.The spectral index n (defined as in the expression $S \propto f^{n}$) varied from -2 to -6 and the average value is - 4.65 $\pm$ 1.6. The spectral index for type III bursts calculated from the average flux density at 169,80,and 43 MHz (Suzuki & Dulk 1985) gives a value of -4.6. In the case of curved spectra, spectral peaks were found to occur at 45.7 or 55.5 MHz. Fig.7.9 shows a typical example. Weber (1978) has found spectral peaks in the case of interplanetary type III bursts. Out of 50 microbursts we have studied 24 bursts showed straight spectra, 13 bursts showed peaks at 45.7 MHz 10 bursts showed spectral peaks at 55.5 MHz and 3 bursts showed zig zag spectra.

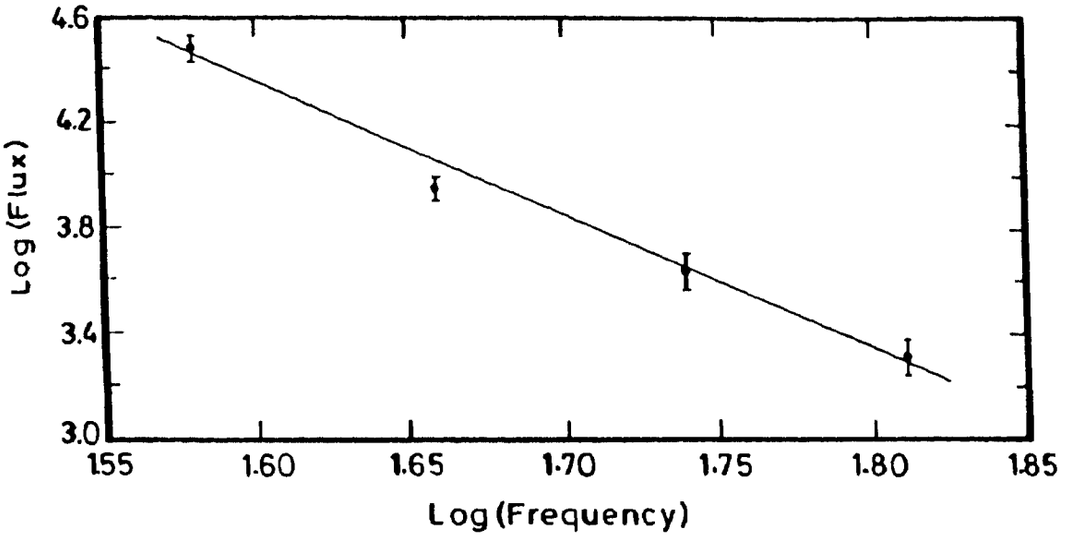

Fig. 7.8.Peak flux density spectra of microbursts showing straight spectra.

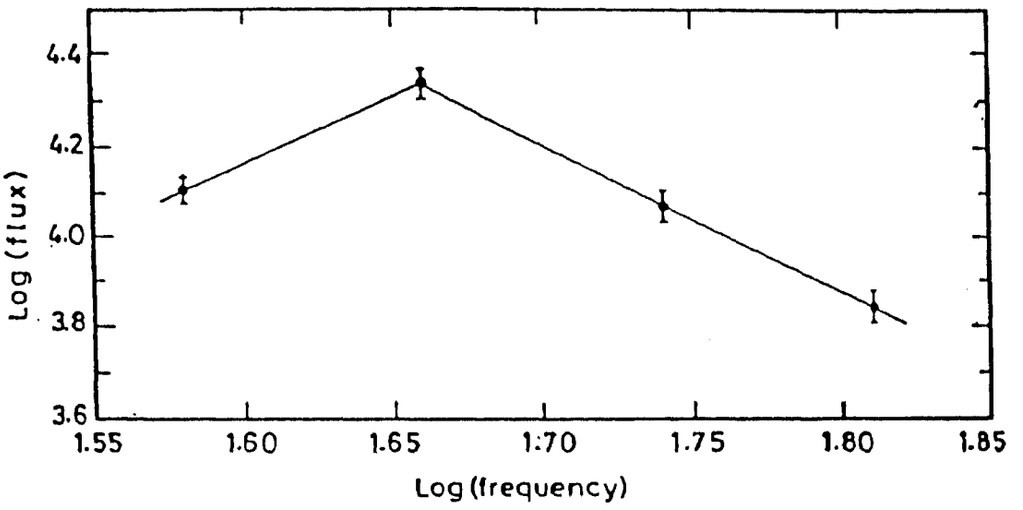

Fig. 7.9. Peak flux density spectra of microbursts showing curved spectrum.

7.3.6 Energy spectra

To study the variation of the amplitude of bursts with frequency in a way which is independent of time, we can evaluate the total energy per unit frequency interval that flows normally through unit area at the earth during the burst, which is given by $E_f = \int S_f dt$ where S_f is the intensity at frequency f and dt is duration of the burst. Wild (1950) was the first to determine the energy spectra of type III burst in the frequency range of 70 to 120 MHz. Elgaroy (1972) measured the energy of type III bursts at 225 MHz and found that the energy in the frequency range of 3.5 MHz to 225 MHz (Haddock and Graedal 1970) can be expressed by a relation of the form $E_f \propto f^{-n}$ where $2.8 < n < 3.6$. Below 70 MHz there are no measurements of the energy spectra of solar radio bursts. The energy of microbursts at 38, 45.7, 55.5 and 64.25 MHz were obtained by intergrating the time profiles at the corresponding frequencies.

Fig. 7.10 shows the energy spectra obtained by plotting the average energy at each frequency against frequency, also and least square fit. The value of n in the expression $E_f \propto f^{-n}$

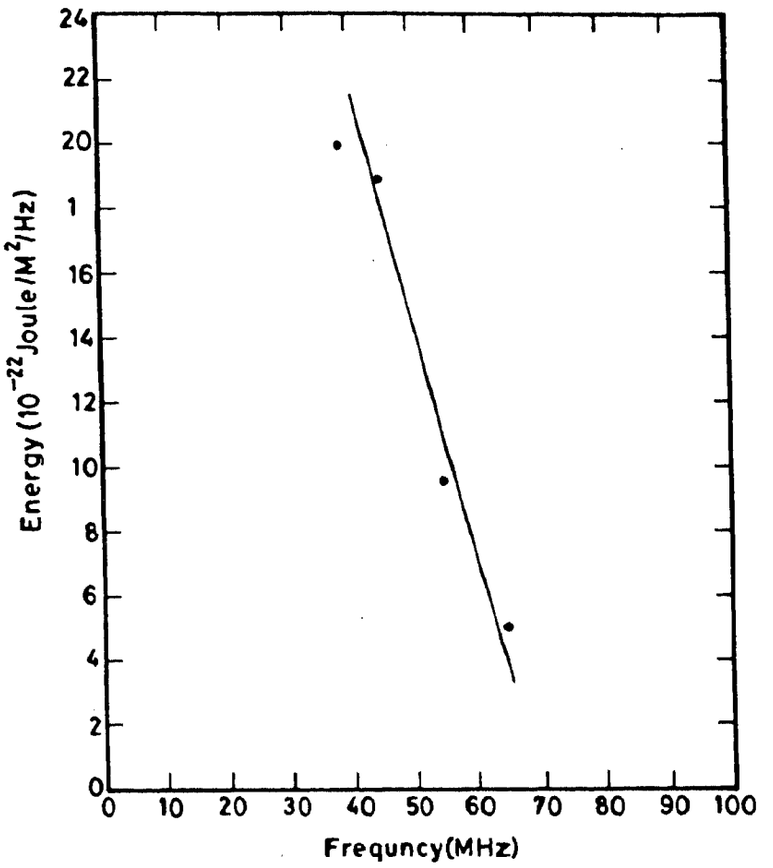

Fig. 7.10 Average energy spectrum of microbursts.

is 2.62 $\pm$ 0.12 ,which is slightly lower than the value of n for type III bursts obtained in the frequency range of 3.5 MHz to 225 MHz.

7.4 Discussion

The time profile characteristics of microbursts agree with that of type III bursts. Microbursts have characteristics similar to type III bursts in the shape of the flux density spectrum and and the value of the spectral index. But the exciter velocity and brightness temperature are lower compared to type III bursts.

Micobursts can not be produced by induced scattering of Langumir waves off ions since the brightness temperature of microbursts are below the threshold value. The induced scattering is important when the effective temperature of the transverse wave exceeds a threshold value T_0. The threshold value is given by $T_0 = \omega' T_i / \Delta\omega$,where ω' is the frequency of the scattered wave, $\Delta\omega$ is the bandwidth of emission and T_i is the temperature of the scattered particle. For scattering off Langumir waves into fundamental transverse waves

$$T_0 \approx V_\phi T_i / V_i$$

since $\Delta\omega \approx \omega_p V_i / V_\phi$, $\omega' \approx \omega_p$

For $V_\phi = 0.3c$ and $T_i = 10^6 K$, $T_0 \approx 3 \times 10^9 K$.

Since the observed brightness temperature of microbursts is $10^6 K$, induced scattering off ions is not the likely candidate for beam stabilization. Models without a threshold such as quasi-linear theory with effficient absorption, but with out any plateau formation can explain the microbursts. The quasi-linear model is valid for weak beams. (Low n_b/n_e, v_b; Galeev et al 1977). In the quasi-linear model the beam relaxes to a plateau distribution and get stabilized by the particles trailing behind the front of the beam (Zaitsev 1972;Takakura and Shibahashi 1976; Magelssen and Smith 1977). In the quasi-linear theory the wave energy density is comparable to the energy in the stream when plateau is formed. Maglessen and Smith (1977) found that the wave energy W^1 is $\approx$ 10% of the beam energy $n_b m v_b^2/2$.

Then $W^1/n_e T_e = n_b v_b^2 / 20 n_e v_e^2$

If microbursts are radiation at the fundamental

frequency and are due to the scattering of plasma waves on ion density fluctuations of the background the brightness temperature is given by (Zaitsev & Stepanov 1983) as

$$T_b = 3 \times 10^{15} W^l / n_e T_e$$

For microbursts $T_b \approx 10^6 K$ and therefore $W^l / n_e T_e$ is 10^{-9}. For such beams the growth rate is not very fast enough for relaxation to occur and plateau distribution do not occur. Velocity dispersion can limit the growth of plasma waves at any point in space to a level below saturation.

The other possibility is that the beam growth can be effectively balanced by angular diffusion of plasma waves due to inhomogenities present in the corona. The scattering from inhomogenities can slow down the quasi-linear relaxation process according to Escande and de Genoulla (1978). Muschietti et al (1985) have shown that large scale density fluctuations of the order of 10^{-2} may be extremely effective in shifting waves out of resonance with the beam and therefore in quenching the instability in the case of interplanetary type III bursts. Density inhomogenities of the order of 10^{-2} have been proposed by Steinberg (1971) and Riddle (1972) to

explain the observed source size and height of F-H pairs. Therefore the presence of such inhomogenities in the corona can stabilize the beam in the case of microbursts.

The power emitted by the electron stream of the microburst is calculated now. The angular size of microbursts at 50 MHz was shown to lie between 10.5 arc min to 16.5 arc min by Thejappa et al (1990). Assuming a circular source size of 13.5 arc min , the area of microburst at 50 MHz is about 10^{22} cm^2.The length of the stream may be identified as the persistence time of the burst at any fixed frequency times the velocity of the stream. For microbursts this estimate gives (15secx0.2c) $9X10^{10}$ cms. Therefore the volume of the stream emitting microburst is $10^{33} cm^3$. Since the ratio of density n_b/n_e is about 10^{-8} for microburst (Thejappa 1990),at 50 MHz (n_e = $3X10^7$ cm^{-3}) n_b is $\approx$ $3x10^{-1} cm^3$. For microbursts the number of electrons in the stream is $3x10^{32}$ The power generated spontaneously by an electron in Langumir waves with speed v_b is given by Melrose (1976) as

$$P = e^2(w_p^2/v_b)\ln(v_b/v_e)$$

$$= 1.5x10^{-20} f_p^2 \text{ ergs } s^{-1}$$, where f_p is in MHz, v_b= 0.2c and v_e = $5.4x10^8$ cm/sec for T_e =

10^6K . With $3x10^{32}$ electrons for a stream at plasma level f_p, the total power generated spontaneously in Langumir waves would be 10^{16} erg s^{-1}. So the streams producing microbursts are much weaker than type III bursts which are known to carry 10^{19} to 10^{20} erg s^{-1}.

CHAPTER 8

CONCLUSIONS

In the introduction it was indicated that high time and frequency resolution studies of solar radio bursts at decameter wavelengths are important since they serve as tracers for spatial structure and magnetic field configuration in the outer corona which are inaccesible to optical techniques.

In the second chapter the time structure of type IIIb burst and type III burst were studied. The time profile of type IIIb burst was compared with that of associated type III burst. It was shown that the time profile of type IIIb burst is asymmetric with a sharp rise and a slow decay, similar to type III burst. It was also shown that the duration of type IIIb burst and the associated type III burst are correlated showing the close relation between type IIIb and the associated type III burst. A theoretical model to explain the various aspects of type IIIb burst was presented . The important feature of this model is the direct excitation of the normal electromagnetic modes.

By comparing the time profiles of isolated type III bursts and type IIIb associated type III bursts, it was shown that the exciter duration and decay time constant were correlated in the case of isolated type III bursts and lack off correlation was found in the case of type IIIb associated type III bursts. The correlation in the case of isolated type III burst and lack of it in the case of associated type III bursts was suggested due to the different nature of the exciter in the two cases.

In the next chapter the south arm of the Gauribidanur radio telescope and an eight channel filter bank receiver system built for the study of the fine structure emission of solar radio bursts were described. The system has the sensitivity to study weak (3 SFU) solar radio bursts.

In the fourth chapter, fine structure emission of solar radio bursts observed using the system described in the previous chapter was presented. The main feature of the pulsating bursts reported, were that these pulsations predominantly occured in the saturation phase of the bursts. The temporal and intensity characteristics of pulsating

bursts were presented. These results were explained on the basis of wave - wave interactions. For the first time spectral features of spike bursts at decameter wavelengths were presented. The magnetic field strength in the outer corona was derived from the bandwidth and drift rate of these spike bursts. The magnetic field strength (1 Gauss) derived is in close agreement with other estimates obtained from frequency splitting and polarisation measurements of type I radio bursts. From the time profiles of diffuse echo bursts at 34.5 MHz, the distance between the plasma layers corrsponding to 17.25 MHz and 34.5 MHz, was derived, which agrees with the standard electron density models of the corona.

In the fifth chapter, the importance of studying the solar radio bursts over wide bandwidth was explained. The broadband array built specially for the study of solar radio emission in the frequency range of 35 to 70 MHz was described. The system has the sensitivity to observe strong radio sources which can be used to calibrate the radio emission of the sun.

In the sixth chapter the low frequency radio spectra of the continuum emission from the

undisturbed sun in the frequency range of 35 to 70 MHz was obtained from observations made using the Broadband array. The difficulties of making low frequency measurement of the undisturbed sun were explained. It was found that the spectral index varied from 1.6 $\pm$ 0.4 to 3.9 $\pm$ 0.7. It was shown that either temperature gradient of the order of 1^{o}K / Km in the outer corona or density enhancement by factor of two or three can explain the steep value of the spectral index observed.

In the next chapter the characteristics of microbursts were compared with those of type III bursts. It was shown that except brightness temperature, other characteristics of the microburst such as drift rate, half power and exciter duration, decay time constant , flux and energy density spectra agreed very well with those of type III bursts. It was shown that microbursts are low brightness temperature extension of normal type III bursts.

To study the wide and narrow band characteristics of solar bursts one requires a spectrograph with high frequency and time resolution and wide bandwidth. The acousto optic spectrograph which satisfies the above requirements will be used

in future for solar burst studies.The flux density spectra of only microbursts were obtained in the frequency range of 35 to 70 MHz, using the broadband array.Measurements of the flux densities of other solar bursts are required to understand their emission mechanisms. It is proposed to measure the flux density of solar radio bursts by using a log periodic dipole array in the frequency range of 40 to 150 MHz in future. Also position information of solar bursts at multifrequencies are required simultaneously to study the time and positional variation of several active centers .

In the case of observations on the undisturbed sun, it was not possible able to resolve the sun, due to the poor angular resolution of the Broadband array. The presence of active regions and slowly varying component can be detected only if the sun is resolved. A log periodic dipole array operating in the frequency range of 40 to 150 MHz is presently being designed and is under construction. This array with an angular resolution of $6' \times 10'$ at 150 MHz will be used for mapping the radio sun which has an angular size of 2 degrees. The three dimensional structure of the sun obtained by multifrequency observation will enable us to separate the contribution from active

regions in the radio emission of the undisturbed sun. The multi - frequency observations should also result in determination of electron density in the corona on a regular basis. Position information of solar radio bursts obtained using the Log periodic dipole array will enable us to identify the active centers producing them and should result in a much better physical understanding of the varieties of the complex solar phenomena.

BIBLIOGRAPHY

Abranin,E. P.,Baselyan,L. L. ,Goncharov,N. Yu., Zaitsev,V. V. ,Zinichev,V. A. ,Rapoport,V. O and Tyskbo,Ya. G. :1980,Solar Phys. ,**66**,393.

Achong,A. :1974,Solar Phys. ,**37**,477.

Alvarez,H. and Haddock,F. T. :1973,Solar Phys., **29**,197.

Aschwanden,M. J. and Benz,A. O. :1988,Astrophys. J., **332**,466.

Athay,R. G. :1976,The Solar Chromosphere and Corona:Quiet Sun, D. Reidal,Dordrecht.

Aubier,M. ,Leblanc,Y. and Boischot,A. :1971,Astron. Astrophys. ,**12**,435.

Aubier,M. and Boischot,A. :1972,Astron. Astrophys., **19**,343.

Aubier,M. G ,Leblanc,Y. And Moller -Pedersen,B. :1978 Astron. Astrophys. ,**70**,685.

Barrow,C. H. and Saunders,H. :1972,Astrophys. Lett. **12**,211.

Barrow,C. H. and Achong,A. :1975,Solar Phys.,**45**,459.

Barrow,C. H. ,Flagg,R. S. and Perround,R. :1984,Soalr Phys. ,**90**,111.

Bazelyan,L. L,Goncharov,N. Yu.,Zaitsev,V.V., Zinichev,V. A. ,Rapoport,V. O. and Tsybko,Ya,G.:1974, Solar Phys. ,**39**,214.

Benz,A. O. ., and Wentzel,D. :1981,Astron. Astrophys., **94**,100.

Benz,A. O. ,Zlobec,P. and Jaeggi,M. :1982,Astron. Astrophys. ,**109**,305.

Benz,A. O. and Simmett,G. M. :1986,Nature,**320**,508.

Bohm,A. and Kruger,A. :1973,Report UAG 28,Part I,World Data Center,NOAA.

Boischot,A. :1958,Ann. d' Astrophys. ,21,273.

Brown,G. H. and Woodward,G. M. ,December 1952,RCA Review,VOl 13,No 4,pp 425-452.

Christiansen ,W. N. and Hogbom,J. A.,1969,Radiotelescopes, Cambridge University Press.

de Groot,T. :1962 Inf. Bull. Solar Radio Obs. Europe,9,3.

de Groot,T. :1970,Solar Phys. ,14,176.

de la Noe,J. and Boischot,A. :1972,Astron. Astrophys., 20,55

de la Noe,J. :1974 Astron. Astrophys. ,43,20.

Desphande,A. :1987,Ph. D. Thesis,Indian Institute of Technology,Bombay.

Drodge,F. and Riemann,P. :1961,Inf. Bull. Solar. Radio Obs. Europe,8,6.

Drodge,F. :1967,Z. Astrophys. ,66,176.

Drodge,F. :1977,Astron. Astrophys.. ,57,285.

Dulk,G. A. and Suzuki,S. :1980,Astron. Astrophys., 80,203.

Dulk,G. A,Steinberg,J. L,Loang,S. and Goldman,M. V.: 1987,Astron. Astrophys. ,173,366.

Duncan,R. A. :1979,Solar Phys. ,63,389.

Eckhoff,H. K. :1966,Inst. Theo. Astrophys.Rep. ,18.

Elgaroy,O. :1961,Astrophys. Norv. ,7,235.

Elgaroy,O. and Lyngstad,E. :1972,Astron. Astrophys., 16,1.

Elgaroy,E. O. ,1977,Solar Noise Storms,Pergamon press.

Elgaroy,O. and Sven,O. P:1979,Nature,278,626.

Ellis,G. R. A. and McCulloch,P. M. :1966,Nature,211,-1070.

Ellis,G. R. A. and McCulloch,P. M. :1967,Aust. J. Phys. 20,583.

Ellis,G. R. A. :1969,Aust. J. Phys. ,22,177.

Erickson,W. C. ,Gergely,T. E. ,Kundu,M. R. and Mahoney,M. J:1977,Solar Phys. ,54,57.

Escande,D. F. and de Genouillac,G. V. :1978,Astron. Astrophys. ,68,403.

Fokker,A. D. :1965,Bull. Astron. Inst. Neth. ,18,111.

Fokker,A. D. :1969,Solar Phys. ,8,376.

Fukai,J. ,Krishan,S.and Harris,E. G. :1969,Phys. Rev. Lett. ,23,910.

Galeev,A. A,Sagdeev,R. Z,Shapiro,V. D. and Stevchenko,V. I:1977,Soviet Phys. JETP,45,266.

Gopalswamy,N. ,Kundu,M. R. and Szabo,A. :1987,Solar Phys. ,108,33.

Gopalswamy,N. and Kundu,M. R. :1990,Solar Phys., 128,377.

Gotwals,B. L. :1972,Solar Phys. ,25,232.

Guidice,D. A. and Castelli,J. P. :1975,Solar Phys. , 44,155.

Haddock,F. T and Gradel,T. E. :1970:Astrophys. J. , 160,293.

Harvey,C. C. and Aubier,M. G. :1973,Astron. Astrophys., 22,1.

Heys Penfield. :1976,Mehtods of Experimental Physics,Vol 12,Part B,Academic Press. Chapter 3.4

Ichimaru.:1973,Basic Principles of Plasma physics.W. A. Benjamin Inc,Massachusettes.

Kaplan,S. A. and Tsytovitch,V. N:1968,Sov. Astron. - AJ,11,956.

Kellermann,K. I,Pauliny-Toth,I. I. K and Williams,P. J. S:1969,Astrophys. J. ,157,1.

Kraus,J. D. :1950,Antenna,McGraw Hill Book Company.

Kraus,J. D,1966,Radio Astronomy,McGraw Hill Book Company.

Krishan,V. :1978a,Astrophys. Space Sci. ,57,19.

Krishan,V. Sinha,K. P. and Krishan,S.:1978b, Astrophys. Space Sci. ,53,13.

Krishan,V. :1979,Plasma Physics,22,163.

Krishan,V.,Subramanian,K. R. and Sastry,Ch. V.:1980, Solar Phys. ,66,347.

Kundu,M. R. :1965, Solar radio astronomy,Interscience, New York.

Kundu,M. R. ,Gergely,T. E. and Erickson,W. C. :1977,Solar Phys. ,53,489.

Kundu,M. R. ,Gergely,T. E. ,Turner,P. J. and Howard,R. A. :1983,Astrophys. J. Lett. ,269,L67.

Kundu,M. R. ,Gergely,T. E. ,Szabo,A. ,Loiacono,R. and White,S. M. :1986,Astrophys. J. ,308,436.

Lacombe,C. and Moller-Pedersen,B. :1971,Astron. Astrophys. ,15,406.

Lampe,M. and Papadopoulos,K. :1977,Astrophys. J. ,212,886.

Lang,K. R. :1974,Astrophysical Formulae,Springer Verlag,p. 286.

Lin,R. P., Schwartz,R. A. ,Kane,S. R. ,Pelling,R. M. and Hurley,K. C. :1984,Astrophys. J. ,283,421.

Magelessen,G. R. and Smith,D. F. :1977, Solar Phys., 55,211.

McConnell,D. :1980, Ph. D. Thesis ,Univ. of Tasmania

McLean,D. J. ,Sheridan,K. V. ,Stewart,R. T and Wild,J.P. :1971,Nature,234,140.

McLean,D. J., and Sheridan,K. V. :1973,Solar Phys., 32,485.

McLean,D. J. :1981,Proc. Astron. Soc. Aust. ,**4**,132.

McLean,D. J. and Melrose,D. B. :1985,Solar Radiophysics,Eds. D. J. McLean and N. R. Labrum,Cambridge Univ. Press.

Melrose,D. B. :1976,Proc. ASA. ,**3**,43.

Melrose,D. B. :1980.Plama Astrophysics,Vol 12,Gordon and Breach,Newyork,Chapter 11.

Melrose,D. B. :1983,Proceedings of 4th CESRA workshop on Solar noise storms,Ed. A. O. Benz and P. Zlobec.

Muschetti,L. ,Goldman,M. V.and Newman,D. :1985,Solar Phys. ,**96**,181.

Newkirk,G. :1961,Astrophys. J. ,**133**,363.

Newkirk,G. :1967,Ann. Rev. Astron. Astrophys. ,**5**,213.

Oraevski,lV. N. ,Wilhelmsson,H. ,Kogan,E. Ya. And Pavlenko,V. P. :1973,Phys. Scripta,**7**,217.

Parker,E. N. :1983,Astrophys. J. ,**264**,635.

Perley,R. A. ,and Erickson,W. C. :1984,VLA Memorandum 146.

Pick,M. and Trottet,G. :1978,Solar Phys. ,**60**,353.

Poquerusse,M. :1977,Astron. Astrophys. ,**56**,251.

Riddle,A. C. :1972,Proc. Astron. Soc. Aust. ,**2**,98.

Riddle,A. C. :1974, Solar Phys. ,**35**,153.

Roberts,J. A. :1958,Aust. J. Phys. ,**11**,215.

Robinson,R. D. :1985,Solar Phys. ,**95**,343.

Rosenberg,H. :1970,Astron. Astrophys. ,**9**,159.

Rumsey,V. H. :1966,Frequency Independent Antenna, Academic Press.

Santin,P. :1971,Solar Phys. ,**18**,87.

Sastry,Ch. V. :1969,Solar Phys. ,10,429.

Sastry,Ch. V. :1971,Astrophys. Lett. ,8,115.

Sastry,Ch. V. :1972,Astrophys. Lett. 11,47.

Sastry,Ch. V. :1973,Solar Phys.,28,197.

Sastry,Ch. V. ,Krishan,v. and Subramanian,K. R.: 1981,J.Astrophys. Astron. ,2,59.

Sastry,Ch. V. ,Dwarakanath,K. S. ,Shevgaonkar,r. K. and Krishan,V. :1981,Solar Phys. 73,363.

Sastry,Ch. V. ,Shevgaonkar,R. K. and Ramanuja,M. N.: 1983,Solar Phys. ,87,391.

Sastry,Ch. V. :1989,Indian J. Of Radio & Space Phys., 44,56.

Simnett,G. M. and Strong,K. T. :1984,Astrophys. J. , 284,839.

Slottje,C. :1978,Nature,275,520.

Smith,R. A.and de la Noe. :1976,Astrophys.J.207,605.

Spicer,D.'S. ,Benz,A. O. and Huba,J. D. :1981,Astron. Astrophys. ,105,221.

Stahli,M. and Magun,A. :1986,Solar Phys. ,104,117.

Steinberg,J. L,Aubier-Giraud,M. ,Leblanc,Y. and Boischot,A. :1971,Astron. Astrophys. ,10,362.

Stewart,R. T. :1976,Solar Phys. ,50,437.

Stewart,R. T.,Helen,M. C.and Heisler,L. H.:1985, Proc. Astron. Soc. Aust. ,6,231.

Subramanian,K. R. ,Krishan,V. and Sastry,Ch. V.: 1981,Solar Phys. ,70,375.

Subramanian,K. R. ,Nanje Gowda,C. ,Abdul Hamedd,A. T. and Sastry,Ch. V. :1986,Bull. Ast. Soc. India,14,236.

Subramanian,K. R.:1988,Kodaikanal Obs. Bull. ,9,217.

Subramanian,K. R. and Sastry,Ch. V. :1988,J. Astrophys. Astron. ,9,225.

Suzuki,S. and Dulk,G. A. :1985,Solar RadioPhysics. Eds. D. J. Mclean and N. R. Labrum. Cambridge Press.

Svestka,Z. :1976,Solar flares,D. Reidal Pub. Co.,Dordrecht,Holland, p. 273.

Takakura,T. ,Naito,Y. ,and Ohki,K. :1972 In R. Ramaty and R. G. Stone (Eds.),High Energy Phenomenon on the Sun. P. 573.

Takakura,T. and Yousef,S. :1975,Solar Phys. ,**40**,421.

Takakura,T. and Shibabashi,H. :1976,Solar Phys.. **46**,323.

Tanstrom. G. L. and Philips,K. W. :1972a. Astron. Astrophys. **16**,21.

Tanstrom.,G. L. and Philips,K. W. :1972b,Astron.Astrophys. ,**17**,267.

Tapping,K. F. :1978.,**59**,145.

Tapping,K. F. :1983,Solar Phys. ,**87**,177.

Ter Harr,D. and Tsytovitch,V. N. :1981,Phys. rep., 73,175.

Thejappa,G. ,Gopalswamy,N. and Kundu,M. R. :1990,Solar Phys. **132**,

Tidmann,D. A. and Krall,N. A. :1971,Shock waves in collisionless plasmas,Wiley Interscience,N. Y.

Trottet,G. ,Kerdraon.,A. ,Benz,A. O. and Treumann,R.: 1981,Astron. Astrophys. .**93**,129.

Tsybko,Ya. G. :1984,Solar Phys. ,**35**,153

Viner,M. R. :1973 Ph. D. Thesis Univ. Of Maryland.

Weber,R. R. :1969,Solar Phys. ,**8**,376.

Weiland,J. and Williamsson,H. :1973,Phys. Scripta **7**,222.

Weiland,J. and Williamsson,H. :1977,Coherent non linear interaction of waves in plasmas. Oxford.

Wentzel,D. :1981,Astron. Astrophys. ,100,20.

Wentzel,D. :1982,in Proceddings of the 4th CESRA workshop on Solar Noise Storms,Eds. ,A. O. Benz,P. Zlobec.

White,S. M. ,Kundu,M. R. and Szabo,A. :1986,Solar Phys. ,107,135.

Wild,J. P. :1950,Austr. J. Sci. Res. ,34,541.

Wild,J. P. and McCready,L. L. :1950,Aust,J. Sci. Res. Ser: A.,3,387.

Wild,J. P. :1959,Aust. J. Sci. Res. ,3A,541.

Wild,J. P. ,Sheridan,K. V. and Nelyan,A. A. :1959,Aust. J. Phys.,12,369.

Wild,J. P. and Tlamicha,A. :1964,Nature,203,1128.

Wild,J. P. :1972,High Energy Phenomenoa on the Sun. Eds,R. Ramaty and R. G. Stone.

Zaitsev,V. V. ,:1971,Solar Phys. ,20,95.

Zaitsev,V. V. ,Mityakov,N. A. and rapoport,V. O. :1972 Solar Phys. ,24. 444.

Zaitsev,V. V. and Gomichev,V. V. :1973,Soviet Astron., 16,166.

Zaitsev,V. V. and Stepanov,A. V. :1983,Solar Phys., 88,297.

Zhao,R.Y. and Yin,S.Z. :1982,Scintia Scinia,25,422.

PUBLICATIONS

1. Observations of the structure of Type IIIb radio bursts. Ch. V. Sastry,K. R. Subramanian, & V. Krishan,1980,Radio Physics of the Sun ,Eds (M. R. Kundu & T. E. Gergely) .

2. Observations and interpretation of Solar decameter type IIIb radio bursts. V. Krishan,K. R. Subramanian & Ch. V. Sastry,1980,Solar Phys. ,**66**,347.

3. Exciter duration and decay constant of solar decameter type III radio bursts. K. R. Subramanian, V. Krishan, & Ch. V. Sastry,1981,Solar Phys. **70**,375.

4. Pulsating radio bursts at decameter wavelengths from the sun. Ch. V. Sastry,V. Krishan, & K. R. Subramanian,1981,J. Astphys. Astr. ,2,59.

5. Absorption bursts in the radio emission from the sun at decameter wavelengths,Ch. V. Sastry,K. R. Subramanian, & V. Krishan,1983,Astrophys. Lett.,23,101

6. A broadband low frequency radio telescope at Gauribidanur. K. R. Subramanian,C. Nanje Gowda,A. T. Abdul Hameed & Ch. V. Sastry,1986,Bull.Astr. Soc. India,**14**,236.

7. Diffuse echo bursts at 34.5 MHz. K. R. Subramanian, 1988,Kodaikanal Obs. Bull. ,**9**,217.

8. The low frequency radio spectrum of the continuum emission from the undisturbed sun. K. R. Subramanian & Ch. V.Sastry,1988,J. Astphys.Astr. ,1988,**9**,225.